ADA071170

4059

AMRL-TR-79-4

$\bigcirc l$

MEASUREMENT OF RESISTIVE TORQUES
IN MAJOR HUMAN JOINTS

ALI ERKAN ENGIN

THE OHIO STATE UNIVERSITY
COLUMBUS, OHIO 43210

April 1979

20030109 225

NOTICES

When US Government drawings, specifications, or other data are used for any purpose other than a definitely related Government procurement operation, the Government thereby incurs no responsibility nor any obligation whatsoever, and the fact that the Government may have formulated, furnished, or in any way supplied the said drawings, specifications, or other data, is not to be regarded by implication or otherwise, as in any manner licensing the holder or any other person or corporation, or conveying any rights or permission to manufacture, use, or sell any patented invention that may in any way be related thereto.

TECHNICAL REVIEW AND APPROVAL

AMRL-TR-79-4

The voluntary informed consent of the subjects used in this research was obtained as required by Air Force Regulation 80-33.

This report has been reviewed by the Information Office (OI) and is releasable to the National Technical Information Service (NTIS). At NTIS, it will be available to the general public, including foreign nations.

This technical report has been reviewed and is approved for publication.

FOR THE COMMANDER

HENNING E. VON GIERKE
Director
Biodynamics and Bioengineering Division
Aerospace Medical Research Laboratory

REPORT DOCUMENTATION PAGE		READ INSTRUCTIONS BEFORE COMPLETING FORM
1. REPORT NUMBER AMRL-TR-79-4	2. GOVT ACCESSION NO.	3. RECIPIENT'S CATALOG NUMBER
4. TITLE *(and Subtitle)* MEASUREMENT OF RESISTIVE TORQUES IN MAJOR HUMAN JOINTS		5. TYPE OF REPORT & PERIOD COVERED FINAL REPORT 1 April 1976 - 30 Sept. 1978
		6. PERFORMING ORG. REPORT NUMBER
7. AUTHOR(s) Ali Erkan Engin		8. CONTRACT OR GRANT NUMBER(s) F33615-76-C-0505 DOT-HS-6-01331
9. PERFORMING ORGANIZATION NAME AND ADDRESS Department of Engineering Mechanics The Ohio State University Columbus, Ohio 43210		10. PROGRAM ELEMENT, PROJECT, TASK AREA & WORK UNIT NUMBERS 61102F; 2312-V3-06
11. CONTROLLING OFFICE NAME AND ADDRESS Aerospace Medical Research Laboratory, Aerospace Medical Division, Air Force Systems Command, Wright-Patterson Air Force Base, Ohio 45433		12. REPORT DATE April 1979
		13. NUMBER OF PAGES 156
14. MONITORING AGENCY NAME & ADDRESS *(if different from Controlling Office)*		15. SECURITY CLASS. *(of this report)* Unclassified
		15a. DECLASSIFICATION/DOWNGRADING SCHEDULE

16. DISTRIBUTION STATEMENT *(of this Report)*

Approved for public release; distribution unlimited

17. DISTRIBUTION STATEMENT *(of the abstract entered in Block 20, if different from Report)*

18. SUPPLEMENTARY NOTES

19. KEY WORDS *(Continue on reverse side if necessary and identify by block number)*

Biomechanics	Shoulder Joint
Human Joints	Knee Joint
Resistive Torques	Hip Joint
Resistive Moments	Elbow Joint
	Ankle Joint

20. ABSTRACT *(Continue on reverse side if necessary and identify by block number)*

Effectiveness of the multisegmented total-human-body models to predict accurately live human response depends heavily on the proper biomechanical description and simulation of the articulating joints. The research program presented in this report is designed to supply the vital data needed, related to the resistive torques in major human joints, for a biodynamic model already available for use in Air Force related applications. The major articulating joints which are considered are the shoulder, knee, hip, elbow and ankle. Due

DD FORM 1473 1 JAN 73   EDITION OF 1 NOV 65 IS OBSOLETE

to drastic postmortem changes of the biomechanical response of the body tissues, the research is conducted with some obvious limitations on live human subjects. The major components of the specially designed and built experimental apparatus are a subject restraint system, a global force applicator (GFA), and an exoskeletal device (ESD). The ESD is used in monitoring the kinematics of the motion between the fixed and the moving body segments and the forces are applied to the moving body segment by means of the GFA. Design of both the ESD and GFA are similar, each containing eight high precision potentiometers. The experimental apparatus and the associated theoretical concepts are utilized to achieve at least three major tasks. These tasks are the quantitative determination of (a) the voluntary range of motion (b) the resistive force and moments (c) the resistive torques for the rotational motion of the body segments about their long bone axes. Although the majority of the results presented are on the passive resistive force, moment and torques for the major articulating joints of three subjects, some results on the magnitudes of the active resistive muscle force, moment and torque vectors are also presented for the same subjects.

PREFACE

TABLE OF CONTENTS

2

TABLE OF CONTENTS (CONTINUED)

LIST OF ILLUSTRATIONS

LIST OF ILLUSTRATIONS (CONTINUED)

5

LIST OF ILLUSTRATIONS (CONTINUED)

LIST OF ILLUSTRATIONS (CONTINUED)

10

INTRODUCTION

Mathematical models play a very significant role in understanding the biodynamic response of the human body subjected to expected and/or unexpected external load conditions. Properly developed models provide a sound basis for the design of support-restraint systems and vehicles as well. The most sophisticated versions of these total-human-body models, in particular vehicle-occupant models, are articulated and multisegmented to simulate all the major articulating joints and segments of the human body. During the last decade and a half there have been as many as ten distinct vehicle-occupant models developed in the U.S.A. alone. Formulation of the equations of motion in these models has been done by utilization of Lagrange's equations, Euler's rigid body equations, and Lagrange's form of d'Alembert's principle. Naturally, the first models developed have been two-dimensional and they take their impetus from the original work of McHenry [1]. Since this work, refinements and other two-dimensional models have appeared in the crash victim simulation literature [2,3,4,5,6]. The three-dimensional models developed in various research centers in the USA include three-segment model of HSRI [7] in Michigan, twelve-segment models of TTI [8] in Texas and of UC [9] in Ohio, and fifteen-segment model of Calspan [10,11,12] in New York. The Calspan three-dimensional model in recent years went through several development stages. Its present version can be considered the most sophisticated three-dimensional crash victim simulation model available at the present time. It can have any desired number of body segments limited only by the storage capability of the computer. Multiple impacts between the crash victim and vehicle, modeling of a pedestrian struck by a vehicle, as well as modeling of multiple occupants of a vehicle are some of the salient features of the Calspan model.

By some additional features the Calspan model is now also available for Air Force related applications, in particular, to study the pilot ejection problem. According to Fleck [12] these additions are: the capability of prescribing time-dependent forces on the body segments to simulate aerodynamic forces; allowing joint torques which are functions of both flexure and azimuth angles; inclusion of a generalized restraint

11

belt subroutine which describes and simulates a typical Air Force harness system.

Effectiveness of the multisegmented models to predict accurately live human response depends heavily on the proper biomechanical description and simulation of the articulating joints. Short time response of these models requires proper characterization of the passive resistive force and moment vectors in articulating joints. In this report a description of the research program which is developed to collect the resistive force, moment and torque data in major human joints and the associated numerical results are presented. Throughout this report the term "torque" will be used only for the moment vector associated with the rotational motion of a body segment about its long bone axis. The joints which are considered, in order of descending priority, are the shoulder, knee, hip, elbow and ankle. Due to drastic postmortem changes of the biomechanical properties of the body tissues, the research is conducted with some obvious limitations on live human subjects. In this report, first background information on the joint models according to the order of increasing complexity is presented. This section is concluded with an exposé of a general joint possessing six degrees of freedom and some initial concepts for the development of an exoskeletal device, which will be shortened to the ESD henceforth. This will be followed with a section dealing with the theoretical aspects of the research program. The main emphasis of this section will be on the fundamental concepts of the kinematics of the relative motion in three dimensional space which is cast into a format that provides the prelude for the development of the theoretical and the design guidelines for the ESD. The major components of the specially designed experimental apparatus and their utilization in data collection are discussed in a section on the experimental phase of the research program. In numerical results section, results on all the major articulating joints are presented in some detail for three subjects. The report is concluded by a discussion of the immediate application of the results obtained in this research for the development of more realistic joint models and prospects of further research on the subject.

REVIEW OF THE JOINT MODELS

BRIEF ANATOMICAL CONSIDERATIONS OF THE ARTICULATING JOINTS

Joints in the human skeletal structure can be roughly classified into three categories according to the amount of movement which is available at the joint. These categories are named Synarthroses (immovable), Amphiarthroses (slightly movable) and Diarthroses (freely movable). The skull sutures is an example of a synarthrodial joint. Examples of an amphiarthrodial joint are junctions between the vertebral bodies and the distal tibiofibular joint. Our main interest here is the biomechanics of the major articulating joints of the upper and lower extremities which belong to the last category i.e. the diarthroses. In general, the diarthrodial joint has a joint cavity which is bounded by articular cartilage of the bone ends and the joint capsule.

The "bearing surface" of the articular cartilage is almost free of collogen fibres and is thus true hyaline cartilage. From a biomechanics point of view, articular cartilage may be described as a poroelastic material composed of solid and fluid constituents. When the cartilage is compressed, liquid is squeezed out, and, when the load is removed, the cartilage returns gradually to its original state by absorbing liquid in the process. The time dependent behavior of cartilage suggests that the articular cartilage might also be modelled as a viscoelastic material, in particular, as a Kelvin solid.

The joint capsule encircles the joint and its shape is dependent on the joint geometry. The capsule wall is externally covered by the ligamentous or fibrous structure (fibrous capsule) and internally by synovial membrane which also covers intraarticular ligaments and tendons. Synovial membrane secretes the synovial fluid which is believed to perform two major functions: it serves as a lubricant between cartilage surfaces and also carries out metabolic functions by providing nutrients to the articular cartilage. The synovial fluid is non-Newtonian in behavior, i.e. its viscosity depends on the velocity gradient. Cartilage and synovial fluid interact to provide remarkable bearing qualities for the articulating joints. More information on properties of articular cartilage and synovial fluid can be found in reference [13].

13

Structural integrity of the articulating joints is maintained by capsular ligaments and both extra- and intra-articular ligaments. Capsular ligaments are formed by thickening of the capsule walls where functional demands are greatest. As the names imply, extra- and intra-articular ligaments at the joints reside external to and internal to the joint capsule, respectively. Extra-articular ligaments have several shapes, e.g. cord-like or flat depending on their locations and functions. These types of ligaments appear abundantly at the articulating joints. However, only the shoulder, hip and knee joints contain intra-articular ligaments. For example, the cruciate ligaments at the knee joint are probably the most well known intra-articular ligaments. Further information about the structure and mechanics of the joint can be found in reference [14].

Returning to the modeling aspects of the articulating joints, in particular, kinematic behavior of the joints we can state that in each articulating human joint, a total of six degrees of freedom exist to some extent. One must emphasize the point that the "degrees of freedom" used here should be understood in the sense it is defined in mechanics, because the majority of the anatomists and the medical people have different understanding of this concept; e.g. both Steindler [15] and MacConaill [16] imply that three degrees of freedom is the maximum number required for anatomical motion. In the following paragraphs a brief survey of the various joint models reported in the literature is presented. This survey by no means is all inclusive, but an attempt was made to include all representative studies on joint models. The classification of the joint models is made according to the order of increasing complexity.

HINGE OR REVOLUTE JOINT (SINGLE DEGREE OF FREEDOM JOINT)

This is probably the most widely used articulating joint model and related publications are extensive. When the articulation between two body segments is assumed to be a hinge type, the motion between these two segments is characterized by rotation about a single axis fixed in one of the segments. Thus, only one independent coordinate, i.e. the angle

formed between two reference lines inscribed on the segments, is sufficient
to determine the position of one segment with respect to the other one.
Some representative publications assuming hinge joint models in the order
of their appearance in the literature, are: for the elbow by Murphy et al.
[17], Adrian [18], Ringer and Adrian [19] and by Murray et al. [20]; for
the hip by Clayson et al. [21], Murphy et al. [17] and Shoup [22]; for the
knee by Saunders et al. [23], Leighton [24], Young [25], Finley and
Karpovich [26], Contini et al. [27], Lieberson [28], Murphy et al. [17],
Klissouras and Karpovich [29] and Beckett and Chang [30]; for the ankle
by Saunders [23], Finley and Karpovich [26], Gollnick and Karpovich [31],
Lieberson [28], Murphy et al. [17], and Beckett and Chang [30]. Even the
shoulder joint has been modeled in a particular plane as a hinge joint,
Freedman and Munro [32].

SPHERICAL JOINT (LIMITED TO TWO DEGREES OF FREEDOM)

This type of joint is a special case of the three degrees of freedom
spherical or ball and socket joint. There are two versions of this joint
which received some attention in literature. The first version differs
from the three degrees of freedom spherical joint only by the absence of
the axial rotation, i.e. ψ is equal to zero in Fig. 1; thus, the motion
is determined by the two independent coordinates ϕ and θ. Whereas, in the
second version, the axial rotation is allowed but the motion is restricted
to a plane passing through the center of the sphere. In Fig. 1 this type
of motion is illustrated as a slotted ball and socket joint. The slot is
defined by θ equal to a constant and the independent coordinates are
ϕ and ψ. Some representative publications for the first version are: for
the wrist by Taylor and Blaschke [33]; for the elbow by Engen [34]; for
the shoulder by Roebuck [35]; for the hip by Paul [36]; and for the knee
by Eberhart and Inman [37], Hallén and Lindahl [38] and Morrison [39].
The second version of the two degrees of freedom spherical joint has been
used primarily for the elbow by Taylor and Blaschke [33], and by Dempster
[40]; for the knee by Dempster [40], and Lamoreux [41].

SPHERICAL OR BALL AND SOCKET JOINT (THREE DEGREES OF FREEDOM)

Needless to say, this type of joint is most frequently used for the modeling of hip and shoulder joints. The motion is characterized as shown in the left hand side of Fig. 1 by the independent coordinates ϕ, θ and ψ. For the hip we can cite the publications by Dempster [40], McKee [42], Johnston and Smidt [43], Chao [44], Lamoreux [41] and Smidt [45]; for the shoulder the publications by Taylor and Blaschke [33], Dempster [40], Bahniuk and Wijnschenk [47], Steindler [15], Bousso [48], and Risteen and Torfason [49].

PLANAR JOINT (THREE DEGREES OF FREEDOM)

As the title suggests, this type of joint permits motion on a single plane and allows the arbitrary location of the instantaneous axes which are always normal to the plane of motion. The primary application of planar joint model has been the knee joint as shown in Fig. 2. Naturally, the three independent coordinates for determination of this type of motion are two cartesian coordinates, i.e. the coordinates of point C, and one coordinate, θ, defining the amount of rotation about an axis perpendicular to the plane of motion. The rotation angle θ is equal to the angle between P_1Q_1 and P_2Q_2. The points P_1, P_2, Q_1 and Q_2 will be explained in the following second paragraph.

Planar motion can be studied by a technique called "Instant Centers", more explicitly instantaneous centers of rotation. Dempster [40] appears to be the first one who applied this kinematic principle to the planar motion study of the knee joint. This principle is based upon the notion that for a body executing a general plane motion one can show that at any given instant the velocities of the various points of the body are the same as if the body were rotating about a certain axis perpendicular to the plane of motion, called the <u>instantaneous axis of rotation</u>. The intersection of this axis with the plane of motion is called the <u>instantaneous center of rotation</u> (<u>or instantaneous center of zero velocity</u>). As the motion of the body proceeds, the instantaneous center moves on the plane. If these centers are marked each time on the body or on the hypothetical extension of the body, they describe a curve on the body, called <u>body centrode</u>. If the same thing is done with respect to a

16
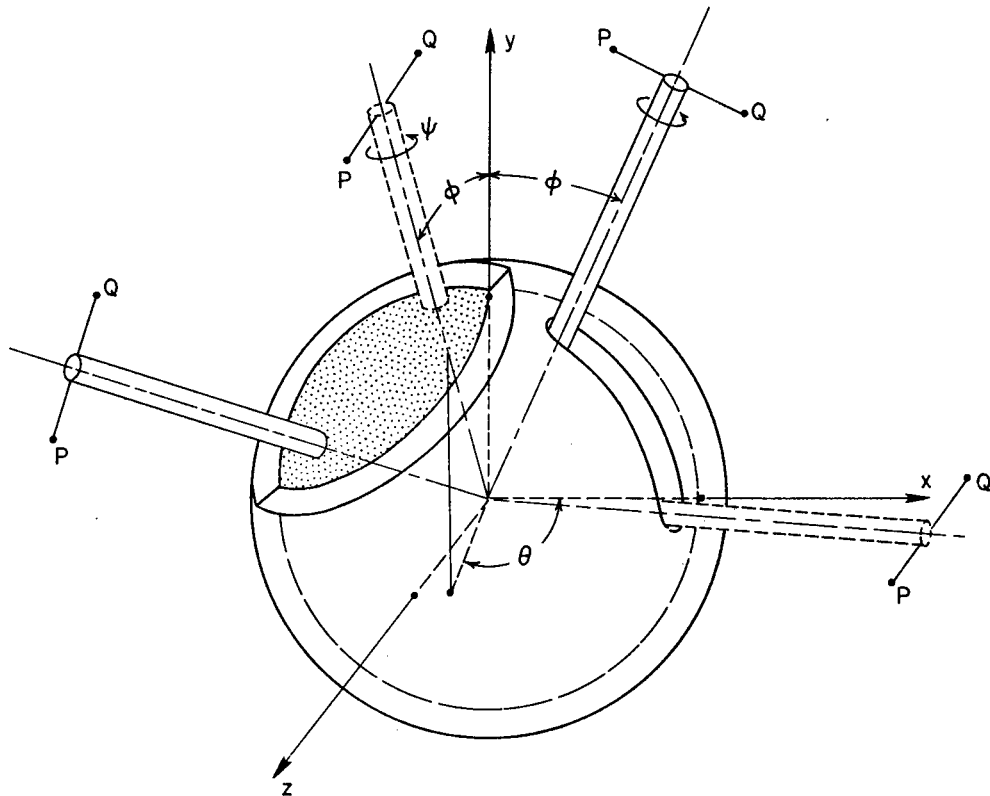
Fig. 1. Spherical or ball and socket joint is illustrated. Figure displays both versions of the two degrees of freedom as well as the most general three degrees of freedom spherical joint.
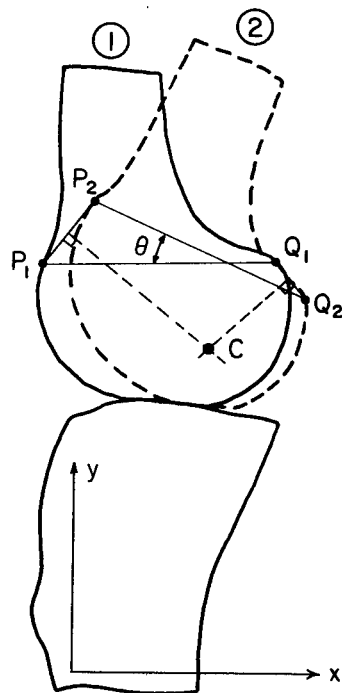
Fig. 2. Planar joint having three degrees of freedom is illustrated by the example of the knee joint. Figure also shows the application of the method of Rouleaux in determination of the instant centers.

fixed reference another curve is obtained, called <u>space centrode</u>. At any instant these two curves are tangent at the corresponding instantaneous center and, as the body moves, the body centrode appears to roll on the space centrode.

By the method of Rouleaux (Fig. 2) one can easily determine the instant centers in the following manner: Lateral roentgenograms of the knee are taken with 15-20° increments from full extension to 90° or more flexion. On the first x-ray film two separate points P_1, Q_1 of the femur are identified and the displacements P_1P_2 and Q_1Q_2 of these two points are determined as the femur moves from one position (1) to another (2) by viewing the two subsequent x-ray films simultaneously on top of each other and drawing lines between the successive positions of each point. These lines connecting the successive positions represent the displacement of the corresponding point. The intersection of the bisectors of the displacements of the two points will be the instant center for the displacement. The locus of these displacement centers is also the body centrode. In fact, the displacement centers for the successive positions of the femur lie between the points defining the instant centers of zero velocity. With the knowledge of the location of the instant centers (of zero velocity) for the two moving bodies which are in contact, one can easily determine the type of relative motion between them since an instant center on the contact surface indicates pure rolling, while an instant center away from the surface indicates some sliding compounded with rolling.

Some notable publications for the knee joint using or accepting the planar joint model are by Barnett [50], Radcliffe [51], Burstein and Frankel [52], Shute [53], Freudenstein and Woo [54], Frankel et al. [55], Reilly and Martin [56], and Smidt [46]. Planar joint model has also been used for the shoulder and elbow by Dempster [40] and Evans [57] and for ankle by Sammarco et al. [58].

Most of the studies quoted so far have utilized protractor type goniometers, electrogoniometers, chronophotography, cinematography and sometimes simple instrumented linkages to determine the kinematics of the joint motion up to three degrees of freedom. We will next consider a

18

joint possessing six degrees of freedom and introduce some concepts for the development of the ESD.

GENERAL JOINT (SIX DEGREES OF FREEDOM)

The joint with six degrees of freedom allows all possible motions between two segments of the body. A good application of this type of a joint model is the shoulder joint where a four segment articulation between the humerus, scapula, clavicle and the rib cage exists. Of course, at the shoulder joint the six degrees of freedom refers to the motion of the humerus relative to the torso. If one considers the total number of degrees of freedom for the motions executed by the humerus, scapula, and clavicle relative to the rib cage, one can easily get a number higher than six even with the proper consideration of various constraints present in the joint complex. Most of the previous work on general joint motion has been conducted by the investigators in dentistry and prosthodontia in the study of the temporomandibular joint. Beck and Morrison [59] introduced an instrumented linkage to measure mandibular motion and later a similar system was developed by Cannon [60] and Messerman [61]. Cannon and Messerman used the instrumented linkage to define the locations of three points in the mandible with respect to the maxilla. Knapp et al. [62] studied jaw motion by relating the orientation of a coordinate system on the mandible to the one on the maxilla. Thompson [63] has developed a mechanical linkage system which consisted of monitoring the lengths of six links which are connected via ball and socket joints to the femur and the tibia for the purposes of studying the motion of the human knee. In a relatively recent study, Kinzel et al. [64] used a linkage system which was attached to the scapula and humerus of a dog by Kirschner-Ehmer splints to determine the relative motion between the two articulating surfaces.

The basic concept for the study of the general joint is quite fundamental and its origin probably goes back to the classical work by Chasles [65]. Consider the general motion of two rigid bodies A and B in three dimensional space as shown in Fig. 3. The relative motion of body B with respect to body A can be characterized by a unique axis called the

19
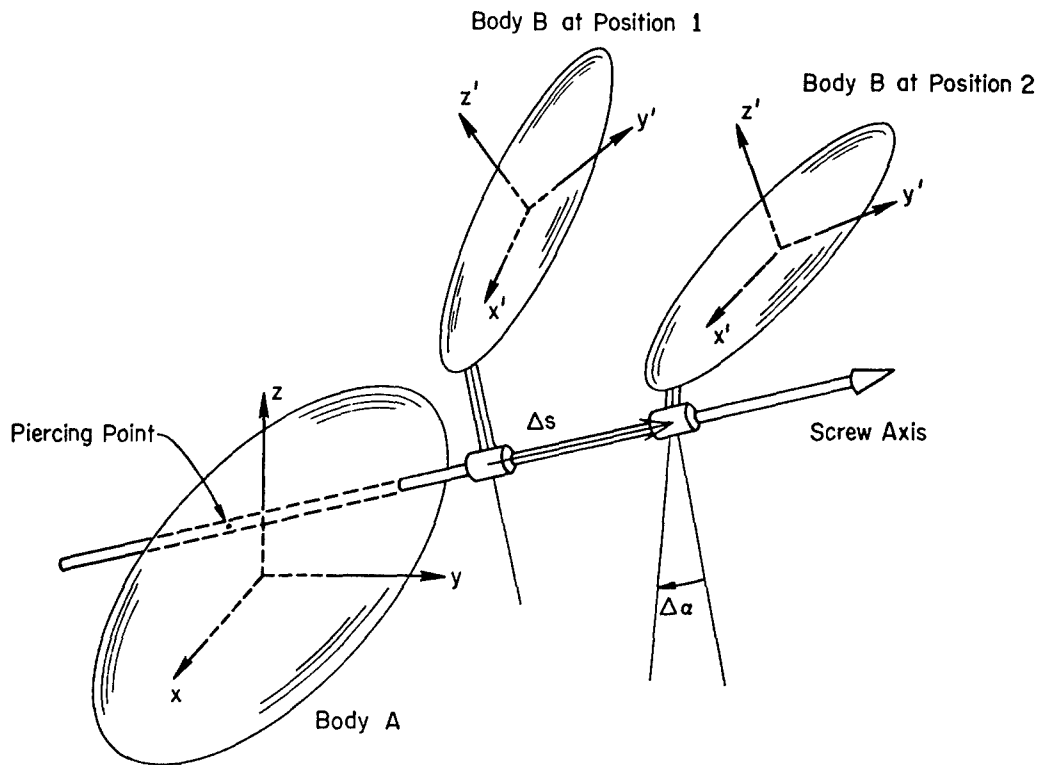
Fig. 3. General motion of two rigid bodies in three dimensional space and
the screw axis used in characterization of the relative motion between
them are illustrated.

screw axis. The relative displacement of body B from position 1 to
position 2 can be defined in terms of a rotation $\Delta\alpha$ about and translation
Δs along the screw axis. For each incremental displacement of body B
with respect to body A, a new screw axis is defined. In fact, if the
increments taken by body B are made infinitesimal in size, the collection
of the screw axes will form a ruled surface called an axode. There are
two unique axodes, one associated with the motion of body B with respect
to body A, and another one is associated with the motion of A with
respect to B. During the relative motion, the two axodes roll and slide
relative to each other along a generator which is momentarily common to
both axode surfaces, [66]. Incidentally, the screw axes and axodes are
the generalization for spatial motion of the instant centers and centrodes
associated with the general planar motion. For a planar motion, the

axodes become two rolling cylinders and the curves formed by the intersection of the motion plane, i.e. the plane which is perpendicular to the generators of the two cylinders, with the cylinders are the centrodes of planar motion. For the spherical joints the axodes become two rolling cones with common apexes at the center of the sphere and for the revolute joints they simply degenerate to a single axis, i.e. the axis of the joint. Of course, in each one of these specialized cases the translation, Δs along the screw axes is zero.

In view of the above remarks, the design of ESD is governed in such a way that any instrumented linkage system must provide us with sufficient data to determine the six parameters associated with the screw axes. The six degrees of freedom between two rigid bodies are in a sense transformed to determination of following six parameters: two parameters which are the coordinates of the piercing point of the screw axes with any one of the three coordinate planes (e.g., xz plane in Fig. 3), two parameters which are the direction cosines of the screw axes, the remaining two parameters are the translations along and rotations about the screw axes.

THEORETICAL PHASE OF THE RESEARCH PROGRAM

The quantitative determination of the nature of the relative motion between two body segments which are connected with a complex anatomical joint is of prime importance to biomechanicians as well as to those in medicine. In the previous section we reviewed various joint models applied in examining the relative motion between two body segments. These joint models range from a simple hinge joint with one degree of freedom to the most general joint model possessing six degrees of freedom. In reality, under both physiological and external loads, each articulating human joint displays a total of six degrees of freedom to some extent. The initial concepts for the development of ESD were already introduced in the previous section. In this section, fundamental concepts of the kinematics of the relative motion in three dimensional space will be cast into a format which will be useful for the development and understanding of the theoretical aspects of the ESD. In particular,

21

we will examine first, the relative position of a point on the upper arm executing a motion with respect to the torso and, second, the displacement of that point during motion. We will derive matrix expressions relating the position and displacement concepts in the light of the screw axis analysis.

Let us consider the relative motion of the arm designated as body segment B in Fig. 4 with respect to the torso which is designated as body segment A. For the intention of studying the relative motion between these two body segments, let us assume that one of them e.g., body segment A, be fixed and the other one, body segment B, is moving relative to body segment A. Note that the range of motion between body segments A and B is controlled by the joint anatomy and ligamentous as well as muscle
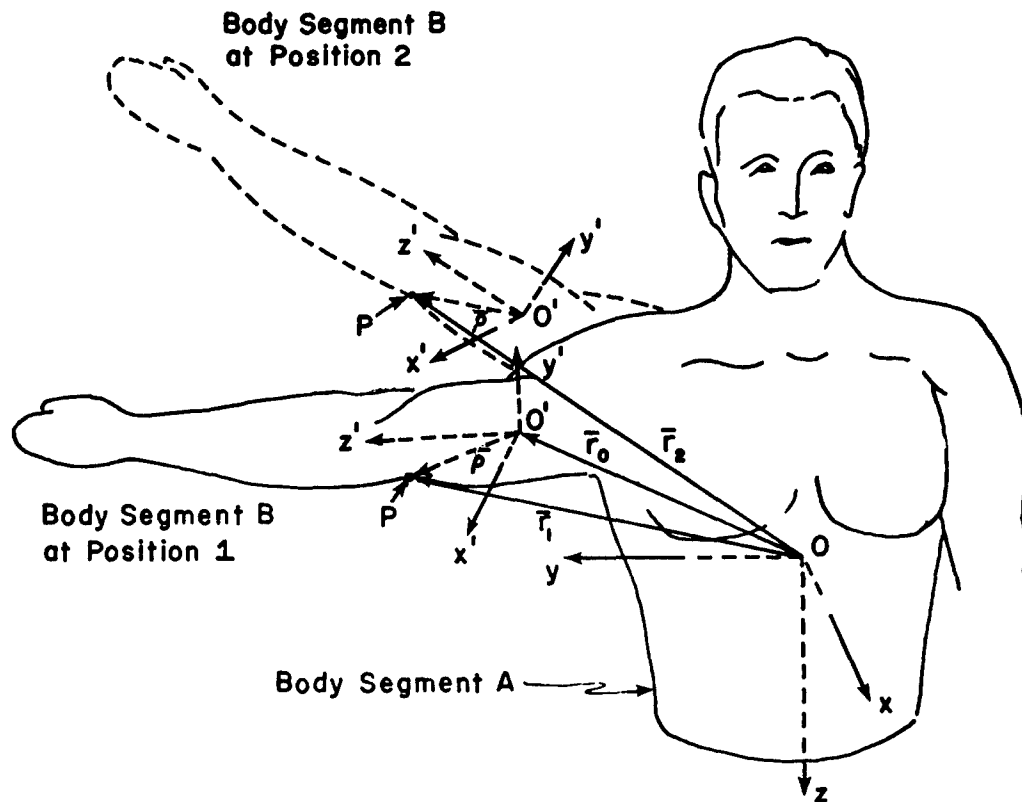
Fig. 4. Motion of body segment B with respect to body segment A in three dimensional space. Displacement of body segment B from position 1 to position 2 is illustrated.

22

forces present during motion. It is very essential to point out before we proceed further that no human body segment is a rigid body in the sense defined in mechanics. However, for the purposes of studying the nature of motion in a given anatomical joint the adjacent body segments to this joint can be assumed to be rigid bodies if certain precautions, which will be discussed in conjunction with the ESD attachment techniques to the body segments, are observed. Let the unprimed xyz and the primed x'y'z' cartesian coordinate systems be attached to the body segments A and B, respectively. These coordinate systems can be also referred to as fixed and moving coordinate systems since body segment A is assumed to be fixed and body segment B is considered to be moving.

Let P be an arbitrary point in body segment B whose position is designated by vectors $\bar{\rho}$ and $\bar{r}_1$ ($\bar{r}_1$ @ position 1; $\bar{r}_2$ @ position 2) in references x'y'z' and xyz, respectively. Since point P is fixed in a moving body segment, the components of vector $\bar{\rho}$ in reference x'y'z' will remain constant, whereas the components of vector $\bar{r}_1$ will change as the body segment B moves relative to body segment A. In fact, the relative position of the moving segment is considered completely determined with respect to the fixed segment if for every point in the moving segment and its associated local position vector $\bar{\rho}$, the corresponding $\bar{r}_1$ can be found. From Fig. 4 the relationship between vectors $\bar{r}_1$, $\bar{r}_o$ and $\bar{\rho}$ can be written in compact matrix form

$$[r_1] = [r_o] + [T][\rho] \tag{3.1}$$

where the elements of matrix T, t_{ij} are the direction cosines of the Ox, Oy and Oz axes relative to the axes of the x'y'z' reference. Thus, matrix T represents rotational orientation of x'y'z', whereas matrix $[r_o]$ represents translation of x'y'z' with respect to the fixed xyz reference. It is more convenient to express Eq. (3.1) in terms of augmented vectors $\bar{r}_{1a}$, $\bar{\rho}_a$ whose first component is 1, and a single 4 x 4 matrix T_a by adding the equation 1 = 1 to the system of equations contained in Eq. (3.1). Thus, Eq. (3.1) takes the following expanded and compact forms:

23

$$
\begin{bmatrix} 1 \\ x_1 \\ y_1 \\ z_1 \end{bmatrix} = \begin{bmatrix} 1 & 0 & 0 & 0 \\ x_o & t_{11} & t_{12} & t_{13} \\ y_o & t_{21} & t_{22} & t_{23} \\ z_o & t_{31} & t_{32} & t_{33} \end{bmatrix} \begin{bmatrix} 1 \\ x_1' \\ y_1' \\ z_1' \end{bmatrix} \quad \text{or} \quad [r_{1a}] = [T_a][\rho_a] \qquad (3.2)
$$

In this report the augmented vectors and matrices will be designated by the subscript or additional subscript "a". Note that there is a new matrix T_a for each position of body segment B, however, at a given position the matrix T_a is the same for all points of body segment B. Hence, determination of the matrix T_a is sufficient to know the position of the moving body segment relative to the fixed one. The primary goal of ESD and the related theoretical development is the determination of matrix T_a and via T_a the achievement of a unique description of the instantaneous position of the moving body relative to the fixed body.

For the total description of the relative motion between two body segments, besides the knowledge of the instantaneous positions of the one body segment relative to another, we must have a description of the nature of the displacement during the motion of the moving segment from position 1 to position 2. Needless to say, instantaneous positions and displacements are very closely related. Displacement analysis results in determination of the set of screw axes; thus, it is essential for the accurate determination of the locations of the joint centers. As was stated in the previous section, displacement of body segment B from position 1 to position 2 can be defined in terms of a rotation α about and translation s along the screw axis, Fig. 5. If the two positions considered are close enough, then the displacements are incremental and refer to a new screw axis each time.

Let us consider a point P fixed in body segment B. As the body segment B moves from position 1 to position 2, we can define the position vectors $\bar{r}_1$ and $\bar{r}_2$ which are expressed in terms of components in xyz references:

$$
\bar{r}_1 = x_1\hat{i} + y_1\hat{j} + z_1\hat{k} \quad \text{and} \quad \bar{r}_2 = x_2\hat{i} + y_2\hat{j} + z_2\hat{k} \qquad (3.3)
$$

24
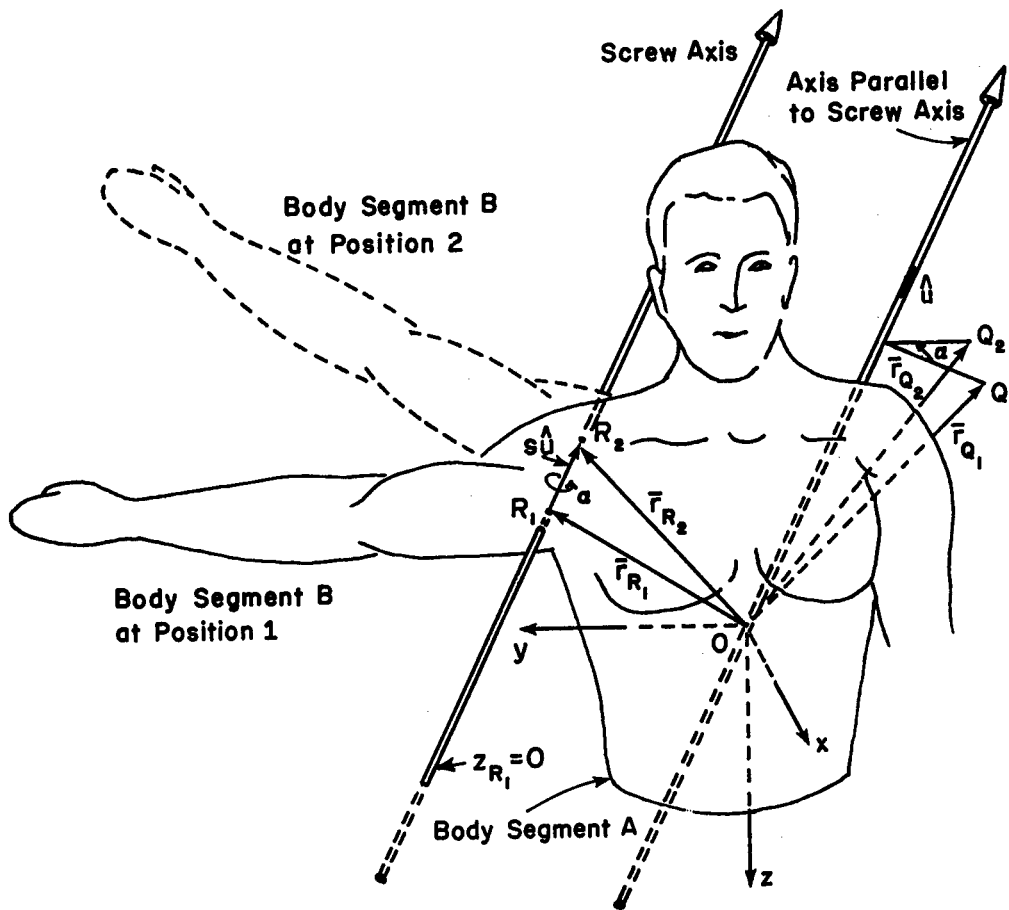
Fig. 5. Representation of the motion of body segment B from position 1 to position 2 in terms of a rotation α about and translation s along the screw axis. A pure rotation of magnitude α of a point Q about an axis parallel to the screw axis is also displayed.

The components of $\bar{r}_2$ will be related to the components of $\bar{r}_1$ by the following special case of an affine transformation [67]:

$$
\begin{bmatrix} x_2 \\ y_2 \\ z_2 \end{bmatrix} = \begin{bmatrix} m_{11} & m_{12} & m_{13} \\ m_{21} & m_{22} & m_{23} \\ m_{31} & m_{32} & m_{33} \end{bmatrix} \begin{bmatrix} x_1 \\ y_1 \\ z_1 \end{bmatrix} + \begin{bmatrix} a_x \\ a_y \\ a_z \end{bmatrix} \tag{3.4}
$$

Eq. (3.4) can be written in augmented form as

25

$$
\begin{bmatrix} 1 \\ x_2 \\ y_2 \\ z_2 \end{bmatrix} = \begin{bmatrix} 1 & 0 & 0 & 0 \\ a_x & m_{11} & m_{12} & m_{13} \\ a_y & m_{21} & m_{22} & m_{23} \\ a_z & m_{31} & m_{32} & m_{33} \end{bmatrix} \begin{bmatrix} 1 \\ x_1 \\ y_1 \\ z_1 \end{bmatrix} \tag{3.5}
$$

Eqs. (3.4) and (3.5) can be expressed in a more compact form as

$$
[r_2] = [M][r_1] + [a] \quad \text{and} \quad [r_{2a}] = [M_a][r_{1a}], \tag{3.6}
$$

respectively. From a mathematical point of view, the augmented form describes the motion of a three-dimensional set of points contained within body segment B relative to a hyperplane, [68]. In Eq. (3.6) matrix M represents a pure rotation about the screw axis and also contains direction cosines information for the screw axis. The augmented matrix M_a in Eqs. (3.5) and (3.6) has the total information for determination of the displacement of the moving body. We will next consider specification of the rotation matrix M.

SPECIFICATION OF THE ROTATION MATRIX M

Since the elements of the rotation matrix M contain only the information concerning the rotation about the screw axis, the translational component of the motion, i.e. the vector whose components are a_x, a_y, a_z in Eq. (3.4), is zero. Thus, the screw axis passes through the origin of xyz reference. In Fig. 5 this is shown as an axis parallel to the original screw axis. Let S be the plane which is perpendicular to the screw axis, Fig. 6. Also, let us define $\bar{r}_1$ as the vector from the origin to a point in the moving body segment. During the motion of the moving body segment from position 1 to position 2, $\bar{r}_1$ will be rotating through an angle α about the screw axis to $\bar{r}_2$. Let $\hat{u} = u_x \hat{i} + u_y \hat{j} + u_z \hat{k}$ be the unit vector along the screw axis. Then, the projections of $\bar{r}_1$ and $\bar{r}_2$ along the screw axis are equal and given by

$$
\bar{r}_{1s} = \bar{r}_{2s} = (\bar{r}_1 \cdot \hat{u})\hat{u} \tag{3.7}
$$
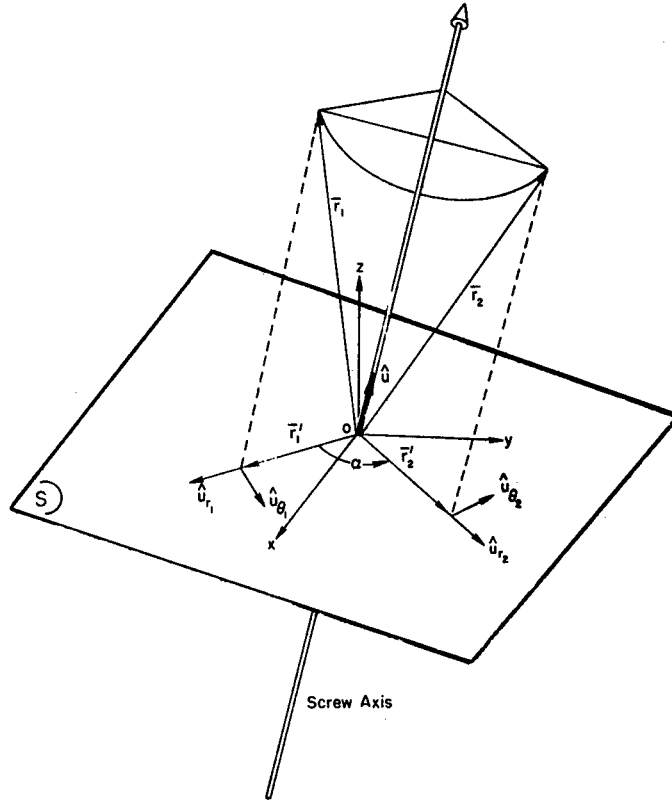
Fig. 6. Coordinate systems and the vectors used in determination of the rotation matrix M.

Let $\bar{r}_1'$ and $\bar{r}_2'$ be the projections of $\bar{r}_1$ and $\bar{r}_2$ in the S-plane, respectively.

Since $|\bar{r}_1'| = |\bar{r}_2'|$, $\quad \bar{r}_2' = (\bar{r}_1 \cdot \hat{u}_{r_1})\hat{u}_{r_2}$ $\quad$ or $\qquad\qquad$ (3.8)

$$\bar{r}_2' = (\bar{r}_1 \cdot \hat{u}_{r_1})(\hat{u}_{r_1} \cos\alpha + \hat{u}_{\theta_1} \sin\alpha) \qquad\qquad (3.9)$$

in view of $\hat{u}_{r_2} = \hat{u}_{r_1} \cos\alpha + \hat{u}_{\theta_1} \sin\alpha$, where the $\hat{u}_{r_1}$, $\hat{u}_{\theta_1}$, $\hat{u}_{r_2}$, $\hat{u}_{\theta_2}$ are the unit vectors for the cylindrical coordinate systems. We can now express vector $\bar{r}_2$ as summation of $\bar{r}_{2s}$ and $\bar{r}_2'$, thus from Eqs. (3.7) and (3.9)

$$\bar{r}_2 = (\bar{r}_1 \cdot \hat{u})\hat{u} + (\bar{r}_1 \cdot \hat{u}_{r_1})\hat{u}_{r_1} \cos\alpha + (\bar{r}_1 \cdot \hat{u}_{r_1})\hat{u}_{\theta_1} \sin\alpha \qquad (3.10)$$

27

Next let us eliminate $\hat{u}_{r_1}$ and $\hat{u}_{\theta_1}$ from Eq. (3.10) by recognizing equivalence of the last two terms of Eq. (3.10) to terms containing cross products of $\hat{u}$ and $\bar{r}$ in the following manner:

$$\bar{r}_2 = (\bar{r}_1 \cdot \hat{u})\hat{u} - [\hat{u} \times (\hat{u} \times \bar{r}_1)] \cos\alpha + (\hat{u} \times \bar{r}_1) \sin\alpha \qquad (3.11)$$

Since $\hat{u} \times (\hat{u} \times \bar{r}_1) = (\bar{r}_1 \cdot \hat{u})\hat{u} - \bar{r}_1$, Eq. (4.11) can be put in the form of

$$\bar{r}_2 = (1-\cos\alpha)(\bar{r}_1 \cdot \hat{u})\hat{u} + \bar{r}_1 \cos\alpha + (\hat{u} \times \bar{r}_1) \sin\alpha \qquad (3.12)$$

This is a vector relation between $\bar{r}_1$, $\bar{r}_2$; it can be cast to matrix form by substituting the components of $\bar{r}_1$, $\bar{r}_2$ and $\hat{u}$ into Eq. (3.12). Thus in the absence of translational component of the motion and in view of Eqs. (3.4) and (3.12), the desired 3x3 rotation matrix M is obtained:

$$\begin{bmatrix} u_x^2(1-\cos\alpha)+\cos\alpha & u_xu_y(1-\cos\alpha)-u_z\sin\alpha & u_xu_z(1-\cos\alpha)+u_y\sin\alpha \\ u_xu_y(1-\cos\alpha)+u_z\sin\alpha & u_y^2(1-\cos\alpha)+\cos\alpha & u_yu_z(1-\cos\alpha)u_x\sin\alpha \\ u_xu_z(1-\cos\alpha)-u_y\sin\alpha & u_yu_z(1-\cos\alpha)+u_x\sin\alpha & u_z^2(1-\cos\alpha)+\cos\alpha \end{bmatrix}$$

Note that the matrix M with elements m_{ij} is the submatrix of M_a as shown in Eq. (3.5). So far, we have determined only the rotational part of M_a. Next, we will focus our attention on the second submatrix of M_a with elements a_x, a_y and a_z to determine the instantaneous orientations of the screw axes.

DETERMINATION OF THE ORIENTATION OF THE SCREW AXIS

In general, the screw axis does not pass through the origin of xyz reference as indicated in Fig. 5. However, if we can find the direction cosines of a line, passing through the origin of xyz and parallel to the screw axis about which the actual motion takes place, we will have the direction cosines of the general screw axis. The elements, m_{ij}, of the rotation matrix M are independent of where the actual screw axis is located; the matrix M was, in fact, determined by considering a rotation about an axis passing through the origin of xyz reference.

Fig. 5 shows a pure rotation of a point Q about an axis passing through the origin. The position vectors of Q, i.e. $\bar{r}_{Q_1}$ and $\bar{r}_{Q_2}$ satisfy

28

the same matrix equation given by Eq. (3.4) excluding the translational component of the motion; thus, in compact form

$$[r_{Q_2}] = [M][r_{Q_1}]$$ (3.13)

Since we are looking for the components of $\hat{u}$, let us move the point Q to the axis, such that $\bar{r}_{Q_1}$ and $\bar{r}_{Q_2}$ are now equal and lie along the same axis. Hence,

$$[M - I][r_Q] = [0]$$ (3.14)

For the nontrivial solution of $\bar{r}_Q$ the determinant of the matrix $[M - I]$ must be zero, [69]. From Eq. (3.14) the vector $\bar{r}_Q$ can be determined only within a constant specifying the length of $\bar{r}_Q$. However, if we designate that constant as 1, then $\bar{r}_Q$ becomes $\hat{u}$ and Eq. (3.14) takes the form of

$$\begin{bmatrix} m_{11} - 1 & m_{12} & m_{13} \\ m_{21} & m_{22} - 1 & m_{23} \\ m_{31} & m_{32} & m_{33} - 1 \end{bmatrix} \begin{bmatrix} u_x \\ u_y \\ u_z \end{bmatrix} = \begin{bmatrix} 0 \\ 0 \\ 0 \end{bmatrix}$$ (3.15)

From the above equation u_y and u_z can be solved in terms of u_x

$$u_y = \frac{m_{23}m_{31} - m_{21}(m_{33}-1)u_x}{(m_{22}-1)(m_{33}-1) - m_{23}m_{32}} \quad , \quad u_z = \frac{m_{21}m_{32} - m_{31}(m_{22}-1)u_x}{(m_{22}-1)(m_{33}-1) - m_{23}m_{32}}$$ (3.16)

Substituting u_y and u_z into $u_x^2 + u_y^2 + u_z^2 = 1$ yields u_x. Thus, the direction cosines of the screw axis, i.e. the orientation of the same axis, are determined in terms of the elements of the rotation Matrix M. Incidentally, once the direction cosines of the screw axis are known, the rotation angle α can be computed very easily from the m_{11} term of the matrix M

$$\alpha = \cos^{-1}\left(\frac{m_{11} - u_x^2}{1 - u_x^2}\right)$$ (3.17)

29

Note that both the direction cosines and the rotation angle α depend on the elements of the matrix M. Before we obtain the remaining parameters, i.e. the translation s along the screw axis and the piercing point coordinates of the screw axis, let us discuss how one can determine the matrix M_a which contains the submatrix M.

DETERMINATION OF THE MATRIX M_A

To determine the matrix M_a, it is sufficient to know the coordinates of four non-coplanar points P_1, P_2, P_3 and P_4 in the moving body segment in both positions 1 and 2. Let us designate the position vectors of these four points by $\bar{\rho}_{ij}$ and $\bar{r}_{ij}$ relative to the moving x'y'z' and the fixed xyz references, respectively. In this subscripted notation, the first subscript i (i = 1,2,3,4) is used to designate a point and the second subscript j (j = 1,2) is used for the designation of positions 1 and 2. The augmented vectors $\bar{r}_{ija}$ for each point can be related via Eq. (3.6).

$$[r_{i2a}] = [M_a][r_{i1a}] \quad (i = 1,2,3,4) \tag{3.18}$$

Eq. (3.18) represents four matrix equations which can be written in one equation by defining a new matrix A whose columns are the augmented vectors, $\bar{r}_{ija}$,

$$[A_j] \stackrel{d}{=} \begin{bmatrix} 1 & 1 & 1 & 1 \\ x_{1j} & x_{2j} & x_{3j} & x_{4j} \\ y_{1j} & y_{2j} & y_{3j} & y_{4j} \\ z_{1j} & z_{2j} & z_{3j} & z_{4j} \end{bmatrix} \quad (j = 1,2) \tag{3.19}$$

Hence, Eq. (3.18) becomes

$$[A_2] = [M_a][A_1] \tag{3.20}$$

The matrix A has a non-vanishing determinant since it is formed by the position vectors of non-coplanar points; thus, it has an inverse and the desired matrix M_a is easily obtained from Eq. (3.20),

$$[M_a] = [A_2][A_1]^{-1} \tag{3.21}$$

30

In theory, by means of Eq. (3.21), the matrix M_a is known and can be determined. However, Eq. (3.21) requires continuous monitoring of four non-coplanar points of the moving body segment. Thus, it does not render a convenient way of determining M_a from an experimental point of view. This situation can be circumvented by utilization of Eq. (3.2) for two instantaneous and close positions of the moving body segment in determining the matrix M_a. In view of Eq. (3.2), the augmented vectors $\bar{\rho}_{ija}$ and $\bar{r}_{ija}$ for each point and position are related as

$$[r_{ija}] = [T_a][\rho_{ija}] \quad \begin{cases} i = 1,2,3,4 \\ j = 1,2 \end{cases} \tag{3.22}$$

Eq. (3.22) represents eight matrix equations or four matrix equations for each position. Let us define a new matrix B whose columns are the augmented vectors $\bar{\rho}_{ija}$, i.e.

$$[B] \overset{d}{=} \begin{bmatrix} 1 & 1 & 1 & 1 \\ x_1' & x_2' & x_3' & x_4' \\ y_1' & y_2' & y_3' & y_4' \\ z_1' & z_2' & z_3' & z_4' \end{bmatrix} \tag{3.23}$$

Then, in view of Eqs. (3.2), (3.19), and (3.23) we have

$$[A_j] = [T_{ja}][B] \qquad (j = 1,2) \tag{3.24}$$

Substituting A_1 and A_2 obtained from Eq. (3.24) into Eq. (3.20) gives

$$[T_{2a}][B] = [M_a][T_{1a}][B]$$

which yields after postmultiplication by $[B]^{-1}[T_{1a}]^{-1}$

$$[M_a] = [T_{2a}][T_{1a}]^{-1} \tag{3.25}$$

where T_{1a} and T_{2a} are the coordinate transformation matrices between xyz and x'y'z' references for positions 1 and 2. The main task of ESD is indeed the continuous monitoring of the necessary parameters for the

31

evaluation of T_a matrices. More will be said on this topic in a later section of this report. We now turn back to the discussion of the parameter s, which is the translation along the screw axis, and the piercing point coordinates.

DETERMINATION OF SCREW DISPLACEMENT AND PIERCING POINT COORDINATES

To find the translational component of the motion along the screw axis, let us consider a point R_1 belonging to the moving body segment or belonging to the hypothetical extension of the moving body segment as shown in Fig. 5. The translation of this point along the screw axis from R_1 to R_2 is designated as $s\hat{u}$ and the corresponding position vectors, $\bar{r}_{R_1}$ and $\bar{r}_{R_2}$, satisfy:

$$[r_{R_2a}] = [M_a][r_{R_1a}] \quad \text{or} \quad [r_{R_2}] = [M][r_{R_1}] + \begin{bmatrix} a_x \\ a_y \\ a_z \end{bmatrix} \tag{3.26}$$

Translation along the screw axis is given as:

$$s[u] = [r_{R_2}] - [r_{R_1}] \tag{3.27}$$

From Eqs. (3.26) and (3.27) we obtain

$$\begin{bmatrix} m_{11}-1 & m_{12} & m_{13} \\ m_{21} & m_{22}-1 & m_{23} \\ m_{31} & m_{32} & m_{33}-1 \end{bmatrix} \begin{bmatrix} x_{R_1} \\ y_{R_1} \\ z_{R_1} \end{bmatrix} = \begin{bmatrix} su_x - a_x \\ su_y - a_y \\ su_z - a_z \end{bmatrix} \tag{3.28}$$

The coordinates of the piercing point of the screw axis and the value of s are found by setting, one at a time, x_{R_1}, y_{R_1} and z_{R_1} equal to zero. For example, the screw axis will intersect x-y plane of the xyz reference when $z_{R_1} = 0$. For this case it can be shown that Eq. (3.28) reduces to:

$$
\begin{bmatrix} x_{R_1} \\ y_{R_1} \\ s \end{bmatrix} = \begin{bmatrix} m_{11}-1 & m_{12} & -u_x \\ m_{21} & m_{22}-1 & -u_y \\ m_{31} & m_{32} & -u_z \end{bmatrix}^{-1} \begin{bmatrix} -a_x \\ -a_y \\ -a_z \end{bmatrix} \qquad (3.29)
$$

Similarly, the intersections of the screw axis with x-z and y-z planes and the screw displacement s are found. With determination of screw displacement and piercing point coordinates of the screw axis we have completed the theoretical groundwork for the development of the ESD which will be one of the essential components of the experimental apparatus for determination of the passive moments at the major articulating human joints.

EXPERIMENTAL PHASE OF THE RESEARCH PROGRAM

Data collection for the kinematic and kinetic analyses of the human motion plays a very significant role in the fields of biomechanics and kinesiology. Among the many devices used in understanding of the human motion are electromyographs, protractor type goniometers, electrogoniometers, stroboscopes, still cameras, normal-and-high-speed motion picture cameras, TV cameras, X-rays, various force and moment transducers, and associated recording and data reducing equipment. The present research program involves monitoring of the motion of a slowly moving body segment with respect to the fixed one and simultaneous recording of the force and moment vectors causing this motion in three-dimensional space. Before we present the description of the major components of the experimental setup to accomplish these tasks we would like to examine briefly the techniques employing film and cameras in studying human motion.

CRITIQUE OF FILM TECHNIQUES USED IN KINEMATIC DATA COLLECTION

Film and camera techniques can be most likely classified into two categories, i.e., those requiring still and those requiring motion picture cameras. Naturally, in each category there exist sub-categories utilizing single and multiple cameras and variations on the established techniques. In the still camera category, the most widely used technique is chronophotography or interrupted light photography which was developed

first by Marey [70] in 1873. Marey's method utilized a rotating disk with a variable number of apertures placed in front of the open shutter of a camera to take successive exposures on a single fixed piece of film, of a walking subject who wore shiny reflecting buttons and bands on various segments of his body which was mostly covered by a black outfit. In 1950 Bresler and Frankel [71], in their study of the kinematics and kinetics of walking subjects, used continuously lighted opthalmoscope bulbs instead of shiny buttons. By exposing a film in a darkened room to the lights 30 times a second, they obtained a photograph containing many points of light. With these data points they were able to calculate displacements, velocities, and accelerations of various segments of the leg by graphic and arithmetic techniques.

The stroboscope can be used to illuminate the subject to make a composite picture of the motion by recording several instantaneous positions on a film of a still camera with open shutter. The number of positions recorded is, of course, controlled by the frequency setting of the stroboscope. If the motion is coplanar it is possible to obtain the kinematic data (i.e. displacements, velocities and accelerations) from the exposed film. However, if the motion is three-dimensional, the stroboscopic picture has the same shortcomings as chronophotography in that they cannot provide sufficient information to determine the actual kinematic data. Naturally, the biggest disadvantage of the stroboscopic photography is the overlapping images of the body segments at the boundaries of the range of motion.

Cinematography with both normal-and high speed motion picture cameras is the second category of collecting data for kinematic analysis of motion. Hyzer [72] and Mascelli and Miller [73] discuss many topics on cinematography dealing with measurement errors due to relative movements of subject with respect to the shutter of the camera, lens aberrations, film distortions, subject-plane relation to film-plane, types of equipment, lighting, exposure, etc. Frame-by-frame analysis of the motion picture film results in composite tracings and "stick figures" showing the positions of the body segments. For the two dimensional coordinate measurements, special equipment such as a Vanguard analyzer is

34

needed. The biggest drawback of cinematographic motion study besides its shortcomings in space and time resolution is the excessive effort requirement for frame-by-frame analysis to obtain the kinematic data.

There are two assumptions usually made in photographic data collecting: (a) the plane of photography can sufficiently approximate or model the spatial motion; (b) the spatial orientation of plane of photography is known exactly at all times. Frequently, these assumptions do not hold and are not verified experimentally. Needless to say, photographic perspective errors increase with the distance of the point of interest from the focus plane. Some investigators used telephoto lenses to minimize perspective errors by increasing camera-to-subject distances. Although there are few corrective formulas derived from trigonometric relationships between two two-dimensional perpendicular views of any position in three-dimensional space, they still depend on the measurements made on the film. Furthermore, the optical axes of multiple cameras must be perpendicular and intersect at a common point. An additional disadvantage of most multiple camera techniques is the requirement of the filming of the landmarks or targets by all cameras for determination of the three coordinates. Because of the solid; irregular, and opaque nature of the body segments, the same landmark or the target may not be seen all the time by all the cameras. Finally, it is extremely difficult to collect more than three degrees of freedom information at a given body joint by means of film techniques. Analyses of the complex body joints require the data collection to be made by considering all six degrees of freedom at the joint. In view of the above comments, it was decided to develop an exoskeletal device which is a spatial linkage system providing one with the capability of studying the six degrees of freedom motion between two body segments. A device such as the ESD is also necessary since the kinematic data must be coupled with the force data during determination of the passive moments at the joints as will be explained later in this section.

MAJOR COMPONENTS OF THE EXPERIMENTAL SETUP

The major components of the experimental apparatus are a subject restraint system (Fig. 7), a global force applicator, GFA (Figs. 8 & 9) and the ESD (Fig. 10). The subject restraint system with its pitch, roll and yaw capabilities can orient the subject to any desired position. This is an important feature of the subject restraint system which assists in the mobilization of subject's appropriate body segment at a constant elevation while the experimentor moves the body segment by means of the GFA throughout its entire range of motion. To eliminate the gravitational component of the moment values at the joint, the force application to the moving body segment is made in a horizontal plane while the elevation of the moving body segment is maintained by a support line in such a way that in the direction of the force application a relaxed floating type of motion of the moving body segment is achieved. Both the security and the support characteristics of the restraint system allow total relaxation, thus minimizing active muscle effects during the experiment. Further details on design criterion, its iteration and the final design form of the subject restraint system are discussed in Appendix A.

Forces are applied to the moving body segments by means of the GFA (Fig. 8) which consists of four links and eight revolute joints containing high precision potentiometers. The outputs of the potentiometers and the length dimensions of the links are utilized to obtain the direction as well as the point of application of the force vector. Note that in Fig. 8 the last two links of the GFA are shown. The GFA is terminated by a force transducer and a force cuff which is free to rotate about its axis. The force transducer is designed and built to measure all three components of the force and moment vectors. Of course, the predominant force component is the one along the direction of the last link of the GFA and all the other force as well as the moment components are relatively small in magnitude if one maintains approximately perpendicular force application on the moving body segment. More details on the design of the GFA and the force transducer are provided in Appendix B.
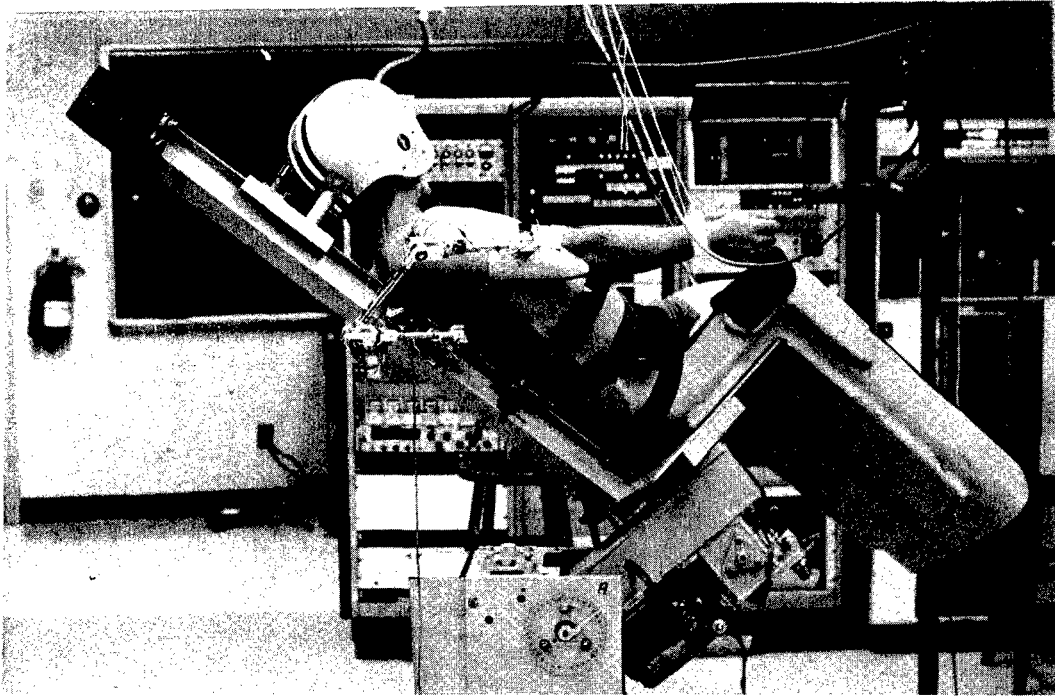
Fig. 7. Overall view of the subject restraint system and data collection equipment. Subject is prepared for the shoulder force and moment data collection.

Fig. 8. Force is being applied by means of the global force applicator (GFA) on the subject's arm.
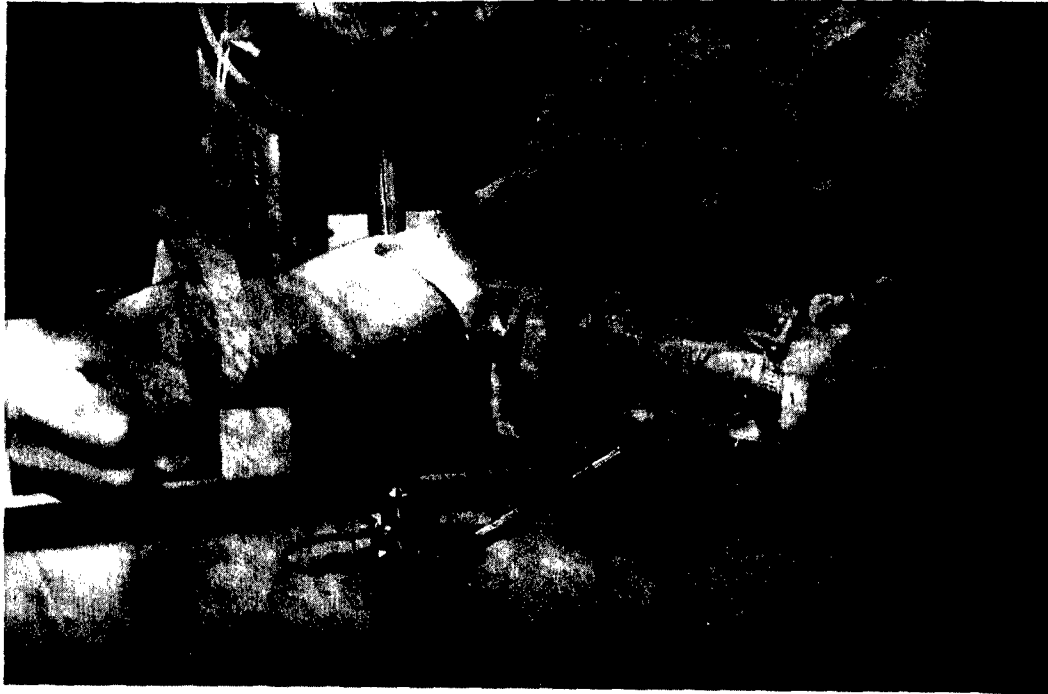
Fig. 9. Close-up view of the force transducer and the force cuff.
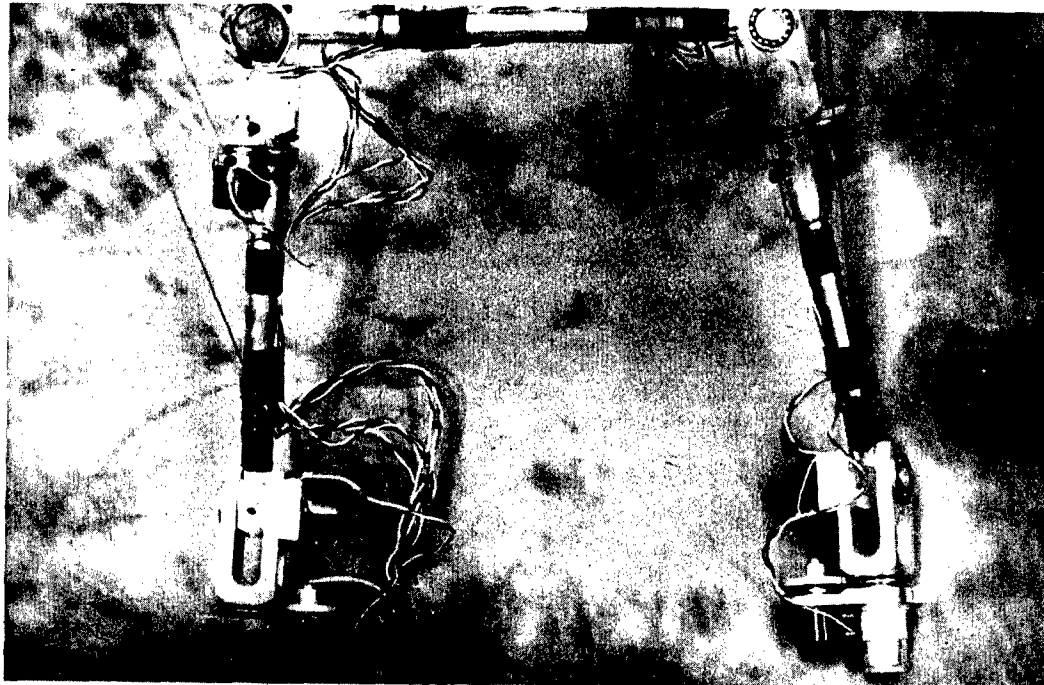
Fig. 10. Close-up view of the exoskeletal device (ESD).

The third major component of the experimental apparatus is the ESD as shown in Fig. 10. The ESD is designed with a capability suitable to study the most complex joint, i.e. the shoulder joint; it also consists of eight revolute joints whose rotations are monitored by means of high precision potentiometers. Although there are major design differences between the ESD and the GFA, from the kinematics point of view the ESD can be considered as a miniaturized version of the GFA. Fundamental design requirements of the ESD are (a) capability of providing complete freedom of motion between two adjacent body segments and (b) capability of providing sufficient data to determine the values of the T_a matrices defined by Eq. (3.2) for all possible motions at the joints. Incidentally, any endeavor to measure directly the so-called rigid-body characteristics of two body segments must include an understanding of certain factors such as: (a) the human body segments have no definite physical demarcation points; (b) no human body segment is a rigid body; (c) the physical structure of these body segments varies from one individual to another. The treatment of these factors varies with respect to the particular joint under study. However, common to the study of all joints is utilization of the principles of orthopedic bracing in attaching the ends of the ESD to the moving and the fixed body segments. Thus, heat formable plastic material is used in forming individually fitted shells for the body segments. Special care is given to locate the bony landmarks of the body segments to minimize relative soft tissue motion. This is also achieved by the light weight and very low friction construction of the ESD. In fact, the ESD is balanced by means of pulleys and small weights in such a way that the subject does not feel its presence or, stated differently, the ESD creates only very negligible resistance to the motion of the moving body segment. In the case of the shoulder joint study, the shell which is attached to the upper arm as shown in Figs. 7, 8, 9 makes close contacts with the medial and lateral epicondyles of the humerus; the torso shell is in contact with pelvis, the rib cage and indirectly with the cranium via a helmet. Appendix C provides more details about the design and construction of the ESD.

DATA COLLECTION SYSTEM

The GFA, the ESD and the force transducers generate 24 analog channels that had to be recorded and analyzed. Our Biomechanics Laboratory did not have a data collection system which was capable of doing this job. Via a search through the Excess ADP Equipment Bulletins of the Defense ADPE Reutilization Office we located a data collection system which was announced on the ADP Equipment Bulletin under DOD Case No: 2618-76-104. With the exception of the Digitronix tape reader which was listed as a part of the system but was kept by the previous users of the equipment, the data conversion system which consists of three consoles weighing approximately 1500 lbs was transported by a rental truck from the Naval Weapons Research Laboratory in Dahlgren, Virginia to our laboratory. In the background of Fig. 7 this data collection system can be seen. Again from the ADP Equipment Bulletins we located an IBM 729-6 Tape Drive which is compatible with the data collection system at Grumman Inc. L.I., New York. This unit was also brought in and connected to the data collection system. The multiplexer of the data collection system had 16 channels. Due to the high cost of buying a new multiplexer and interfacing with the rest of the system we designed and built an additional board to convert the multiplexer from 16 channels to 24. Initially, we had many problems in various sections of the data collection system, some of which are mentioned in Appendix D. This appendix also contains more technical information about the data collection system.

NUMERICAL RESULTS

The development of the ESD, the GFA, the subject restraint system, and the associated theoretical concepts which have been presented in the previous sections were made to achieve at least three major tasks. The first one is the quantitative determination of the range of motion in all major joints; the second one is quantitative determination of passive resistive force and moments at the joints; the third task is quantitative determination of passive resistive torques associated with the rotational motion of the body segments about their long bone axes. In this research

program three subjects were tested and for each joint the tests were repeated at least three times. Selected anthropometric measurements of these three subjects are given in Table 1. In Fig. 11 the cartesian coordinate systems of the fixed-body segments and the ESD attachment point locations are shown. The locations of the ESD attachment points with respect to the coordinate systems attached to the fixed body segments for all three subjects are tabulated in Table 2.

Before we present the plots showing for all three subjects the results of the three major tasks mentioned in the above paragraph we would like to refer to Fig. 12 where θ and ϕ angles define the orientation of the moving body segment with respect to the fixed body segment. These two angles will be used in all subsequent figures of this report to designate orientation. Thus, for the shoulder motion, $\phi = 90°$ corresponds to the motion in the frontal plane. Fig. 12 also shows a centrode path for the shoulder joint when the arm is elevated in the frontal plane. The points of this particular centrode path are obtained by the intersection of the screw axes with the frontal plane. Similar centrode paths can be obtained for various values of constant ϕ, each defining a plane passing through a point such as S in Fig. 12. The significance of the shape of the centrode path can be examined in the light of the anatomical structure of the shoulder joint complex. The most striking feature of the shoulder joint is the presence of four independent articulations. These are: 1. The glenohumeral joint which is a ball and socket joint where the humerus mates with the glenoid cavity of the scapula. 2. The acromioclavicular joint where the clavicle meets the acromion process of the scapula. 3. The sternoclavicular joint where the clavicle meets the manubrium of sternum. 4. The scapulothoracic joint where the scapula rotates on the thorax. In the true sense, the scapulothoracic articulation is not a joint, but this definition is of value when describing the movements of the scapula over the thorax. There are numerous ligaments connecting various components of the shoulder joint. In Fig. 12 the point closest to the origin of the xyz coordinate system corresponds to the initial phase of the arm elevation ($\theta \simeq 25°$). As the angle of elevation increases, the centrode path curves upward, indicating dependence of the

Table 1

SELECTED ANTHROPOMETRY OF SUBJECTS 1, 2, 3.

(All length dimensions are in cm)

	1	2	3
Weight (Newtons)	658	689	734
Stature	160	175	183
Shoulder Circumference	109.2	111.7	111.4
Chest Circumference	89.2	97.8	96.5
Waist Circumference	81	78.8	78.1
Wrist Circumference	16.5	17.2	17.5
Lower Arm Circumference	28	27.8	26.7
Elbow Circumference	29.2	30.2	29.2
Biceps Circumference	31.7	33	30.8
Arm, Axillary Circumference	31.4	33	29.2
Arm, Scye Circumference	44.1	47	45.7
Thigh, Upper Circumference	53.9	58.5	61.0
Thigh, Lower Circumference	39.6	37.8	40.6
Calf Circumference	36.5	36.2	40
Ankle Circumference	22.2	21	24.1
Forearm - wrist length	25.4	29.2	29.2
Shoulder - elbow length	34.3	38	38.1
Shoulder - height, sitting	60.4	58.4	63.5
Sitting height	87.6	88.3	94
Shoulder breadth	45.1	44.5	43.8
Chest breadth	31.2	33	29.2
Chest depth	21.4	25.4	21.6
Waist depth	18.4	20.3	19.1
Buttock - knee length	53.4	60.4	59.7
Buttock - popliteal length	43.2	50.8	52.1
Knee height, sitting	47	55.9	54.6
Elbow - to - elbow breadth	44.5	45.1	47
Hip breadth, sitting	35	34.3	36.2
Knee - to - knee breadth, sitting	20.4	19.2	21.6
Leg length (tibial point - Malleo.)	33.6	34.4	41.9
Trochanterion height	90	99	98
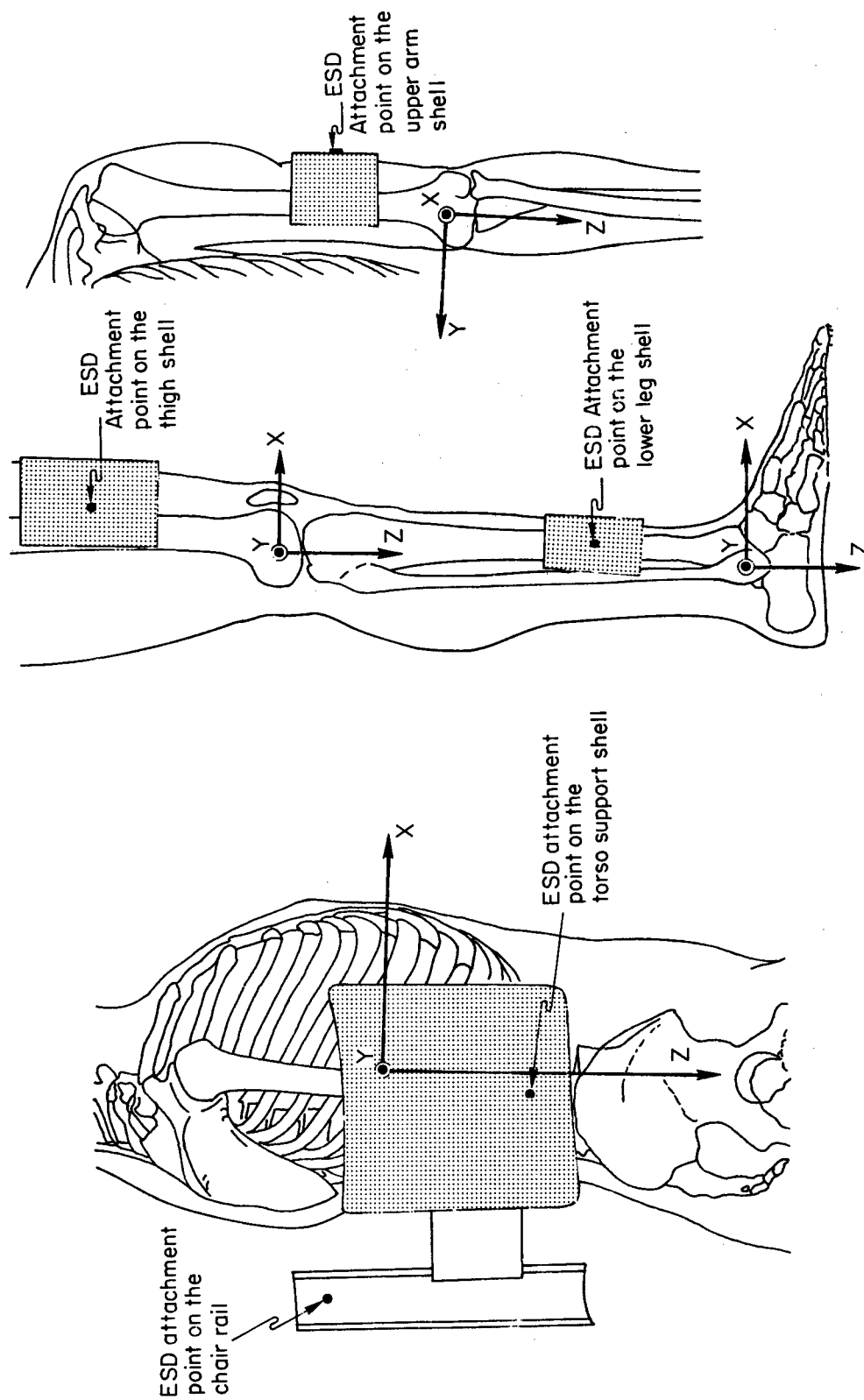
Fig. 11. Coordinate systems of the fixed-body segments and the ESD attachment point locations.

43

Table 2

THE LOCATION OF THE ESD ATTACHMENT POINTS WITH RESPECT
TO THE COORDINATE SYSTEMS ATTACHED TO THE FIXED BODY SEGMENTS

(All Dimensions are in cm)

JOINTS		SUBJECT 1	SUBJECT 2	SUBJECT 3
-SHOULDER- (The origin of the coordinate system is at the mid-torso)	x_s y_s z_s	-24.0 0 - 5.4	-23.9 0 - 0.8	-24.2 0 - 1.4
-HIP- (The origin of the coordinate system is at the mid-torso)	x_h y_h z_h	- 3.1 -15.1 15.3	- 2.9 -15.2 22.1	- 3.2 -14.7 19.3
-KNEE- (The origin of the coordinate system is at the distal end of the femur)	x_k y_k z_k	1.3 5.8 -13.0	1.3 5.8 -13.5	3.2 5.8 -16.5
-ANKLE- (The origin of the coordinate system is at the distal end of the tibia)	x_a y_a z_a	0 4.1 -17.1	0 4.1 -17.8	0.6 4.1 -24.9
-ELBOW- (The origin of the coordinate system is at the distal end of the humerus)	x_e y_e z_e	1.3 4.1 - 8.9	0.5 4.1 -13.2	0 4.1 -14.0
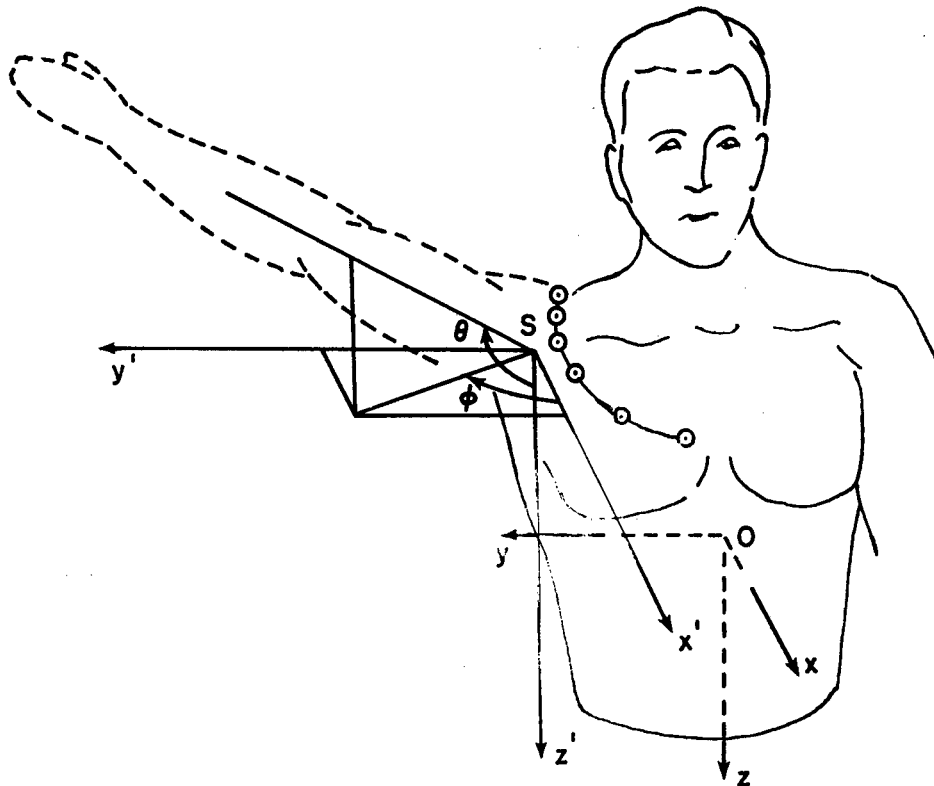
Fig. 12. Centrode curve for the shoulder joint for a motion corresponding to the elevation of the arm in the frontal plane.

joint motion on the glenohumeral and acromioclavicular joints, whereas the initial phases of the arm elevation utilizes primarily sternoclavicular and scapulothoracic articulations. Because of various reasons we did not pursue determination of other joint centers. Thus, the moment values will be given at a fixed point strategically located at the joint. One very important reason of picking a fixed point and evaluating the moment values with respect to that point is to eliminate errors caused by evaluating the moment components at joint centers whose coordinates can have errors themselves. Note that the moment values depend on the coordinates of the point about which they are determined. For the shoulder joint the fixed point chosen, S, coincides approximately with the center of the glenohumeral joint when the arms are on the side of the torso. Of course, when the arm motion starts, the center of the glenohumeral joint moves

45

away from point S. Further note that for any other point in the shoulder joint complex the corresponding moment vector is the sum of the moment vector given at point S and the vector obtained by the cross product of the position vector, which extends from that point to point S, and the force vector itself.

The coordinates of the point S used for the shoulder joint for all three subjects are as follows:

$$x_1 = 0 \qquad x_2 = 0 \qquad x_3 = 0$$

$$y_1 = 0.181 \text{ m} \qquad y_2 = 0.177 \text{ m} \qquad y_3 = 0.186 \text{ m}$$

$$z_1 = -0.152 \text{ m} \qquad z_2 = -0.148 \text{ m} \qquad z_3 = -0.156 \text{ m}$$

The coordinates of the point about which the moments are determined for the hip joint for all three subjects are:

$$x_1 = 0 \qquad x_2 = 0 \qquad x_3 = 0$$

$$y_1 = -0.097 \text{ m} \qquad y_2 = -0.095 \text{ m} \qquad y_3 = -0.1 \text{ m}$$

$$z_1 = 0.325 \text{ m} \qquad z_2 = 0.317 \text{ m} \qquad z_3 = 0.334 \text{ m}$$

The point chosen for the hip joint corresponds to the center of the head of the femur. For the other joints i.e. the elbow, knee and ankle the point chosen is the origin of the coordinate system as shown in Fig. 11.

In this report the results will be presented for the standing erect configuration of the human body as the initial condition rather than some arbitrary set of joint angles being initial conditions. Thus, the positions of the body segments illustrated in Fig. 11 are taken to be the initial condition positions. This choice was made to provide the reader with easy interpretation of the angles involved in terms of extension-flexion, abduction-adduction, and internal-external rotation of the body segments. Naturally, for the shoulder joint the values of θ and ϕ that define the orientation of the upper arm with respect to the torso are the same whether the subject is in standing configuration or seated configuration with arm positioned as if the lower arm were supported by an armrest. Of course, if one desires to have results referred to some

angles other than those shown in Fig. 11, one simply makes $(\theta - \theta_0)$ or $(\phi - \phi_0)$ type of coordinate transformation in expansion equations or simply shifts the abscissa of the figures θ_0 or ϕ_0 amounts.

RESULTS ON PASSIVE RESISTIVE FORCE & MOMENT VECTORS AND VOLUNTARY RANGE OF MOTION AT THE JOINTS

First, results obtained for the shoulder joints of the three subjects are presented. In Fig. 13 the components of the passive resistive force vector at the shoulder joint of the first subject during forced sweep of the arm for the shoulder ab/ad duction (abduction/adduction) is presented. Corresponding passive resistive moment vector components are shown in Fig. 14. During this test, the subject is in a normal seating configuration, i.e. the chair is not rotated in any direction and subject's arm is moved in abduction and adduction directions for a θ value nominally equal to 75°. Zero value of angle ϕ corresponds to straight anterior extension of the arm. Thus, positive values of ϕ designate abduction, which is the motion of the arm in the lateral direction; and negative values of ϕ designate adduction, which is the motion of the arm in medial direction. In these and subsequent figures voluntary range of motion (VROM) for the same motion is shown on the abscissa of the figures. Subjects were first asked to move their arms voluntarily in a prescribed manner and data were collected for this voluntary motion. Later on, the same motion was repeated by the application of the GFA as shown in Figs. 8 and 9 on the freely moving arm when the subject was assumed to be relaxed as much as possible. In Figs. 15-18 results for the same test are presented for the second and third subjects. Incidentally, all figures of this report, unless otherwise stated, are plotted from those data which represent closely the information obtained from at least three sets of tests.

In Figs. 19-24 components of the passive force and moment vectors at the shoulder joint are plotted for all three subjects for the forced sweep of the arm for the shoulder abduction in the frontal plane. For the standing subject this motion corresponds to raising of the arm without allowing rotation about the axis of the humerus. Tests were conducted on the subject when the chair angle was pitched backward such that the torso

support shell and thus, subject's torso, were parallel to the ground.
This effectively converted the raising of the arm motion to a motion that
took place in a horizontal plane. The next six figures (Figs. 25-30)
show the components of the passive resistive force and moment vectors at
the shoulder joint for all three subjects for the forced sweep of the arm
for shoulder extension. To simulate this, the chair was rotated from the
pitched backward position in the direction of 90° roll. These two
rotations placed the subject lying on his side supported by lower limb
and torso supports and helmet. This was probably one of the least
comfortable situations for the subjects.

For the first subject more information in regard to range of motion
of the shoulder joint is displayed in Fig. 31. In this figure voluntary
range of motion is plotted on $\theta - \phi$ plane for three tests in which the
subject, by maintaining approximately 90° between the lower and upper
arm, sweeps all possible θ and ϕ angles for the shoulder joint. In
addition to this voluntary range of motion envelope, Fig. 31 contains a
limited amount of data corresponding to the tolerable levels of range of
motion obtained from various forced sweep tests. By positioning the
subject's torso in various orientations and repeating the forced sweep
tests, one can obtain a more complete picture of the behavior of the
passive resistive force and moment vectors at the shoulder joint.
Figs. 32 and 33 display in essence a summary of numerous tests on the
first subject. In these figures only the maximum values of the magnitudes
of the passive resistive force and moment vectors are plotted.

We next present results obtained for the hip joint of the three
subjects. Fig. 34 shows a picture of a subject seated in the subject
restraint system and prepared for the left hip force and moment data
collection. For the left hip testing the left-hand side of the lower
limb support of the chair is removed so that the left leg has complete
freedom of motion. In Fig. 35 the components of the passive resistive
force vector at the hip joint of the first subject during forced sweep of
the leg for the hip abduction are presented. During this test, the
subject is in a normal seating configuration, i.e. the chair is not
rotated in any direction. Zero value of angle ϕ corresponds to straight

48

anterior extension of the leg with locked knee. Passive resistive moment vector components for the same test for the first subject are shown in Fig. 36. In Figs. 37-40 results for the same test are presented for the second and third subjects.

Components of the passive force and moment vectors at the hip joint are plotted for all three subjects during the forced sweep of the leg for the hip abduction in the frontal plane in Figs. 41-46. For the standing subject this motion corresponds to raising of the leg without allowing femural rotation. Tests were conducted on the subject when the chair angle was pitched backward such that the torso support shell, and thus, the subject's torso were parallel to the ground. This effectively converted the raising of the leg motion in the vertical plane to a motion that took place in a horizontal plane.

The tests on the elbow, the knee and the ankle joints were conducted on a table secured to the floor of the laboratory at the vicinity of the GFA location. Photographs of the experimental setup for these three joints are shown in Figs. 47, 54, and 61 for the elbow, the knee and the ankle joints, respectively. Results for all three subjects are displayed for the elbow joint in Figs. 48-53, for the knee joint in Figs. 55-60, and for the ankle joint in Figs. 62-67.

In addition to the figures displaying the resistive force and moment vector components, polynomial expansions are presented for all the joints of the first subject in Tables 3-5. These expansions approximate in the least squares sense the data and the curves shown in the figures. Note that these expansions constitute only the first attempt at characterizing resistive force and moment transmission characteristics of the joints. More elaborate representation of the data will be considered in the next research program.
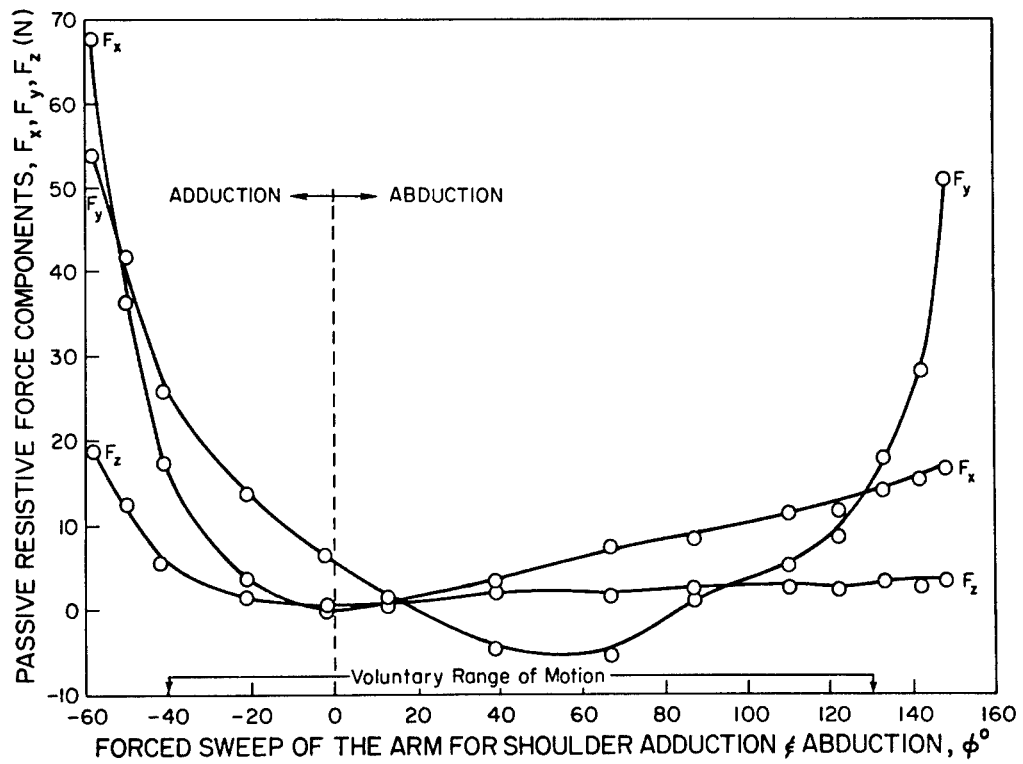
Fig. 13. Components of the passive resistive force vector at the shoulder
joint of the first subject during forced sweep of the arm for the
shoulder abduction & adduction.
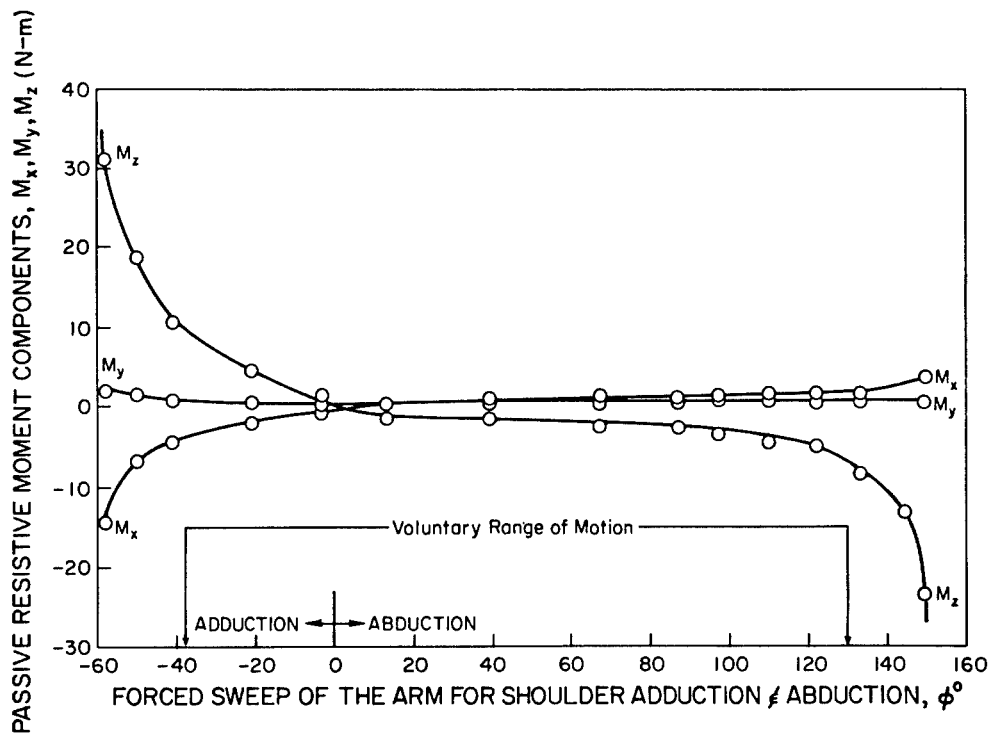
Fig. 14. Components of the passive resistive moment vector at the shoulder
joint of the first subject during forced sweep of the arm for the shoulder
abduction & adduction.

50
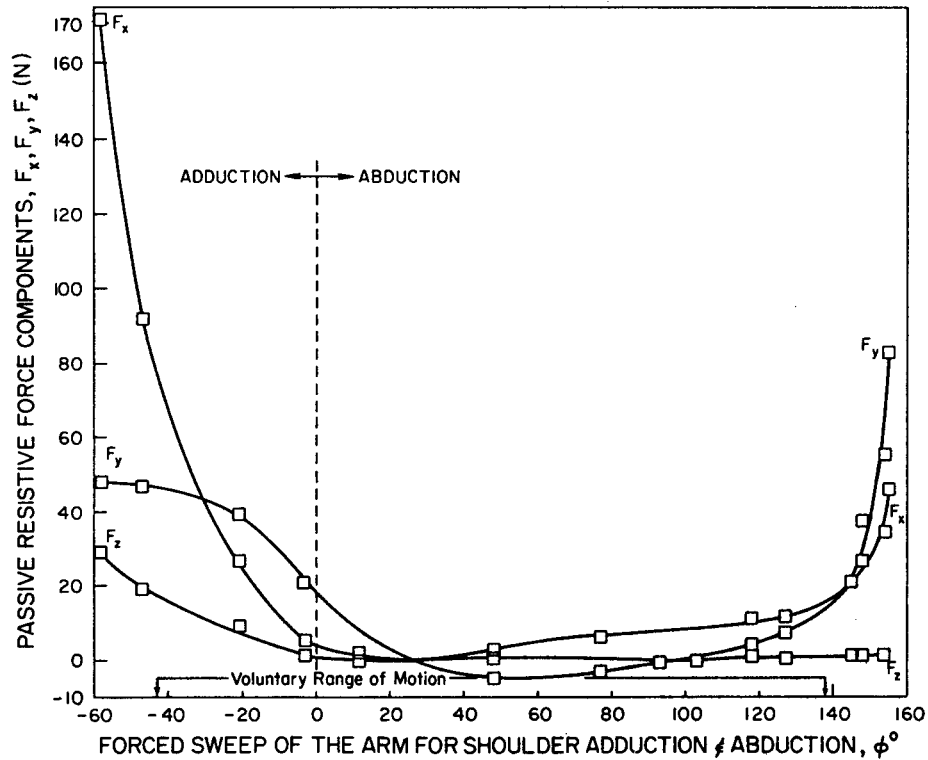
Fig. 15. Components of the passive resistive force vector at the shoulder joint of the second subject during forced sweep of the arm for the shoulder abduction & adduction.
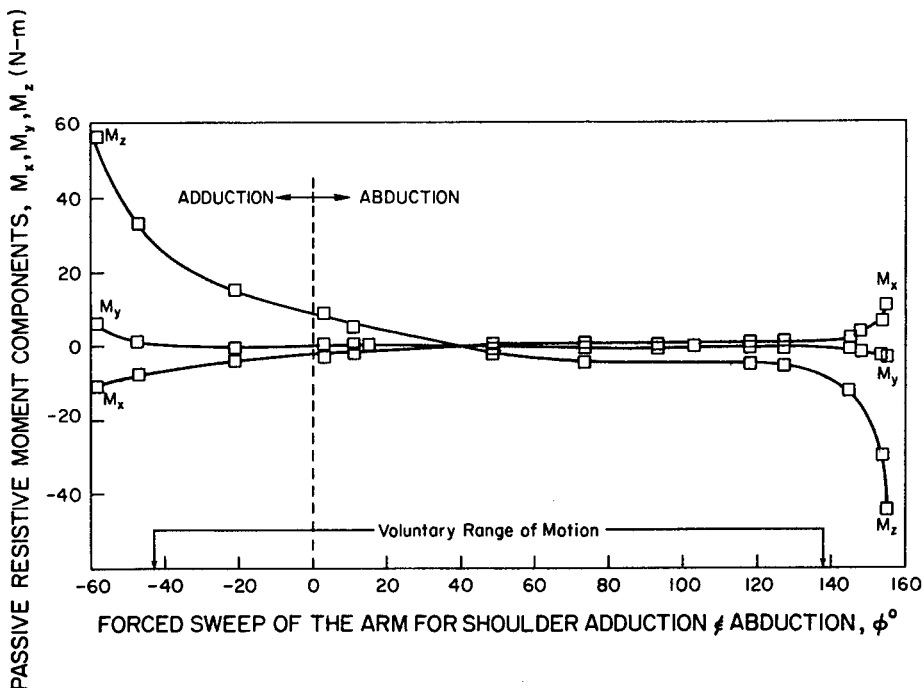
Fig. 16. Components of the passive resistive moment vector at the shoulder joint of the second subject during forced sweep of the arm for shoulder abduction & adduction.

51
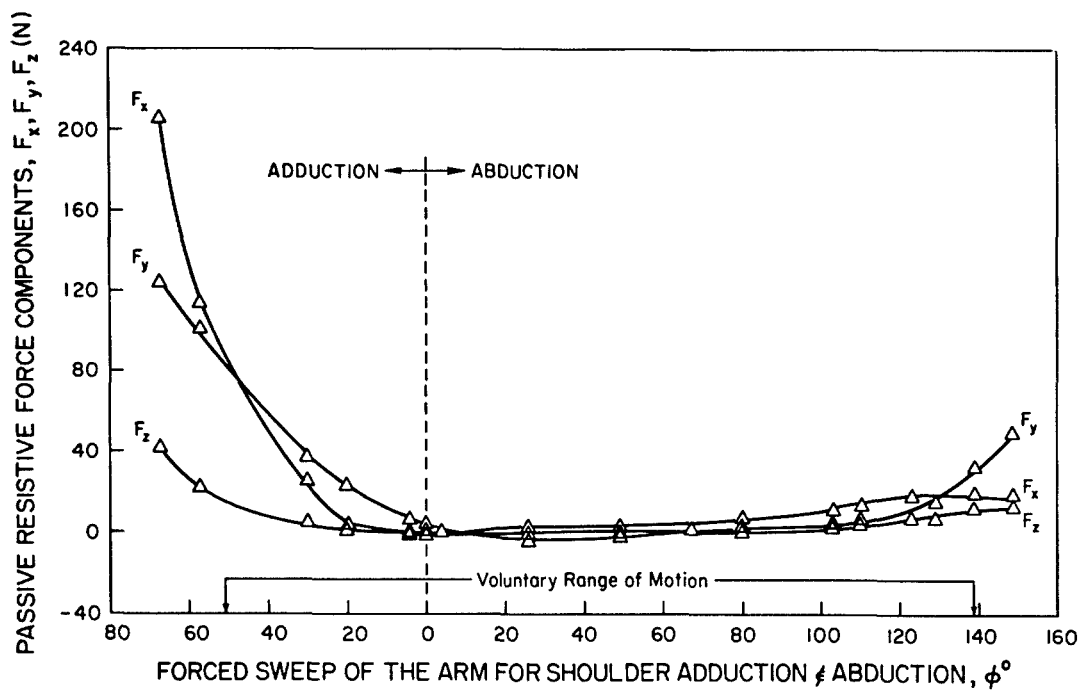
Fig. 17. Components of the passive resistive force vector at the shoulder joint of the third subject during forced sweep of the arm for shoulder abduction & adduction.
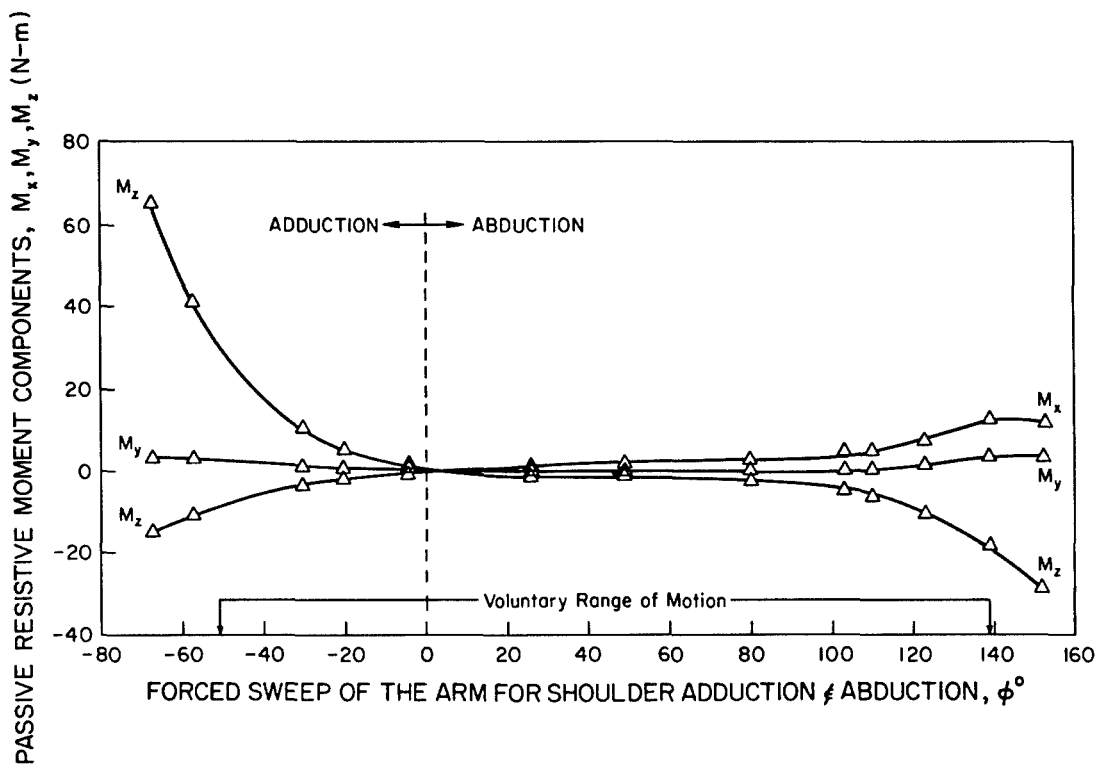
Fig. 18. Components of the passive resistive moment vector at the shoulder joint of the third subject during forced sweep of the arm for shoulder abduction & adduction.
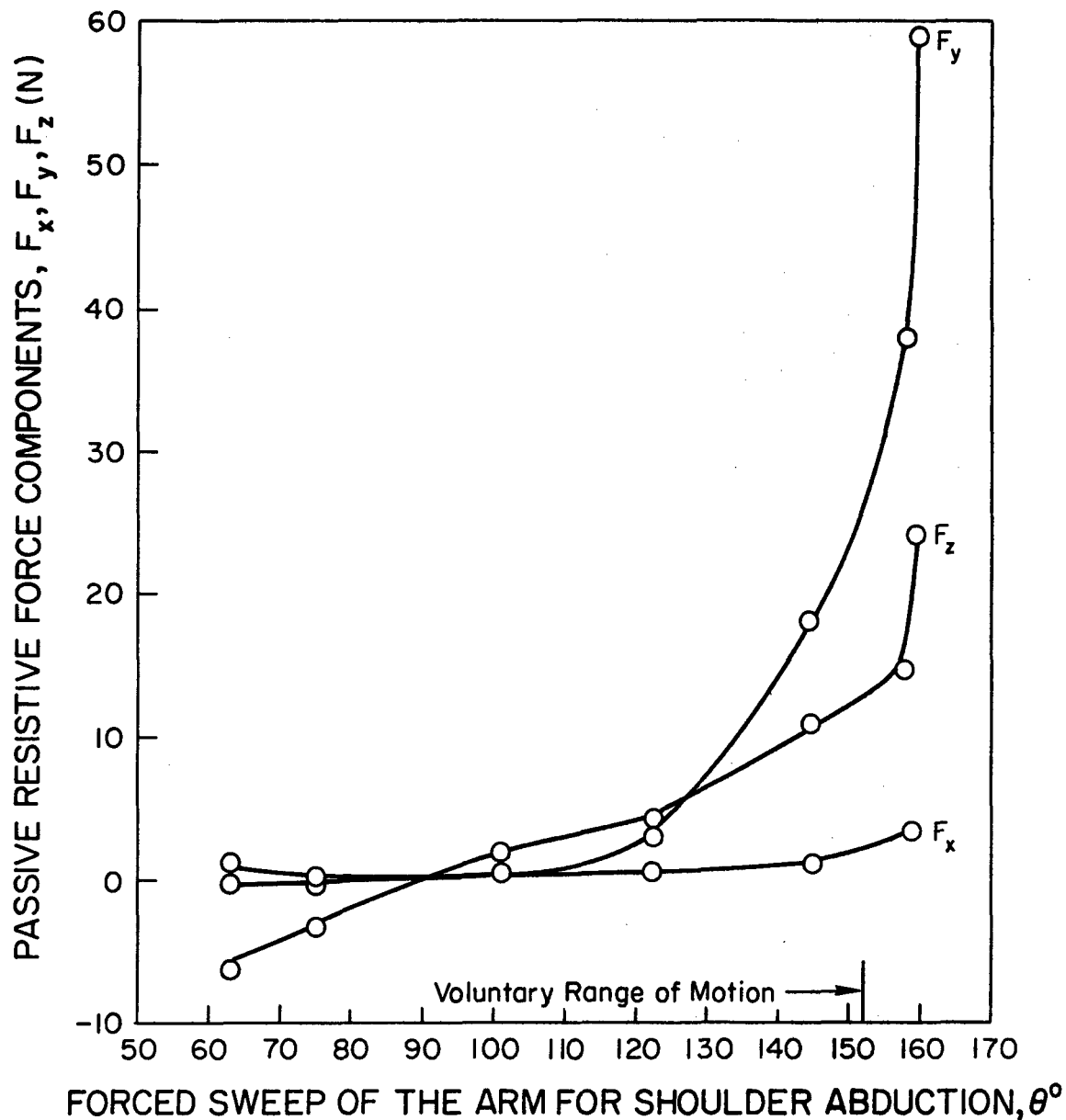
Fig. 19. Components of the passive resistive force vector at the shoulder joint of the first subject during forced sweep of the arm for the shoulder abduction in the frontal plane.

Fig. 20. Components of the passive resistive moment vector at the shoulder joint of the first subject during forced sweep of the arm for the shoulder abduction in the frontal plane.

54
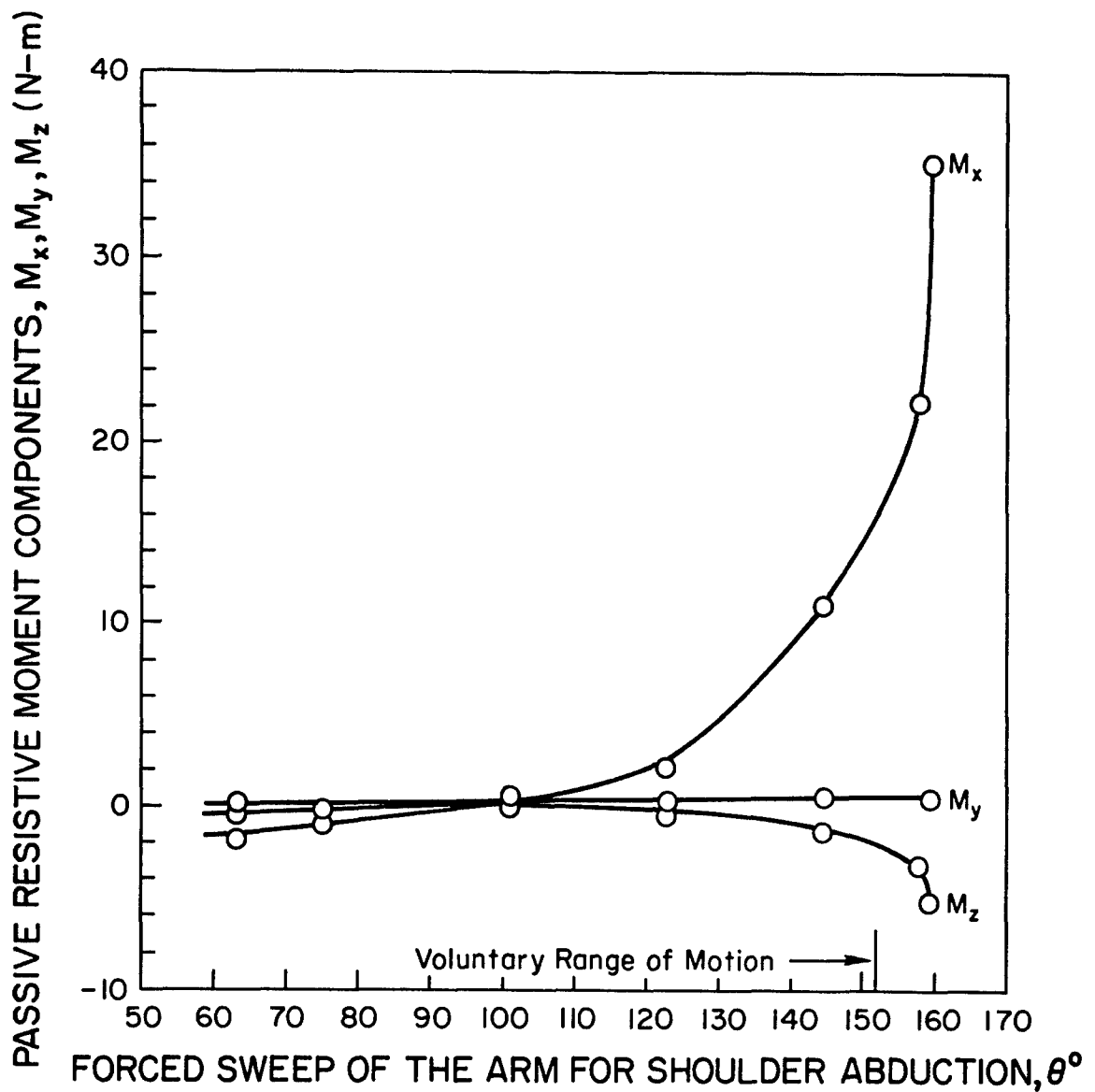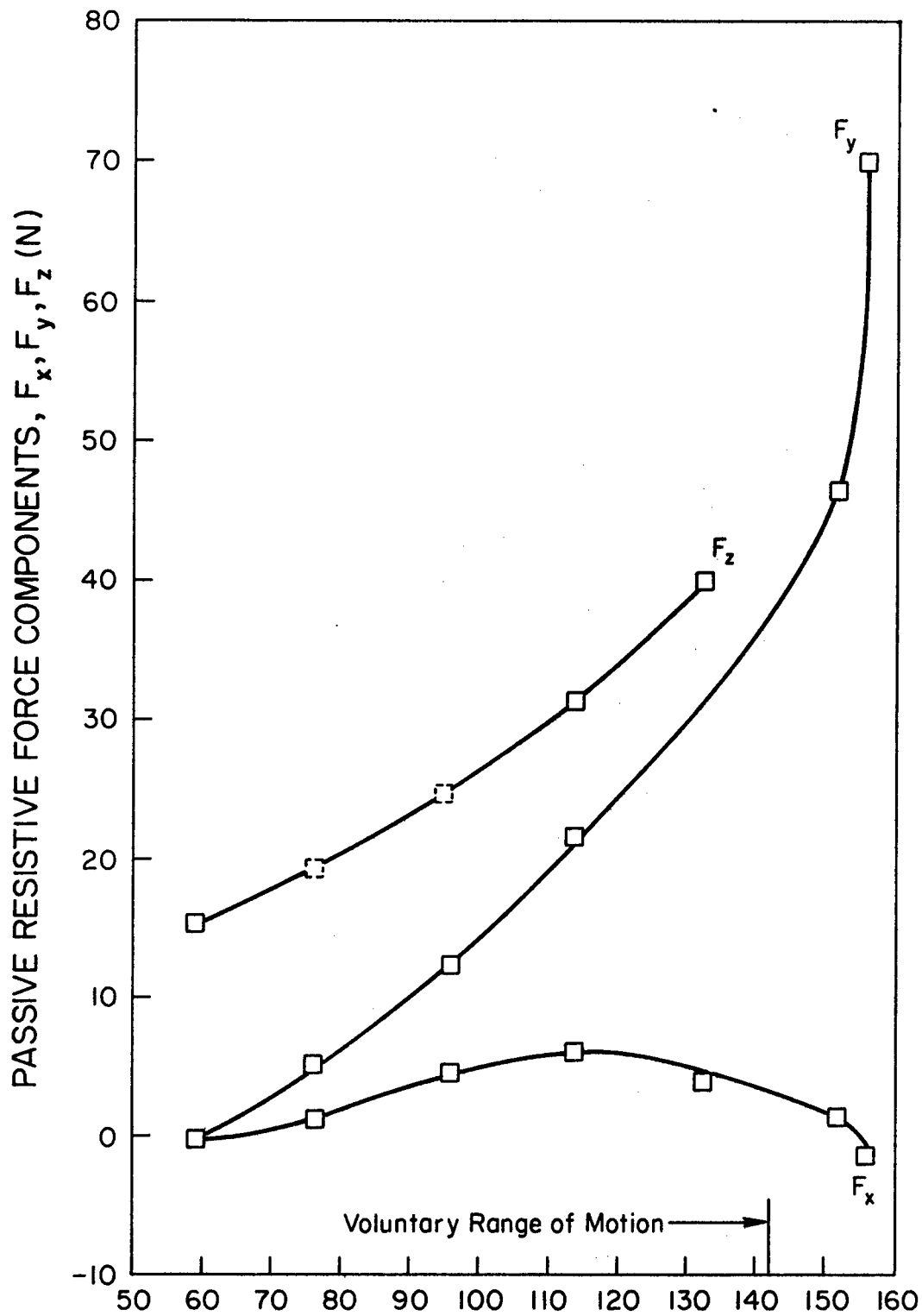
Fig. 21. Components of the passive resistive force vector at the shoulder joint of the second subject during forced sweep of the arm for the shoulder abduction in the frontal plane.

Fig. 22. Components of the passive resistive moment vector at the shoulder joint of the second subject during forced sweep of the arm for the shoulder abduction in the frontal plane.
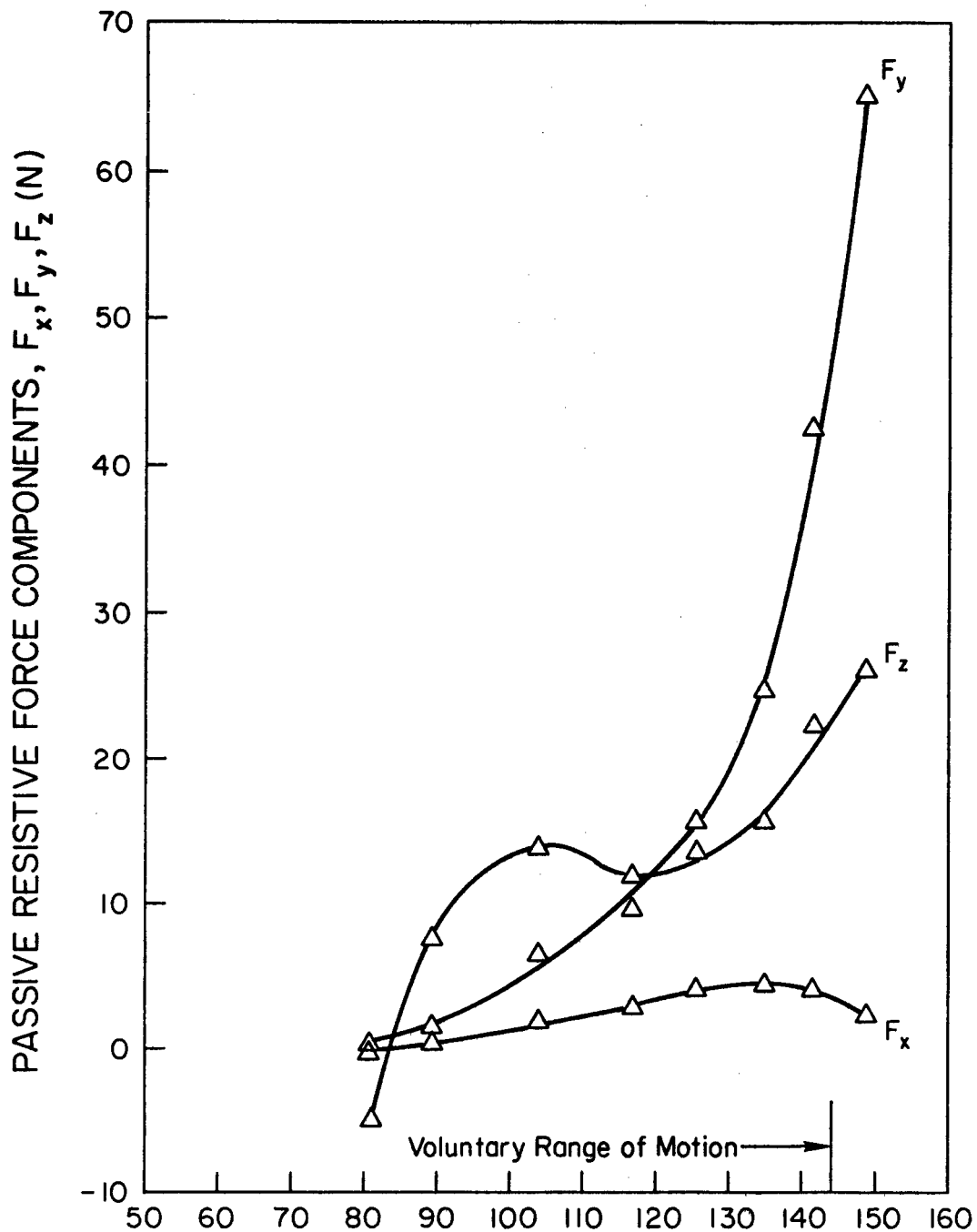
Fig. 23. Components of the passive resistive force vector at the shoulder joint of the third subject during forced sweep of the arm for the shoulder abduction in the frontal plane.

57
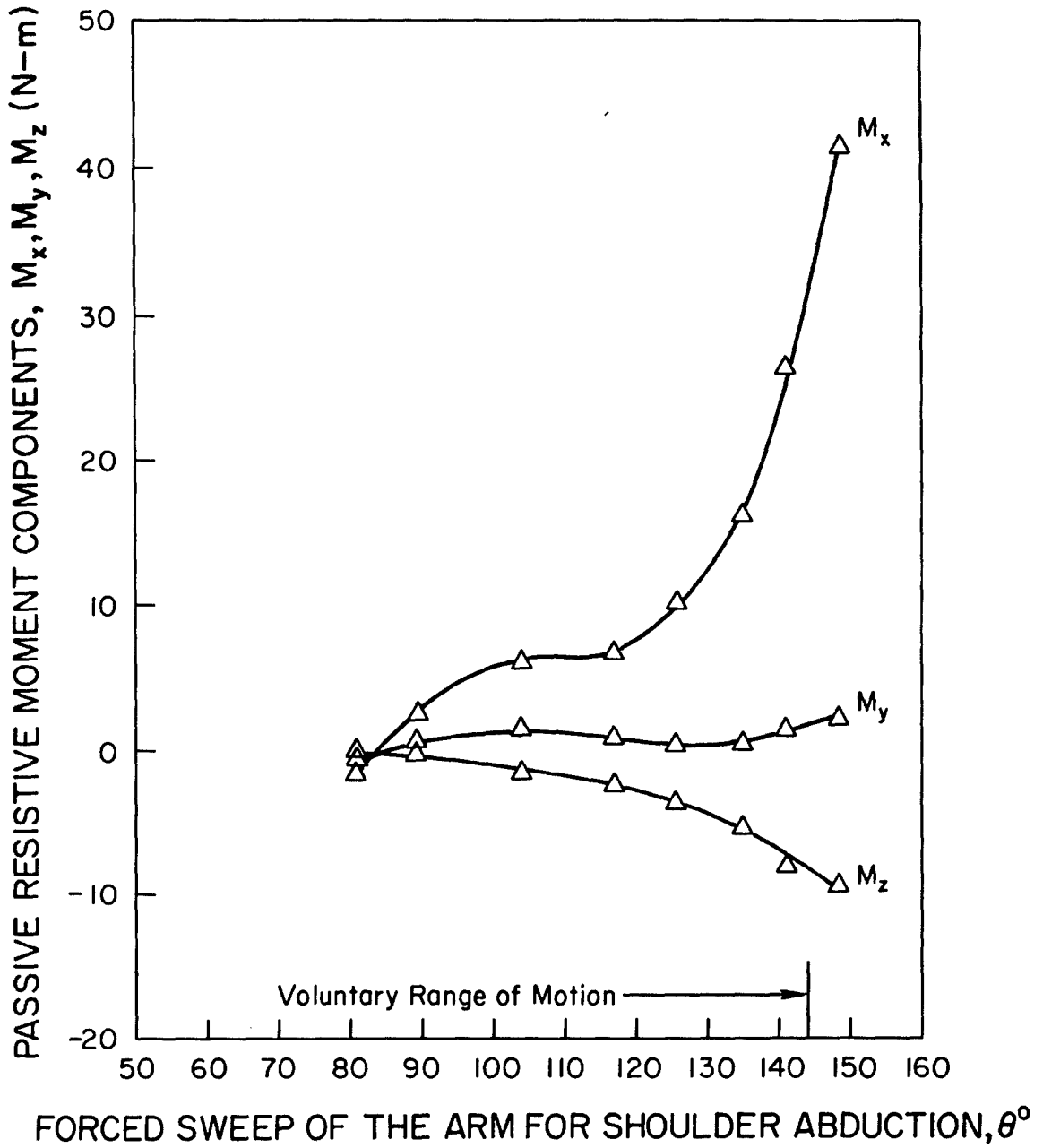
Fig. 24. Components of the passive resistive moment vector at the shoulder joint of the third subject during forced sweep of the arm for the shoulder abduction in the frontal plane.
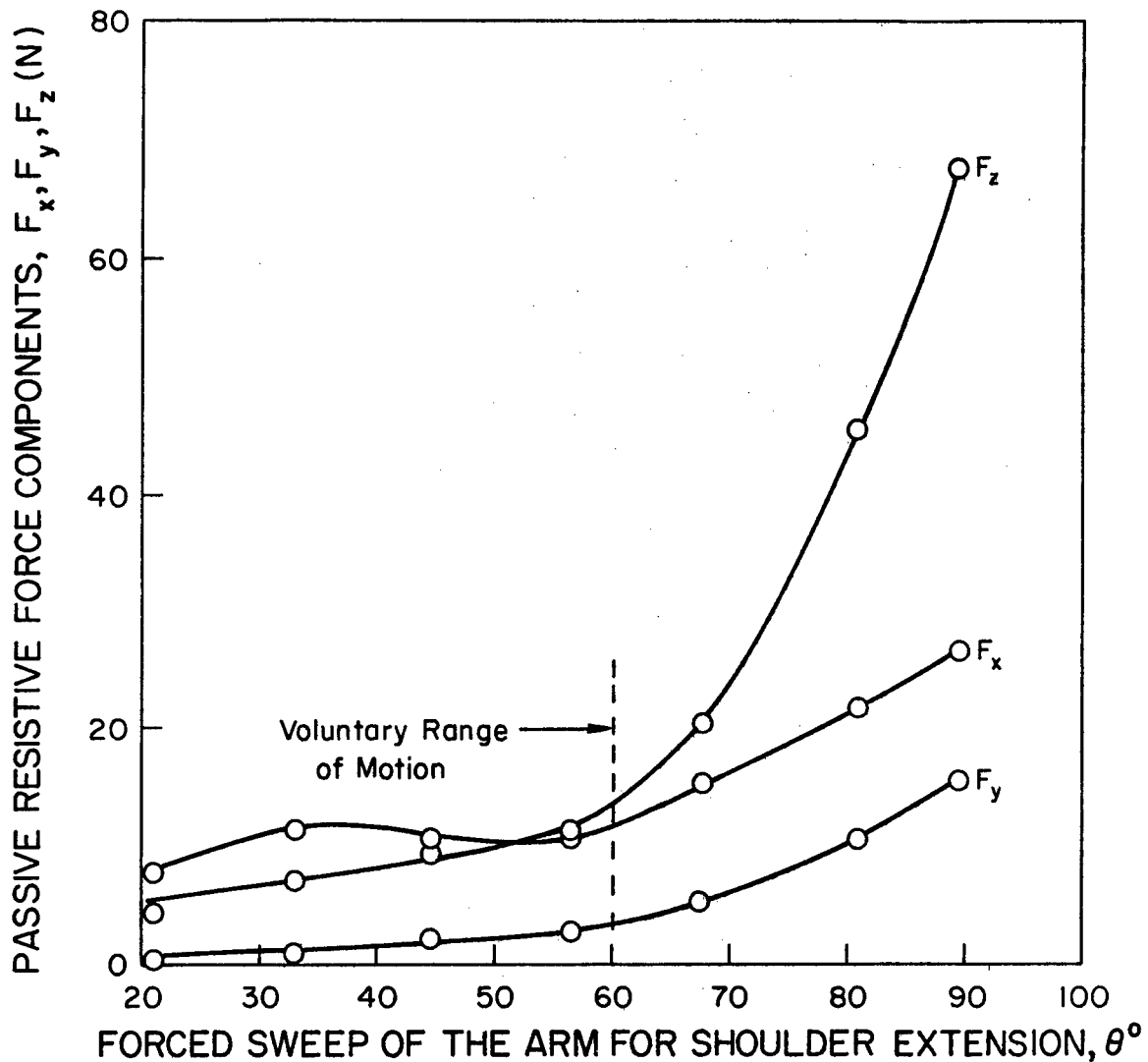
Fig. 25. Components of the passive resistive force vector at the shoulder joint of the first subject during forced sweep of the arm for the shoulder extension.
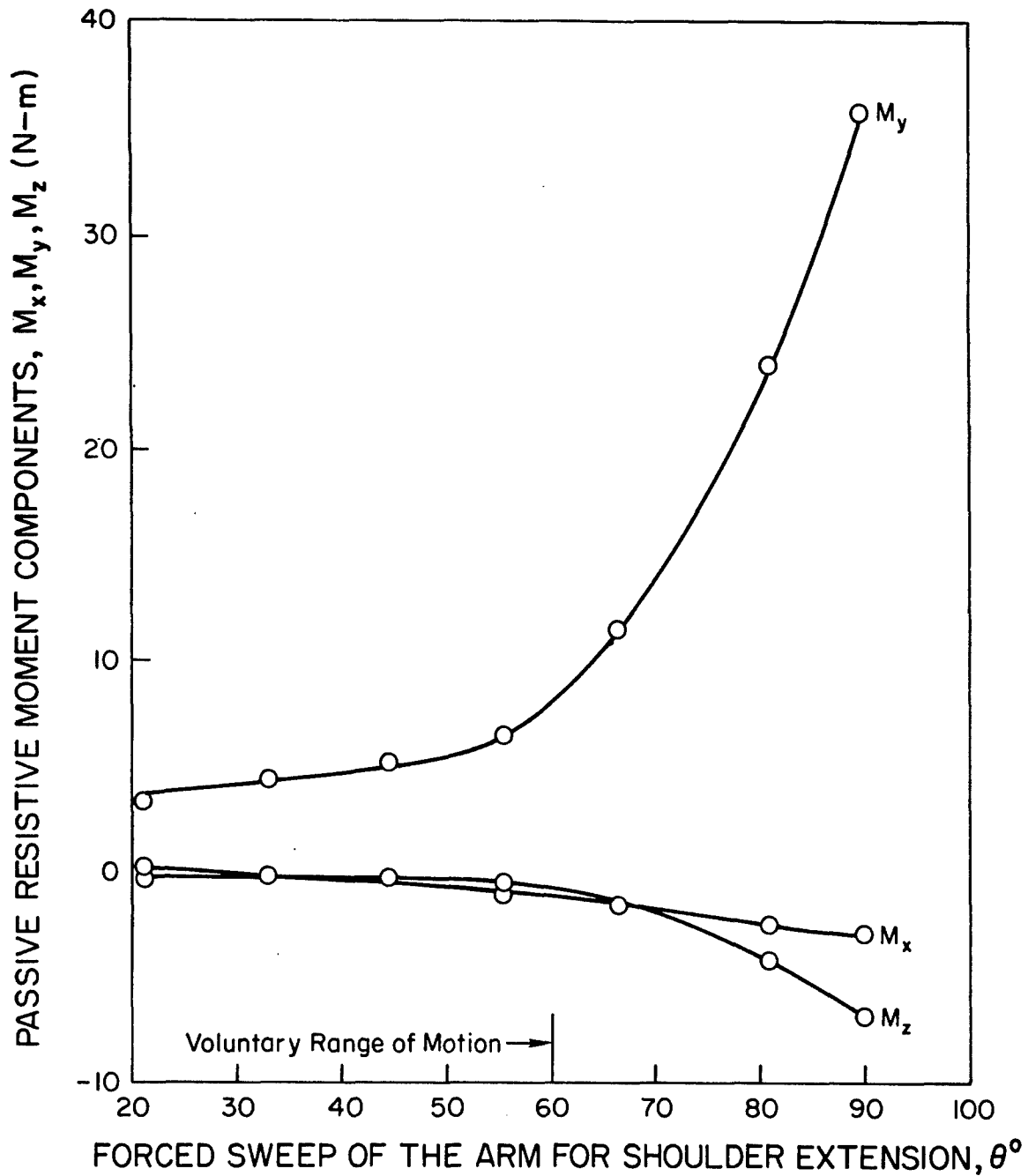
Fig. 26. Components of the passive resistive moment vector at the
shoulder joint of the first subject during forced sweep of the
arm for the shoulder extension.
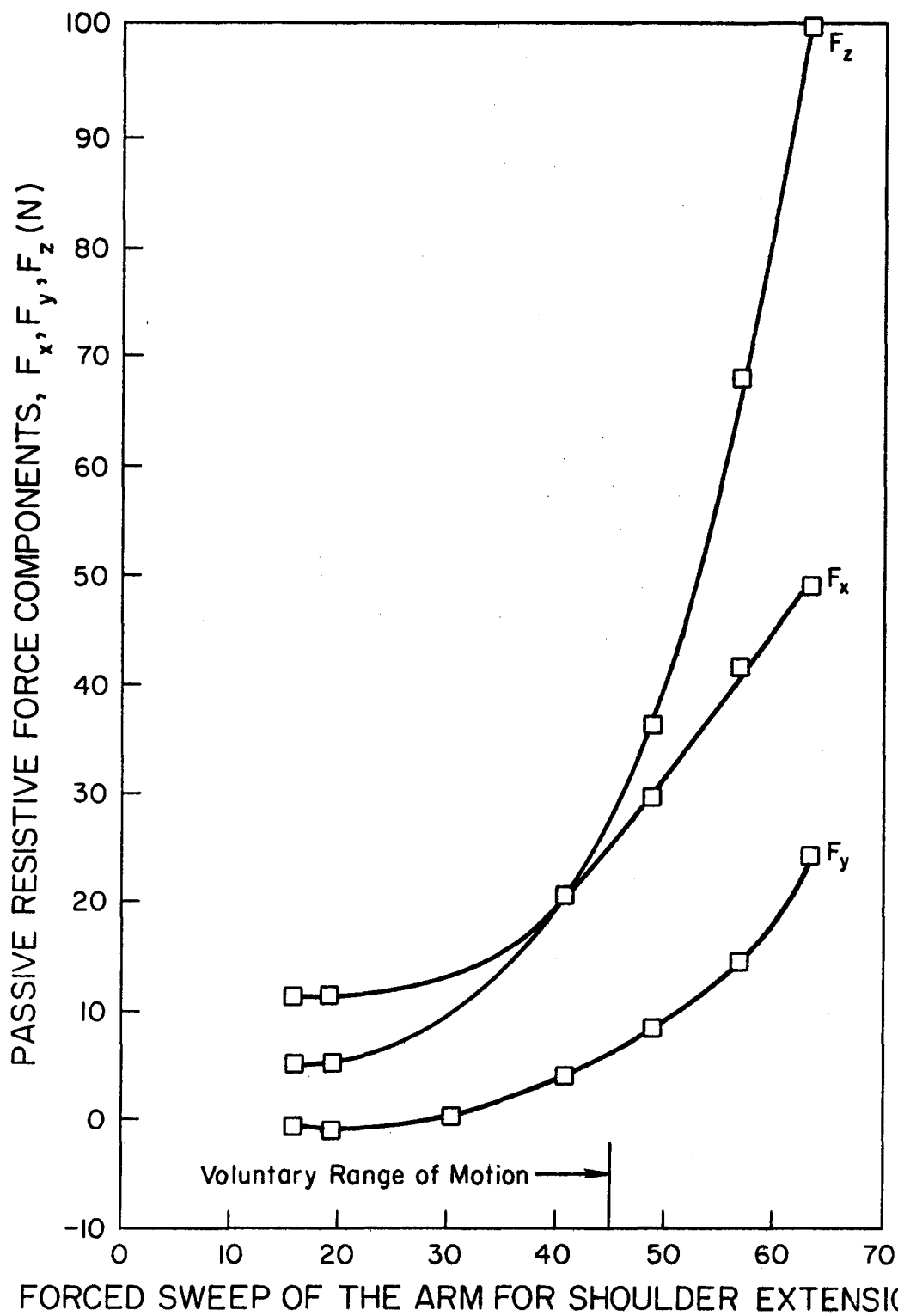
Fig. 27. Components of the passive resistive force vector at the shoulder joint of the second subject during forced sweep of the arm for the shoulder extension.
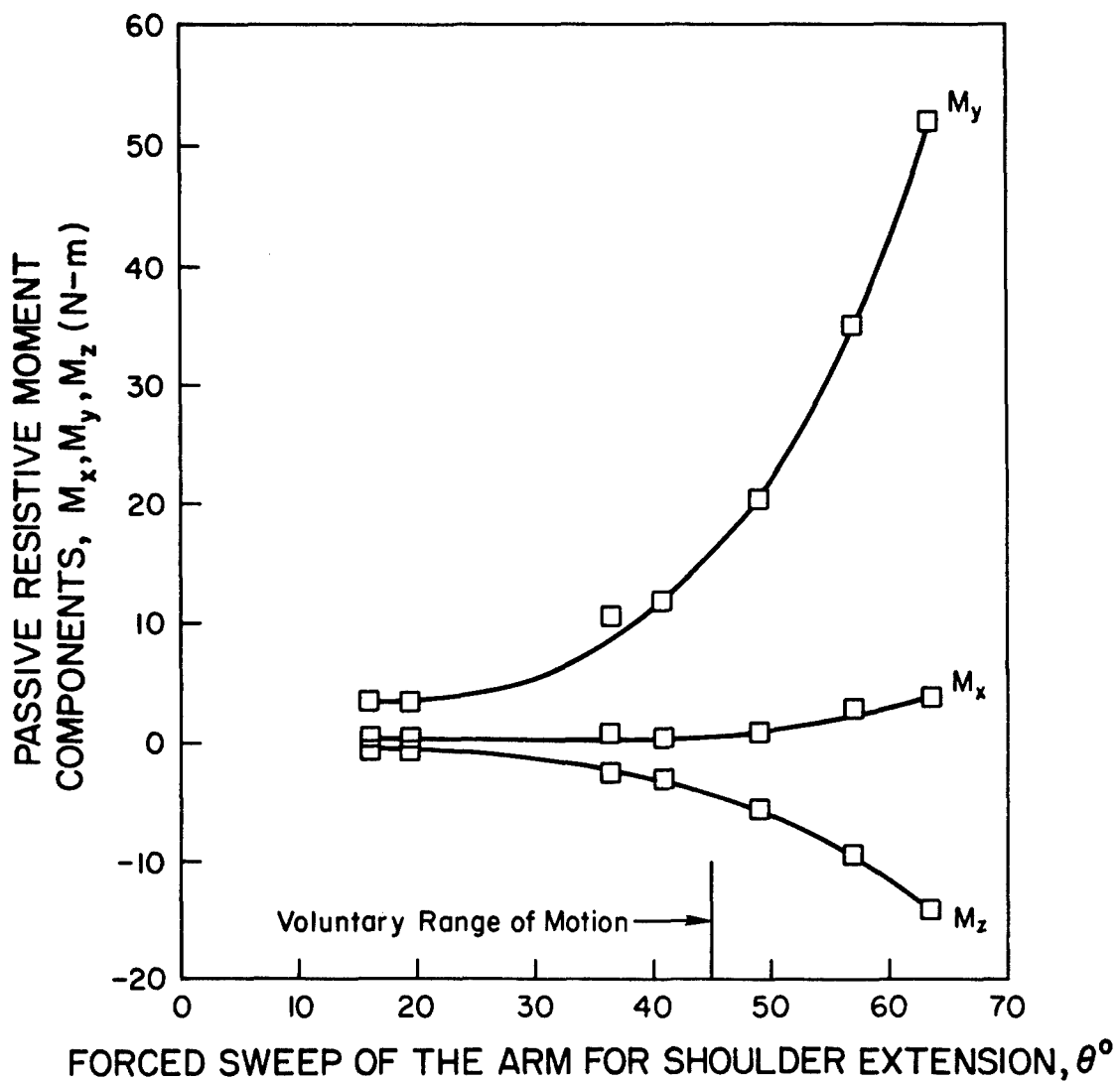
Fig. 28. Components of the passive resistive moment vector at the shoulder joint of the second subject during forced sweep of the arm for the shoulder extension.
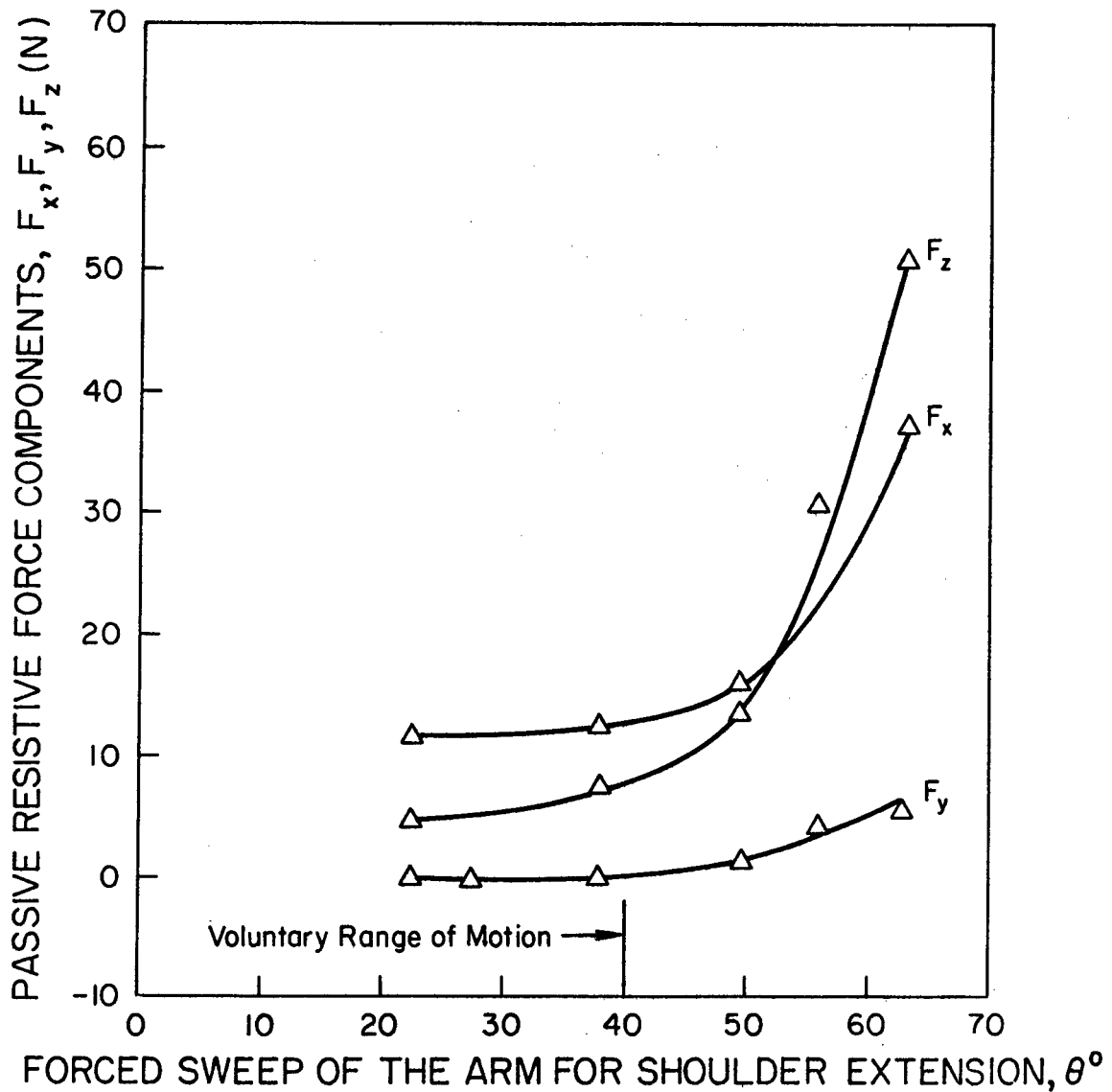
Fig. 29. Components of the passive resistive force vector at the shoulder joint of the third subject during forced sweep of the arm for the shoulder extension.
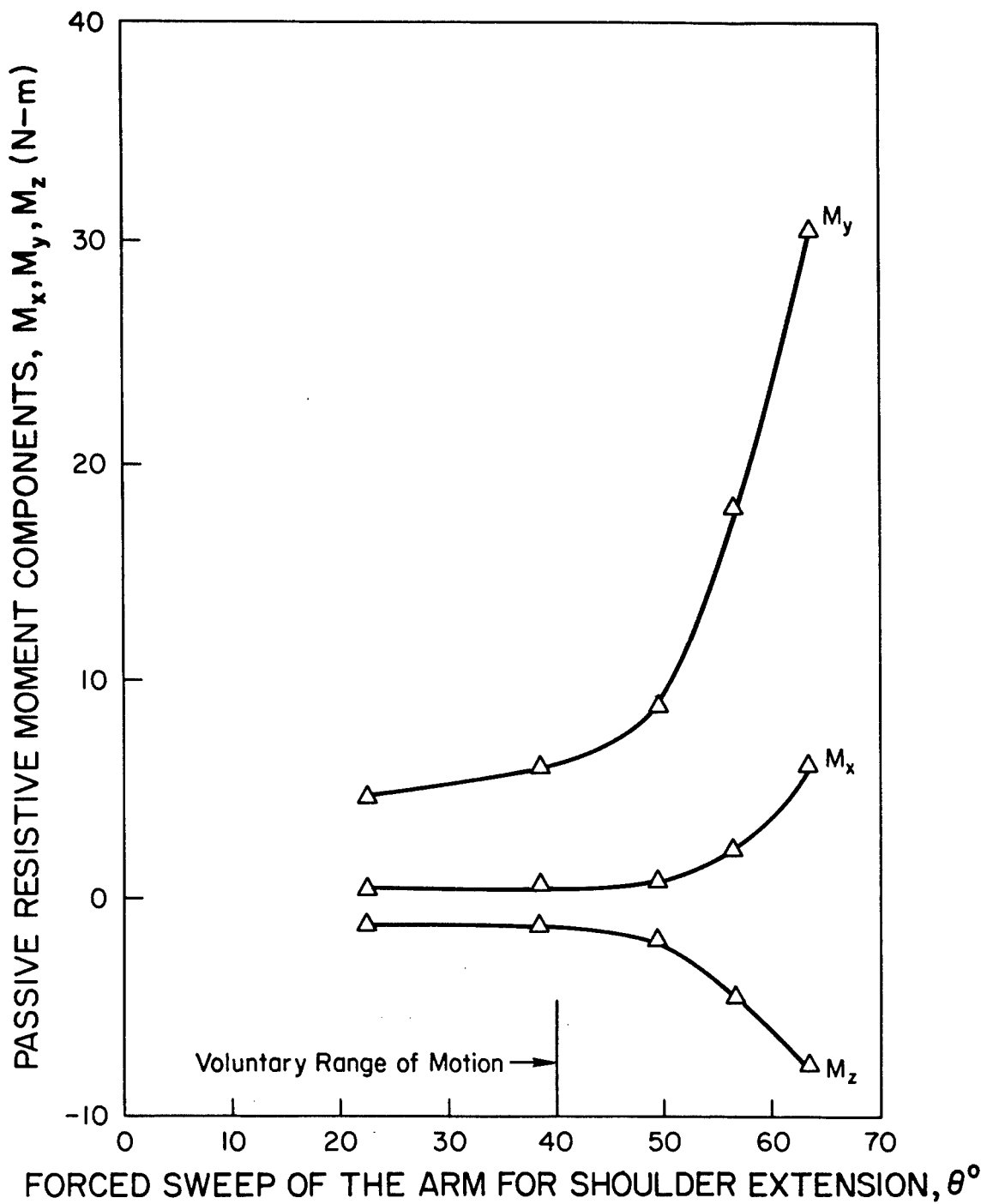
Fig. 30. Components of the passive resistive moment vector at the
shoulder joint of the third subject during forced sweep of the
arm for the shoulder extension.
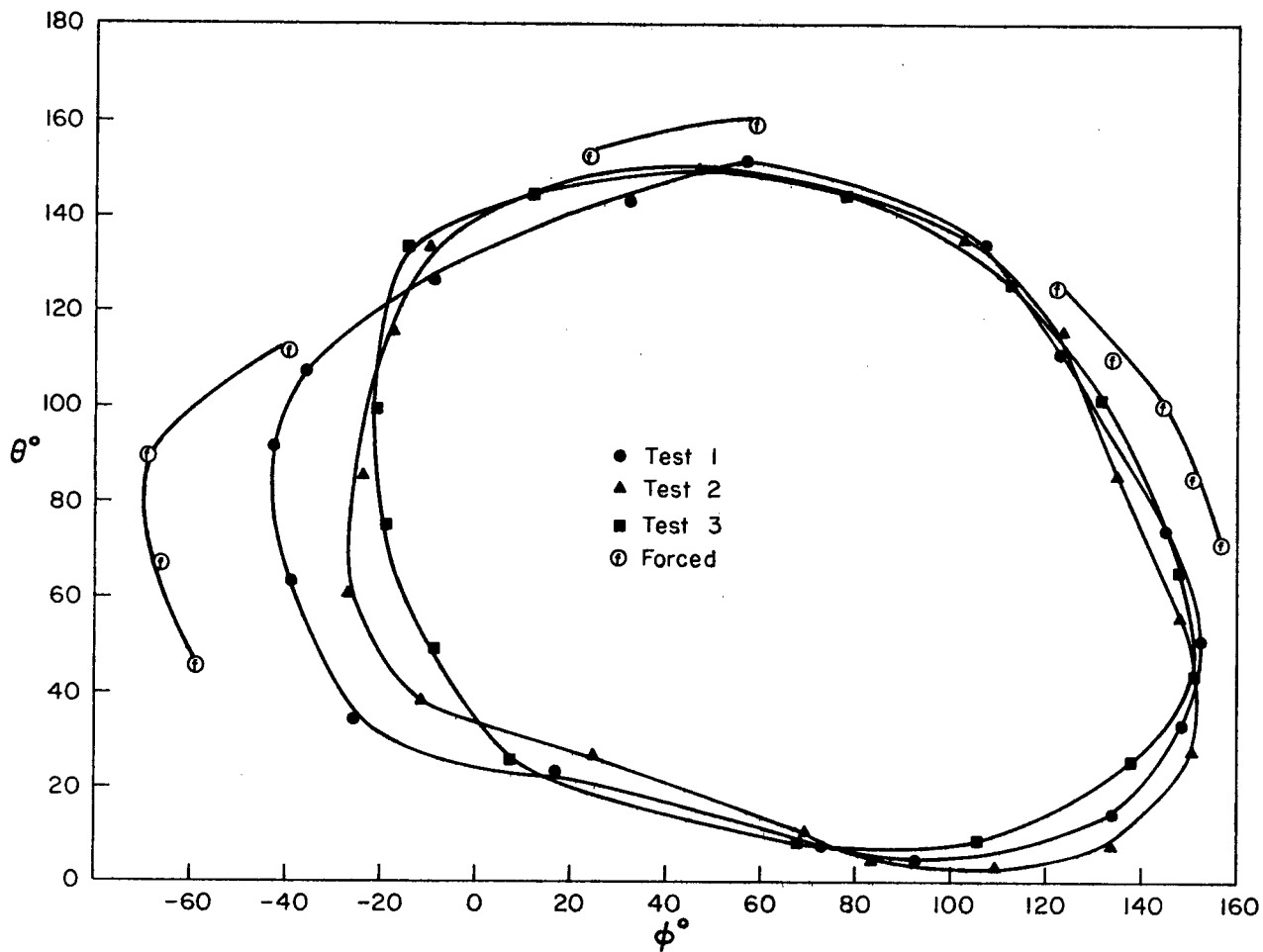
Fig. 31. Voluntary range of motion for a shoulder joint of the
first test subject.
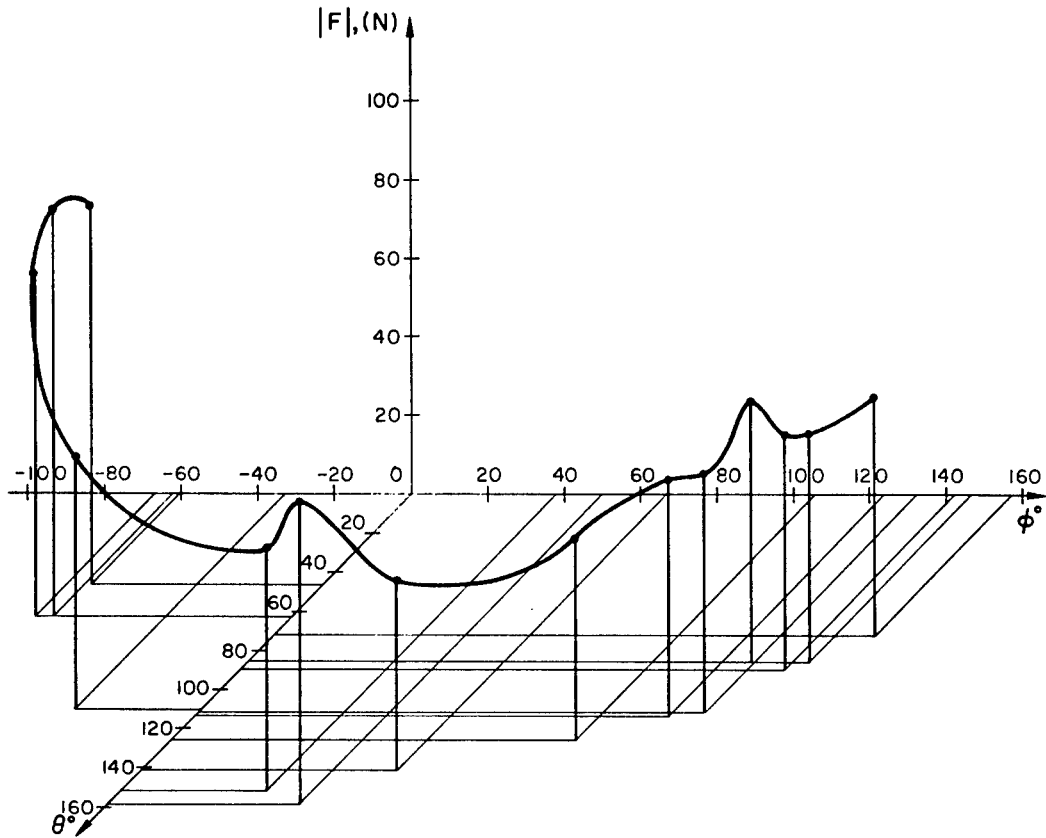
Fig. 32. Maximum values of the magnitude of the passive resistive force vectors at the shoulder joint for various forced sweeps of the arm.
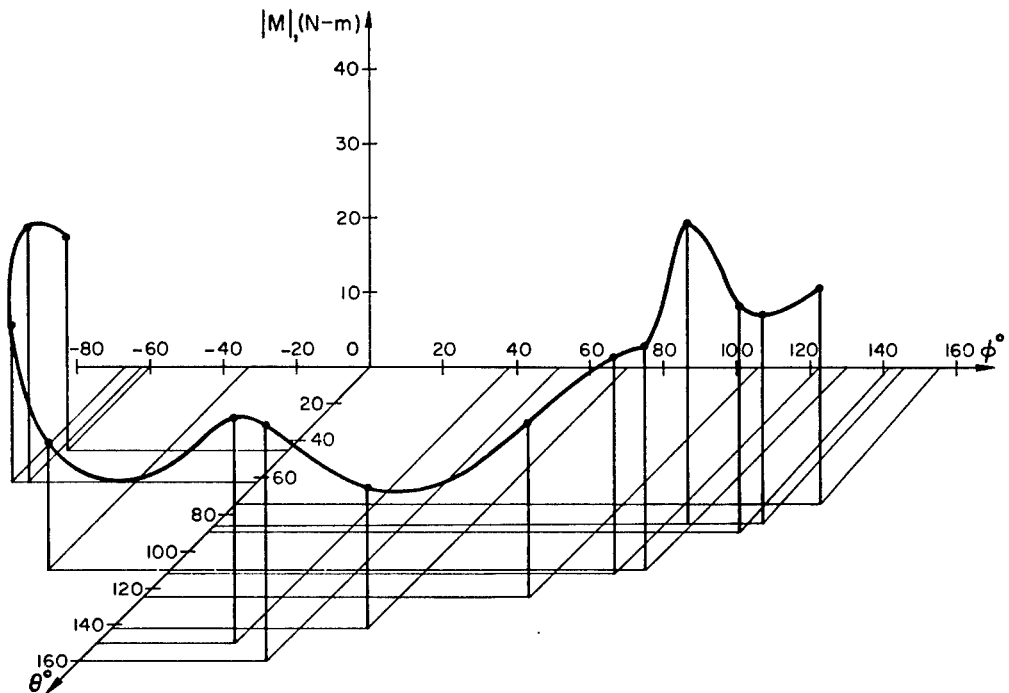
Fig. 33. Maximum values of the magnitude of the passive resistive moment vectors at the shoulder joint for various forced sweeps of the arm.

66
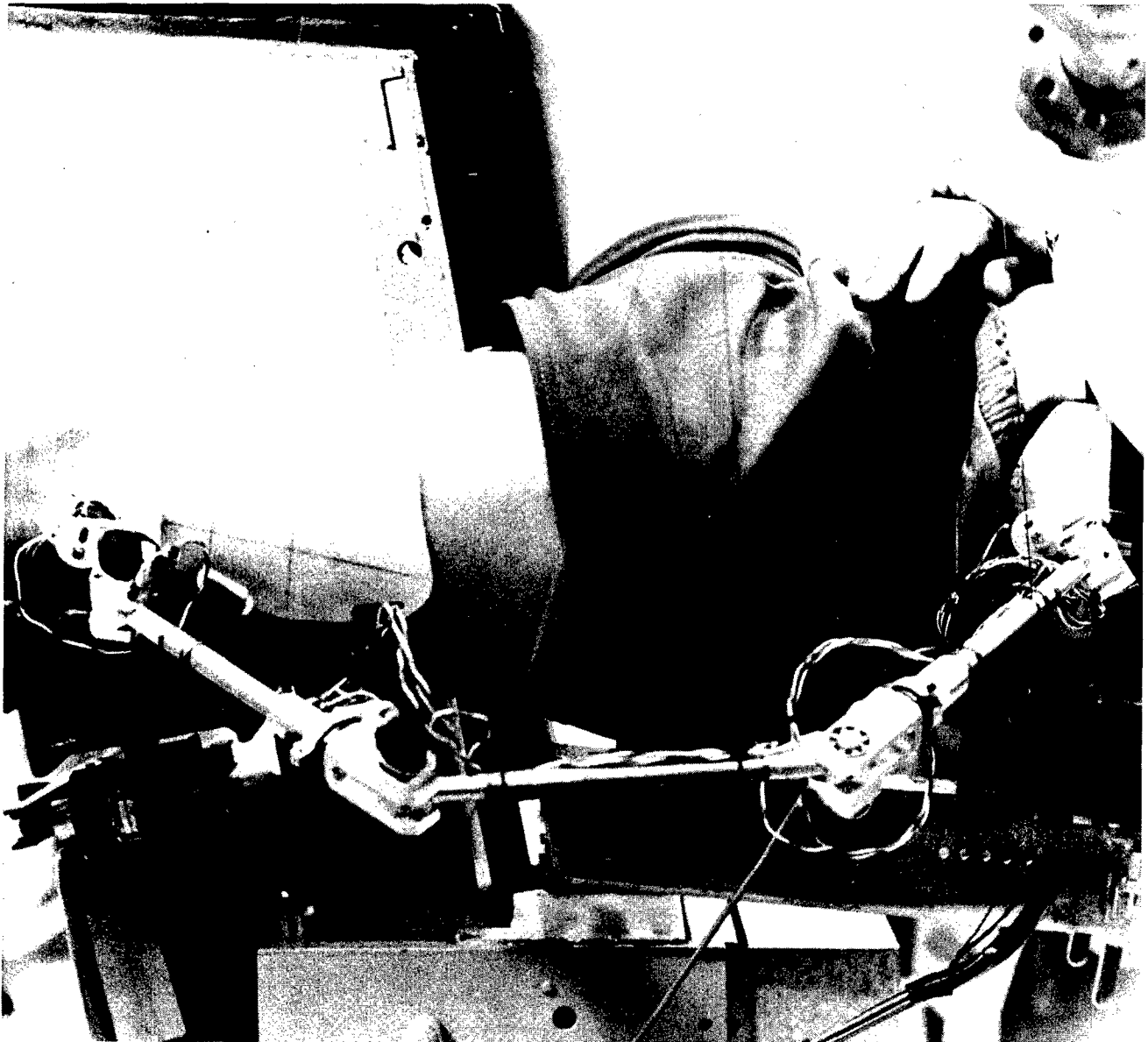
Fig. 34. Subject is prepared for the hip force and moment data collection.
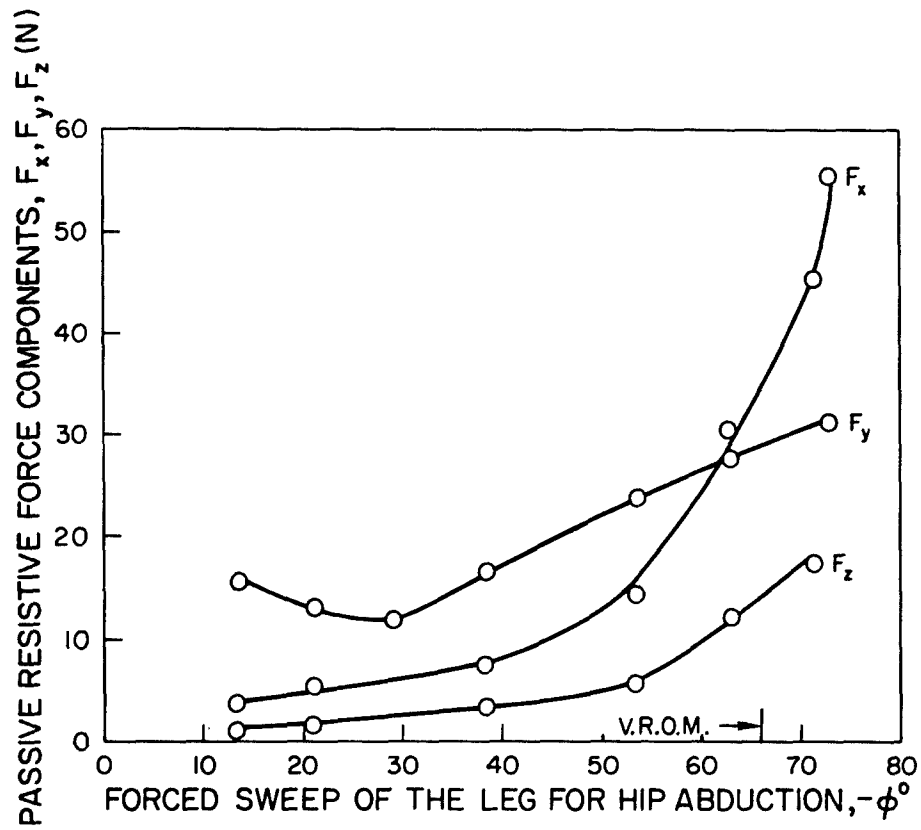
Fig. 35. Components of the passive resistive force vector at the hip joint of the first subject during forced sweep of the leg for the hip abduction.
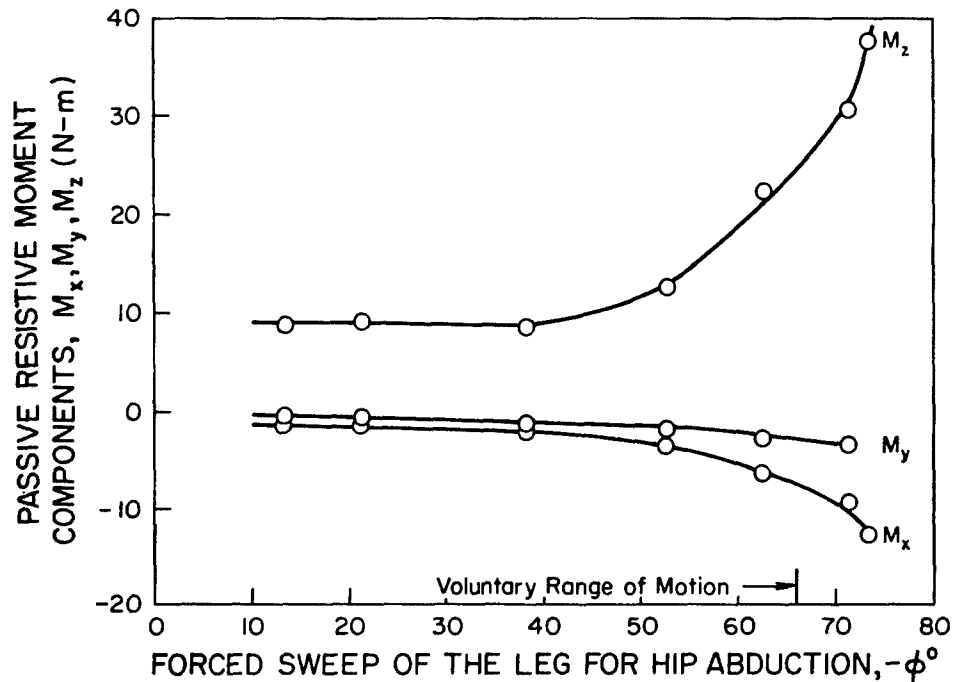
Fig. 36. Components of the passive resistive moment vector at the hip joint of the first subject during forced sweep of the leg for the hip abduction.

68
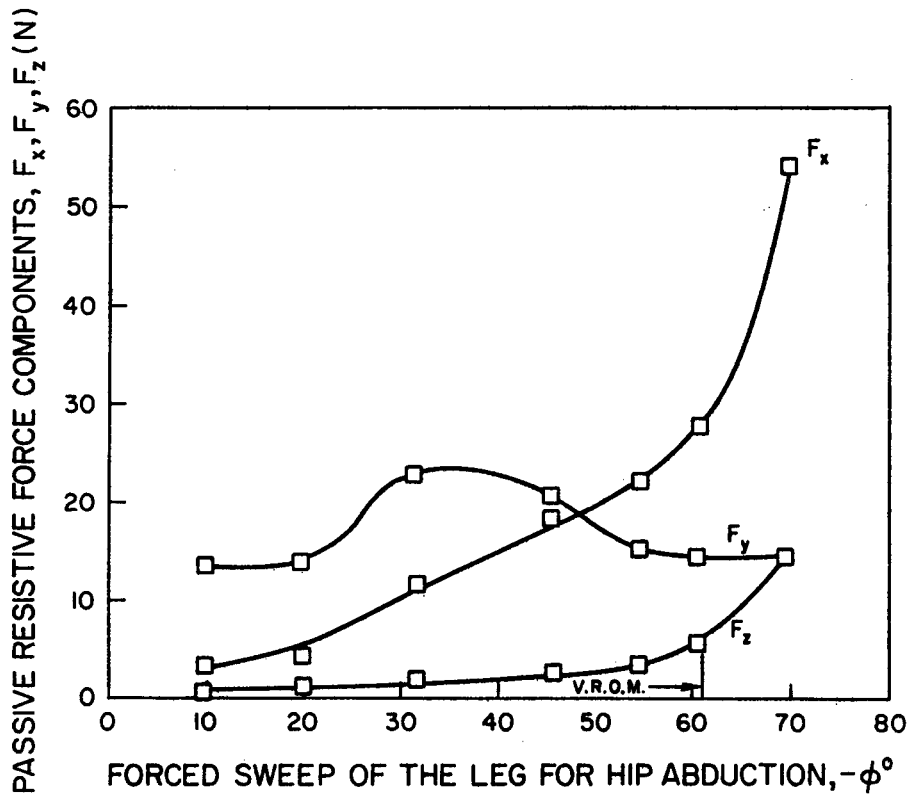
Fig. 37. Components of the passive resistive force vector at the hip joint of the second subject during forced sweep of the leg for the hip abduction.
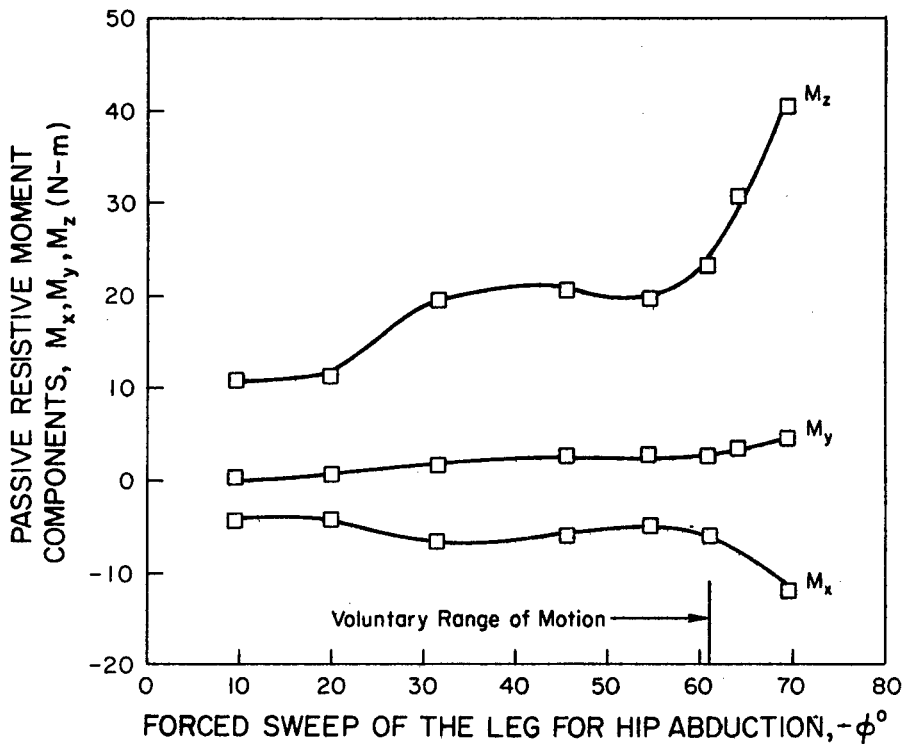

Fig. 38. Components of the passive resistive moment vector at the hip joint of the second subject during forced sweep of the leg for the hip abduction.
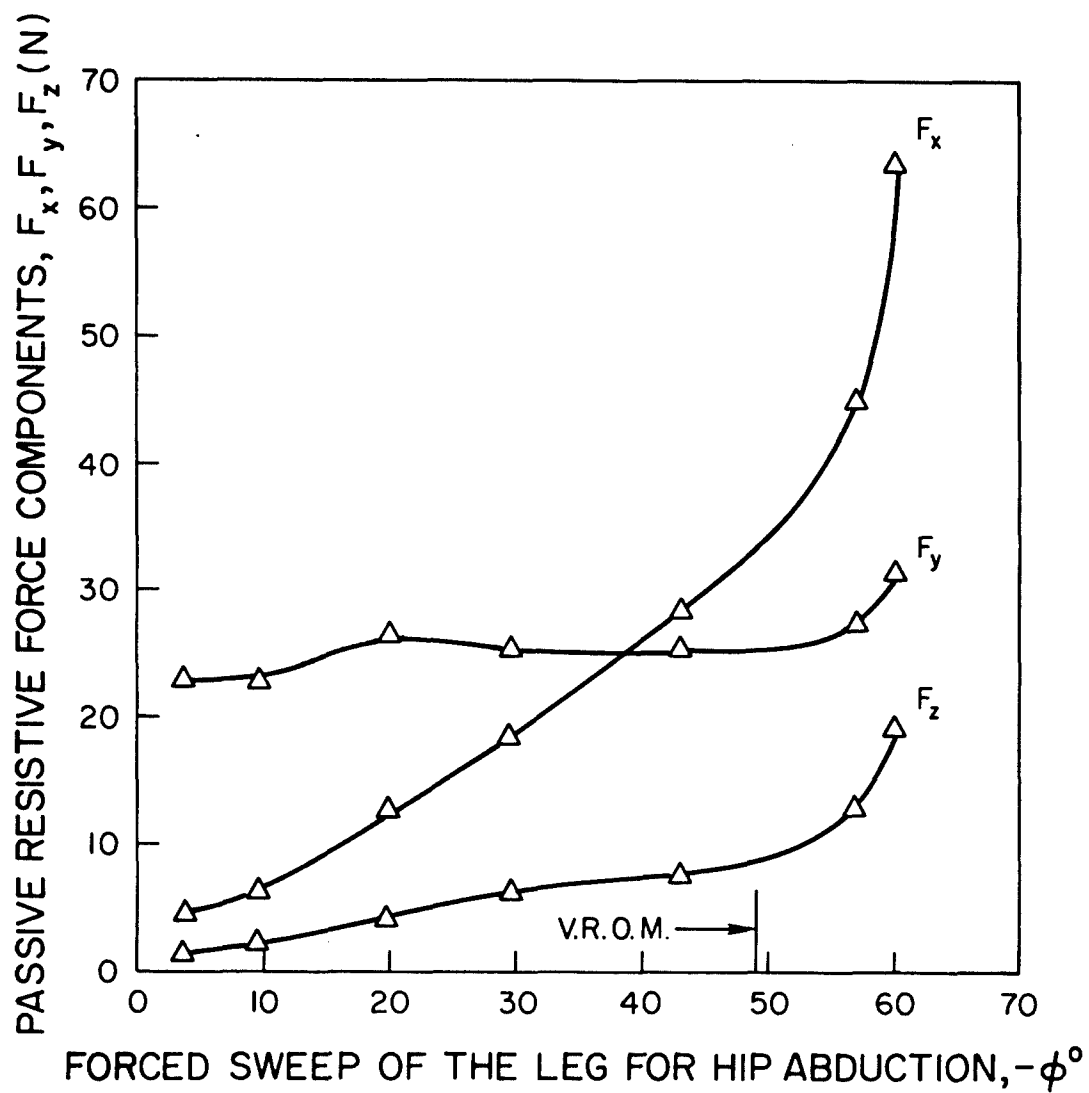
Fig. 39. Components of the passive resistive force vector at the hip joint of the third subject during forced sweep of the leg for the hip abduction.
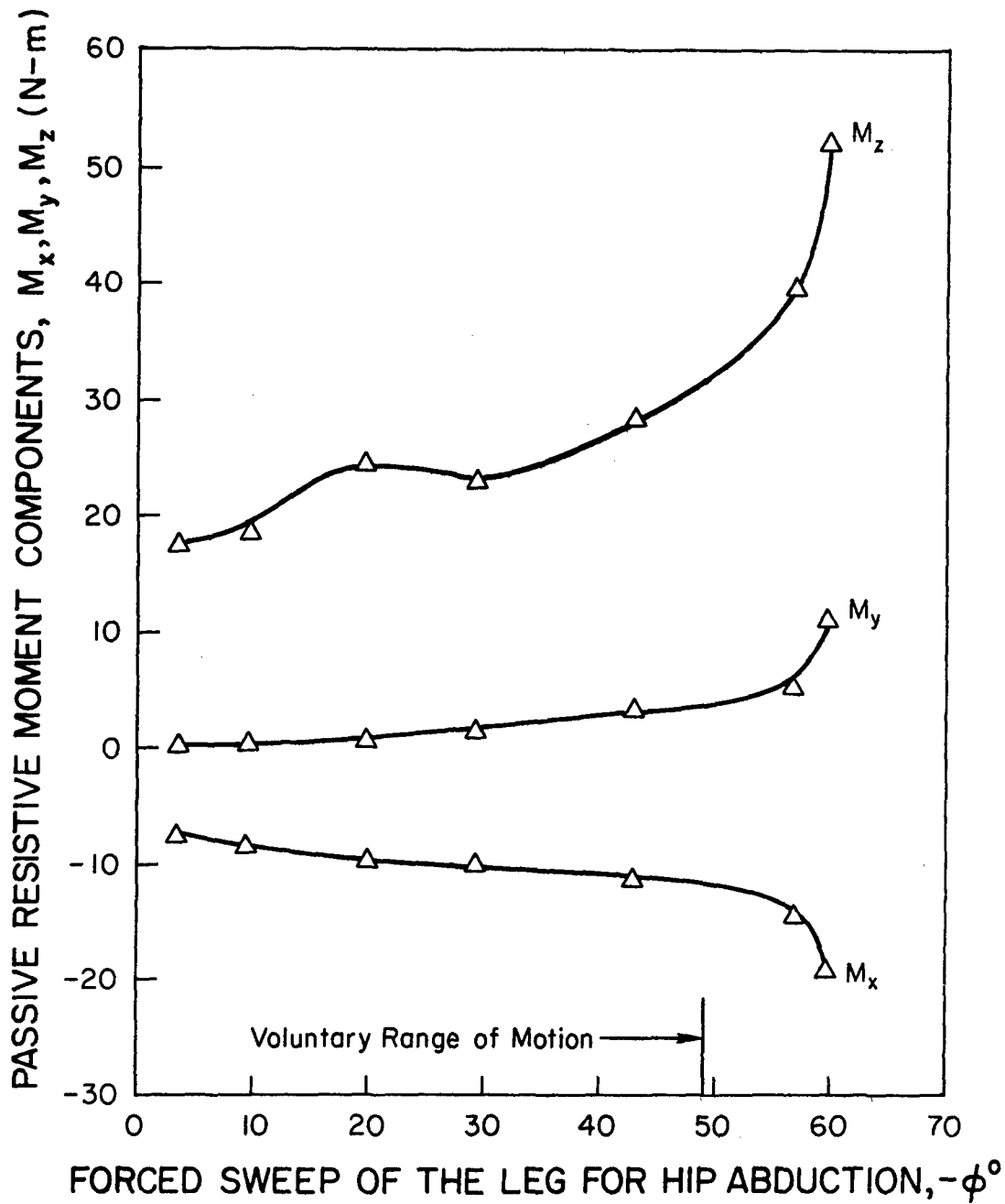
Fig. 40. Components of the passive resistive moment vector at the hip joint of the third subject during forced sweep of the leg for the hip abduction.

71
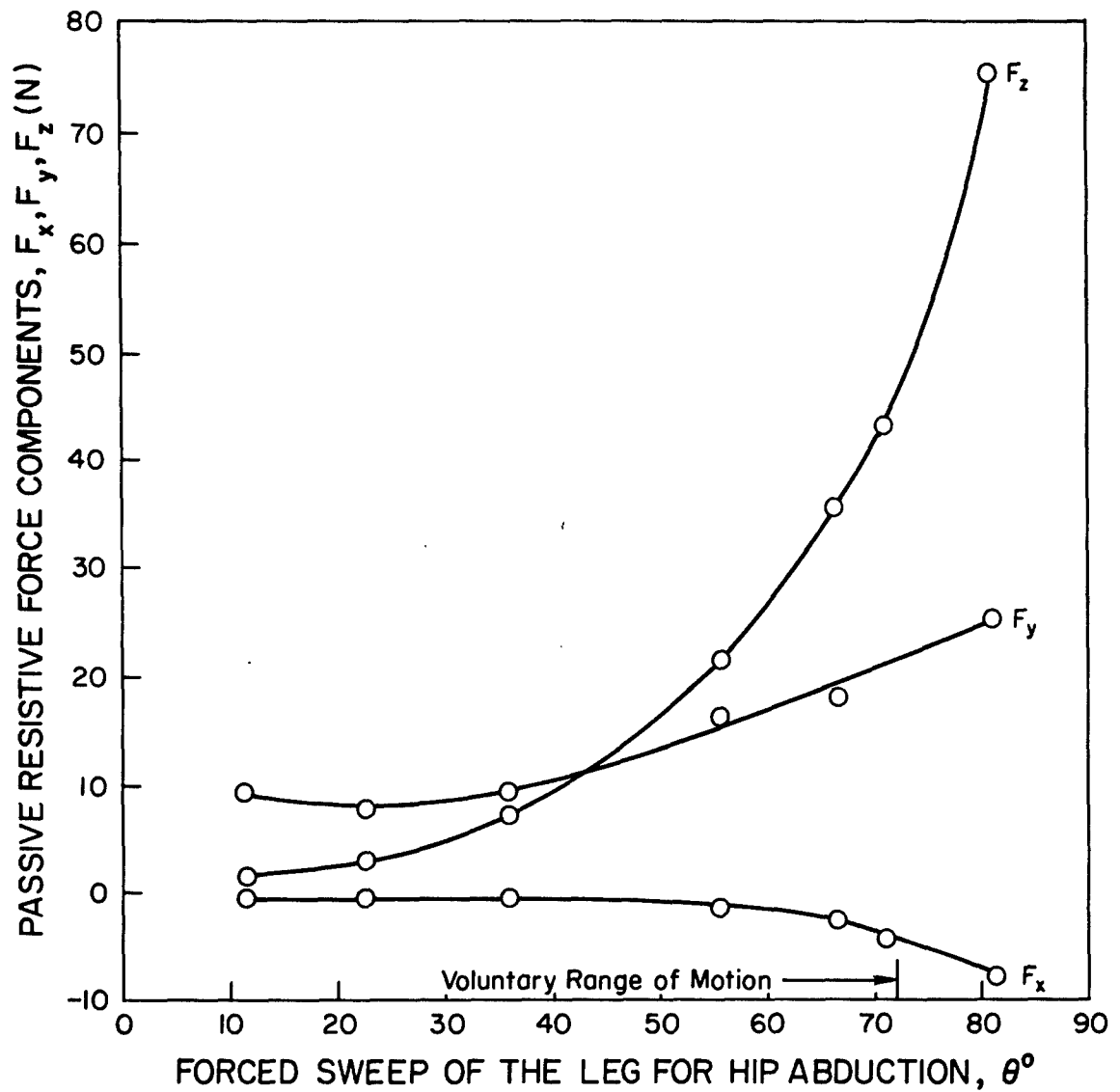
Fig. 41. Components of the passive resistive force vector
at the hip joint of the first subject during forced sweep
of the leg for the hip abduction in the frontal plane.

72
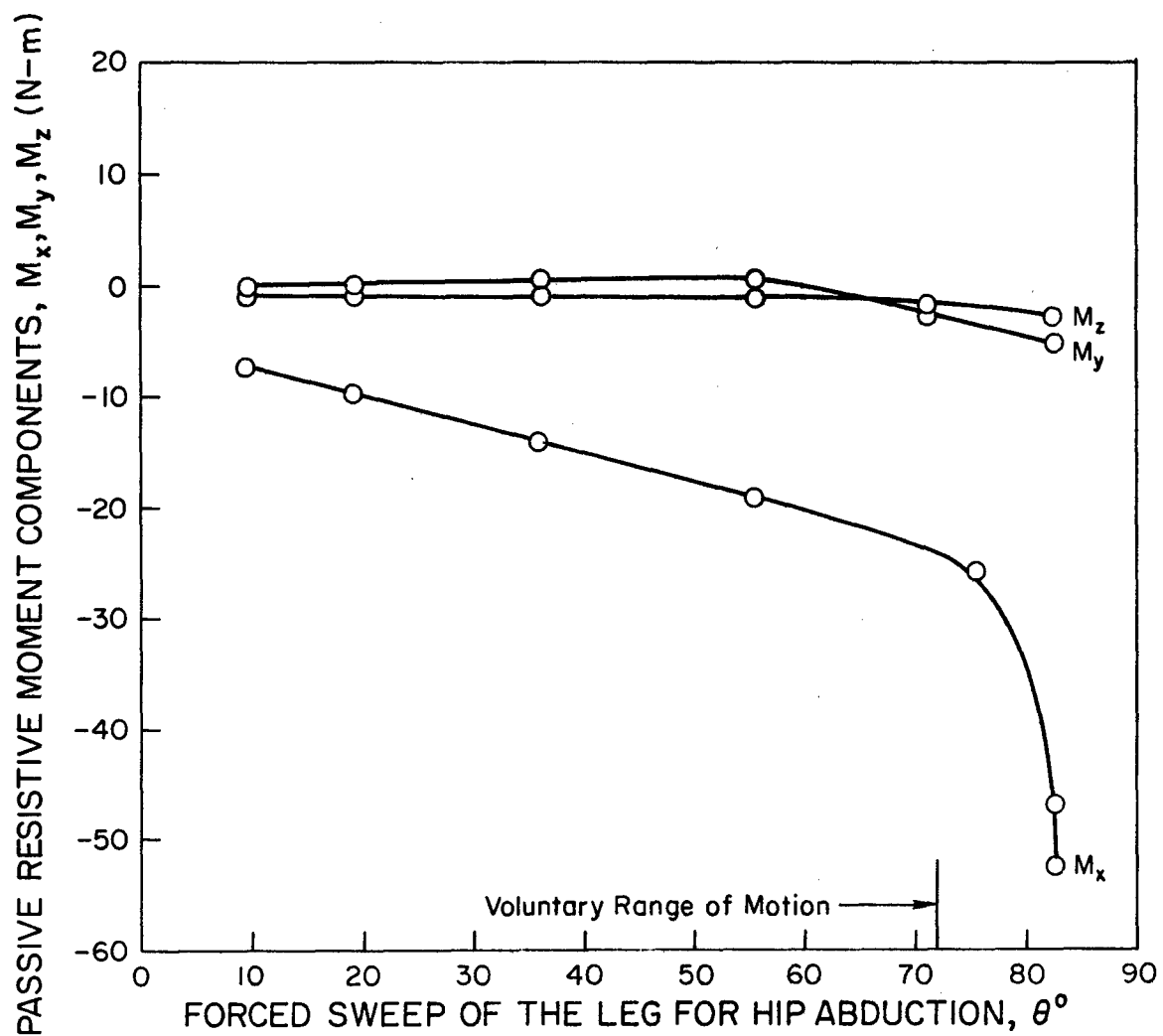
Fig. 42. Components of the passive resistive moment vector
at the hip joint of the first subject during forced sweep
of the leg for the hip abduction in the frontal plane.

73
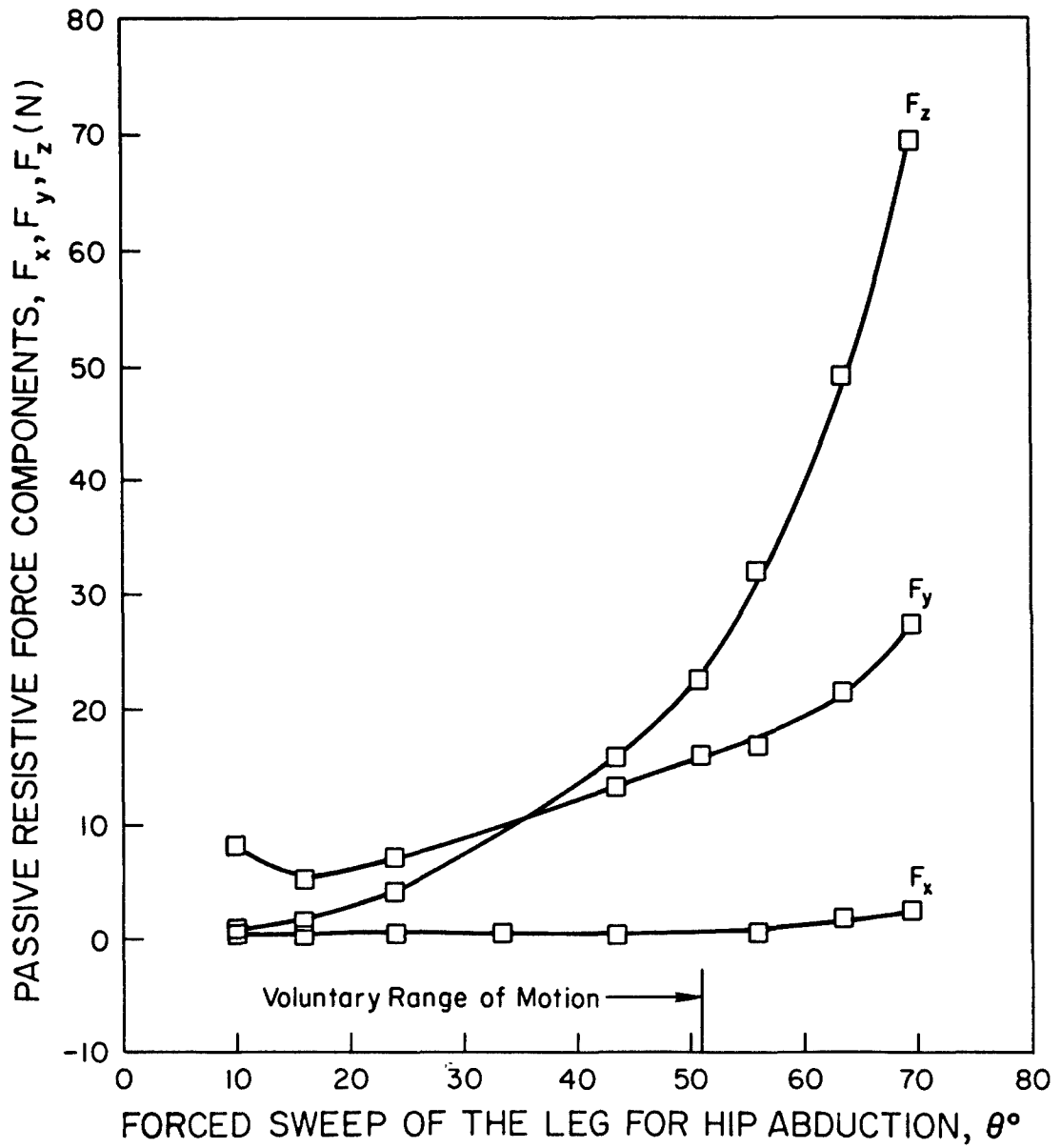
Fig. 43. Components of the passive resistive force vector
at the hip joint of the second subject during forced sweep
of the leg for the hip abduction in the frontal plane.
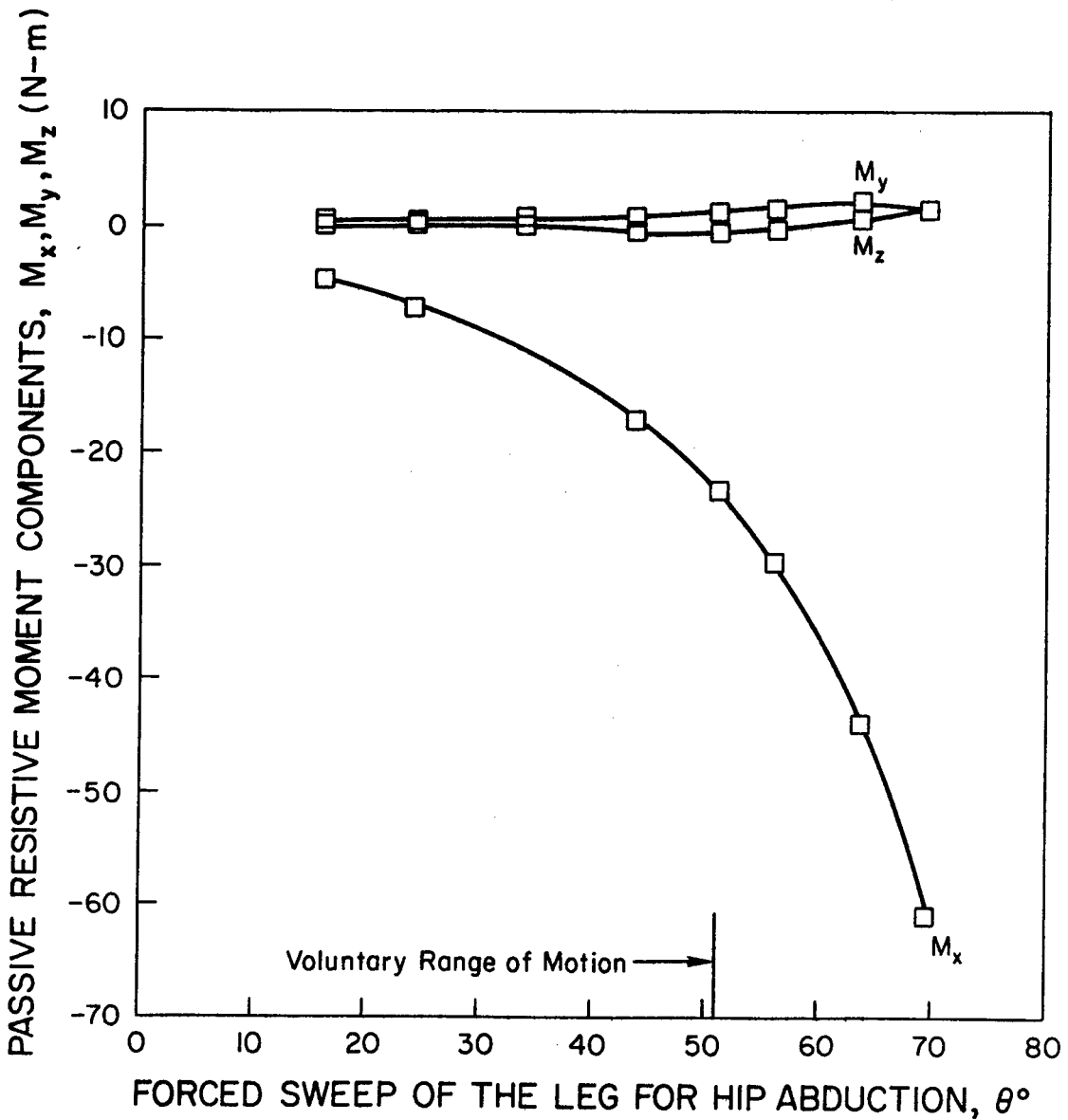
Fig. 44. Components of the passive resistive moment vector
at the hip joint of the second subject during forced sweep
of the leg for the hip abduction in the frontal plane.
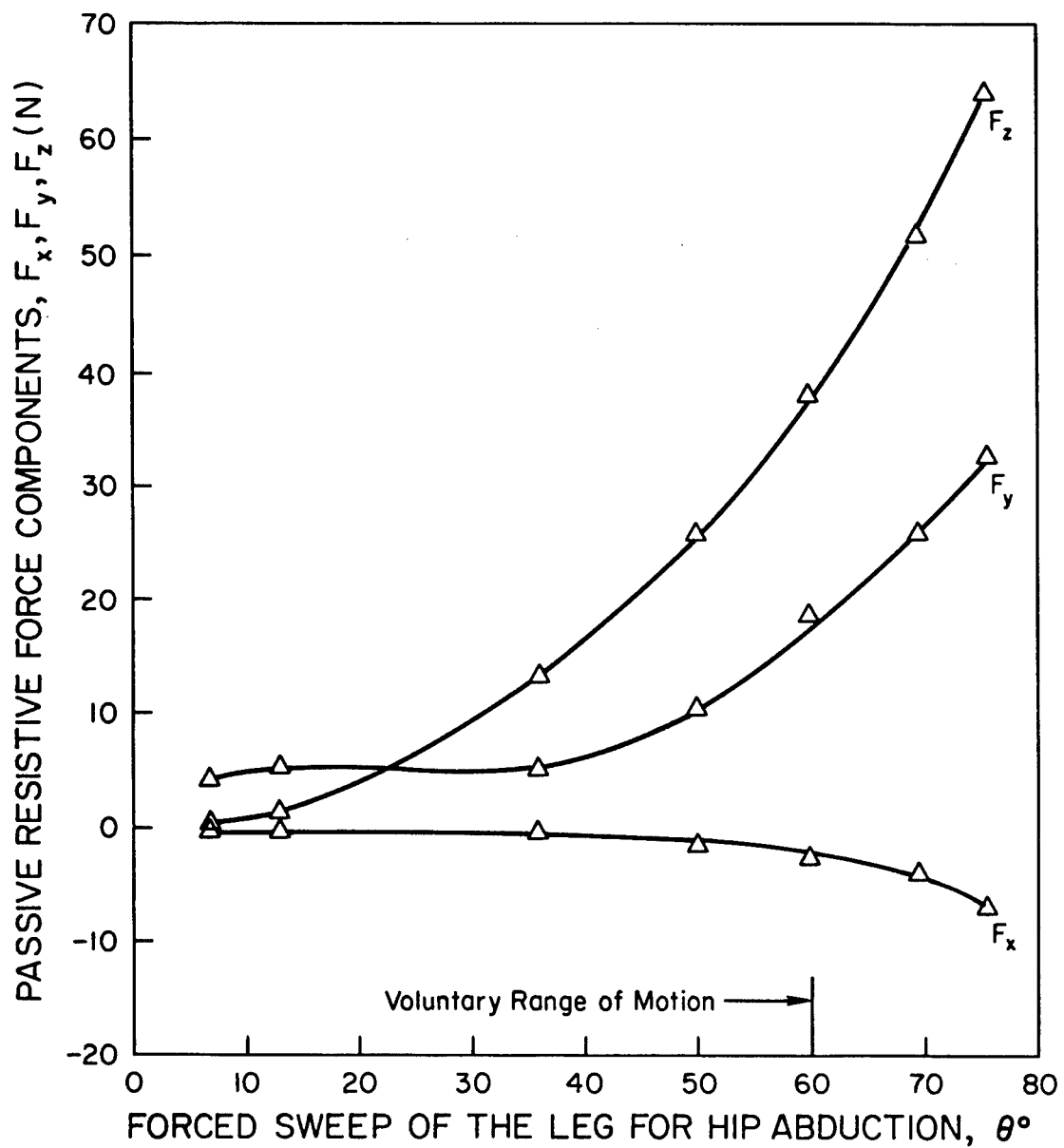
Fig. 45. Components of the passive resistive force vector
at the hip joint of the third subject during forced sweep
of the leg for the hip abduction in the frontal plane.

76
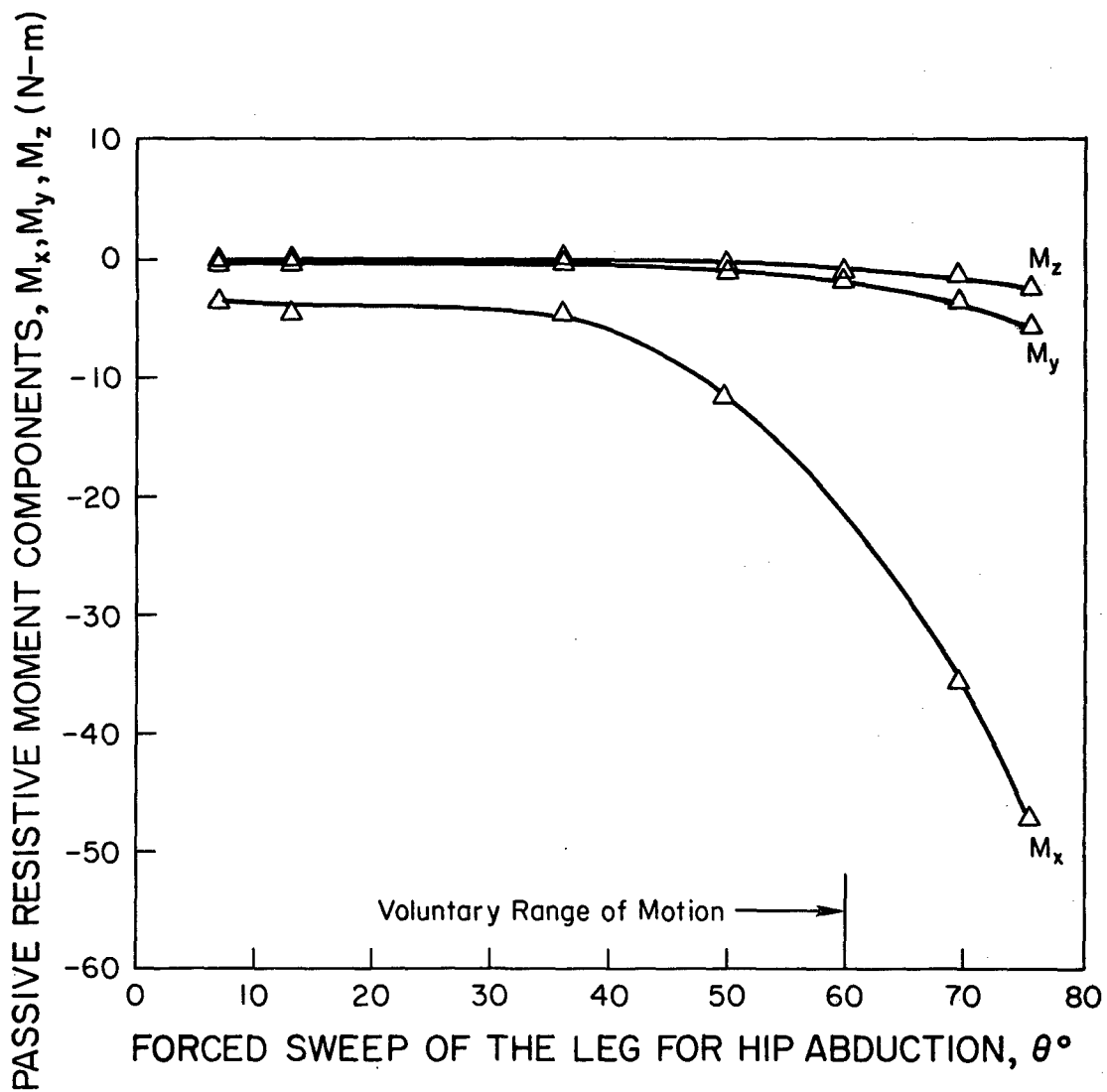
Fig. 46. Components of the passive resistive moment vector at the hip joint of the third subject during forced sweep of the leg for the hip abduction in the frontal plane.

77
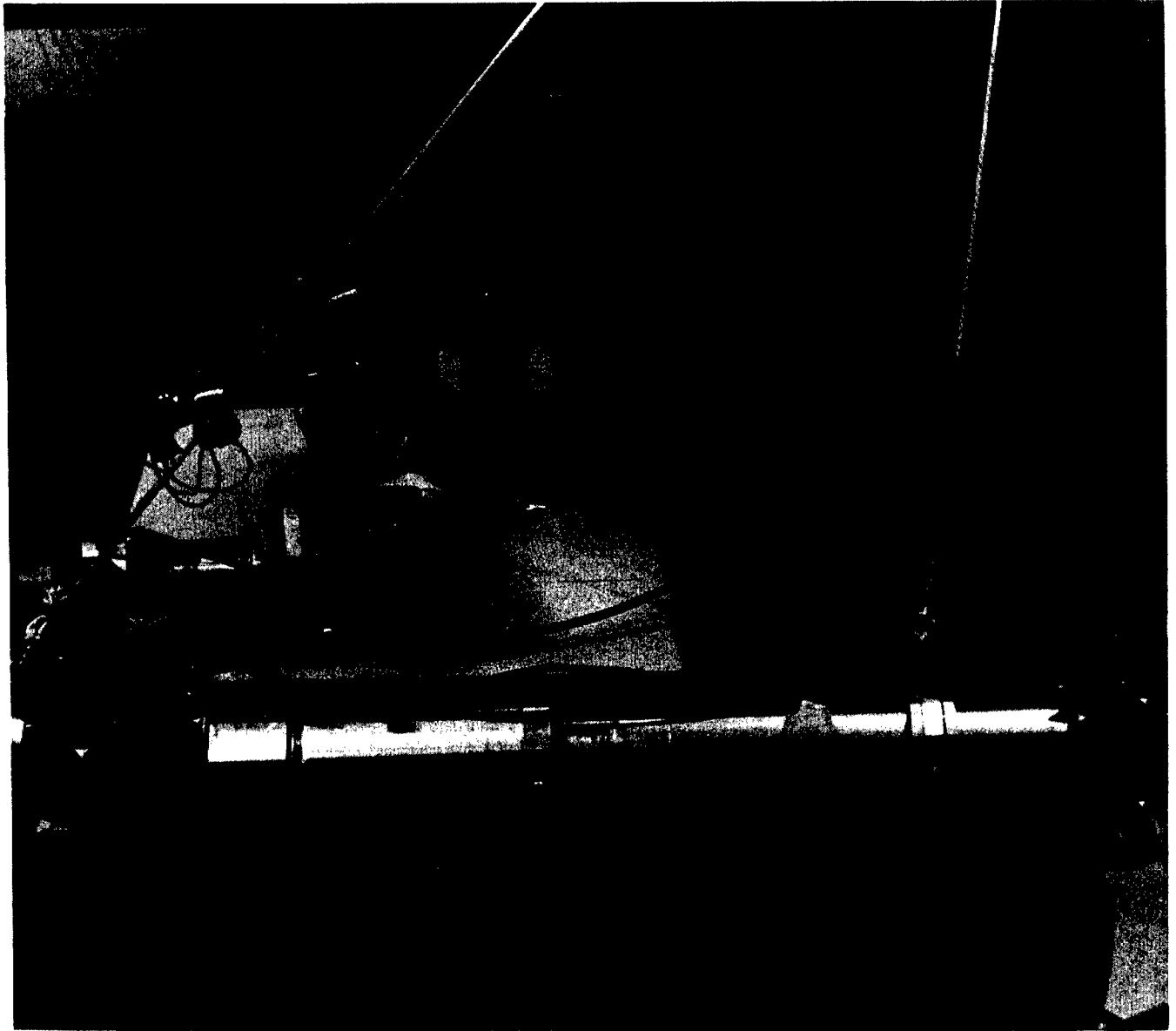
Fig. 47. Force is being applied by means of the GFA on the subject's lower arm for the elbow joint resistive force and moment data collection.
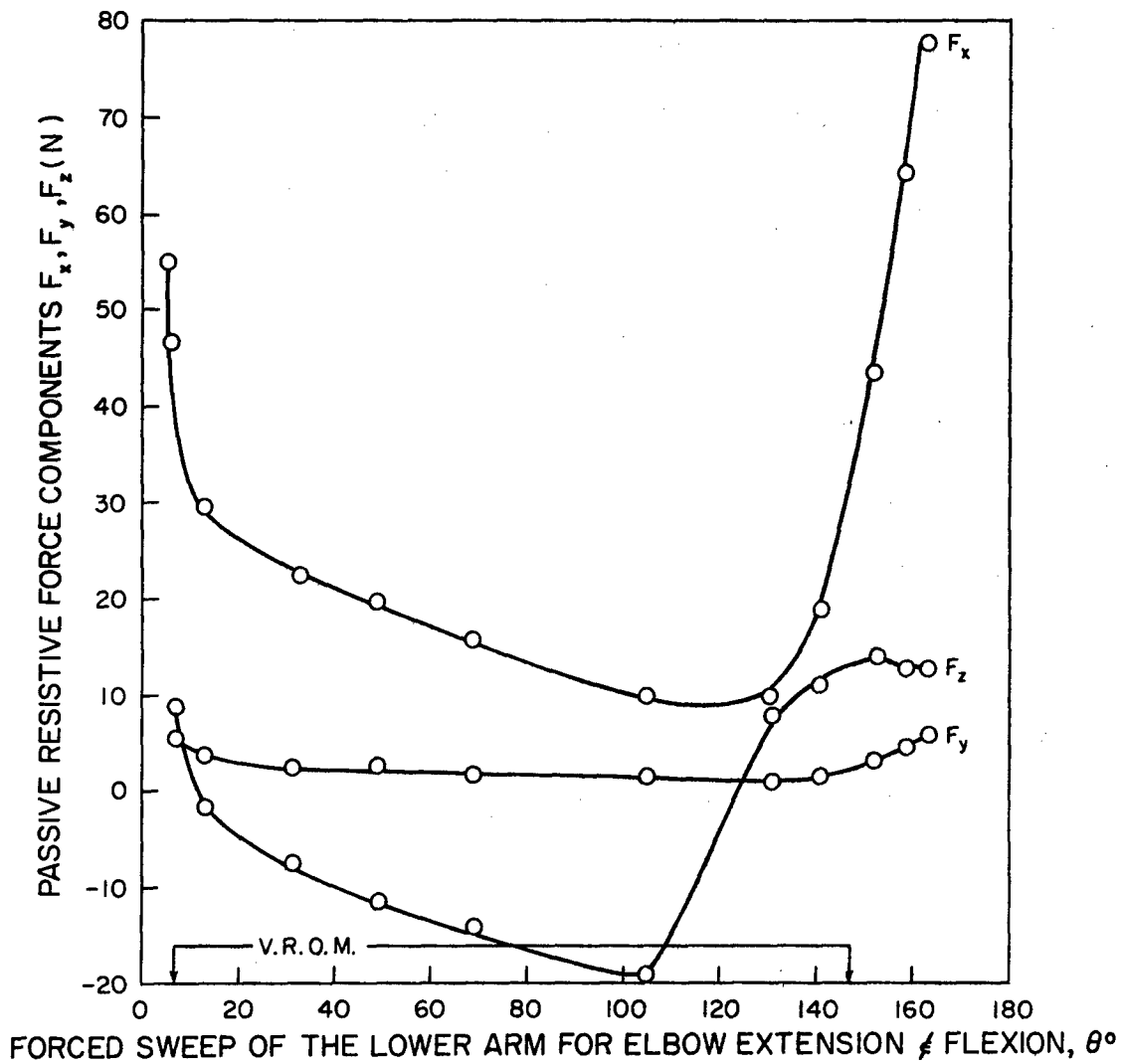
Fig. 48. Components of the passive resistive force vector at the elbow joint of the first subject during forced sweep of the lower arm.
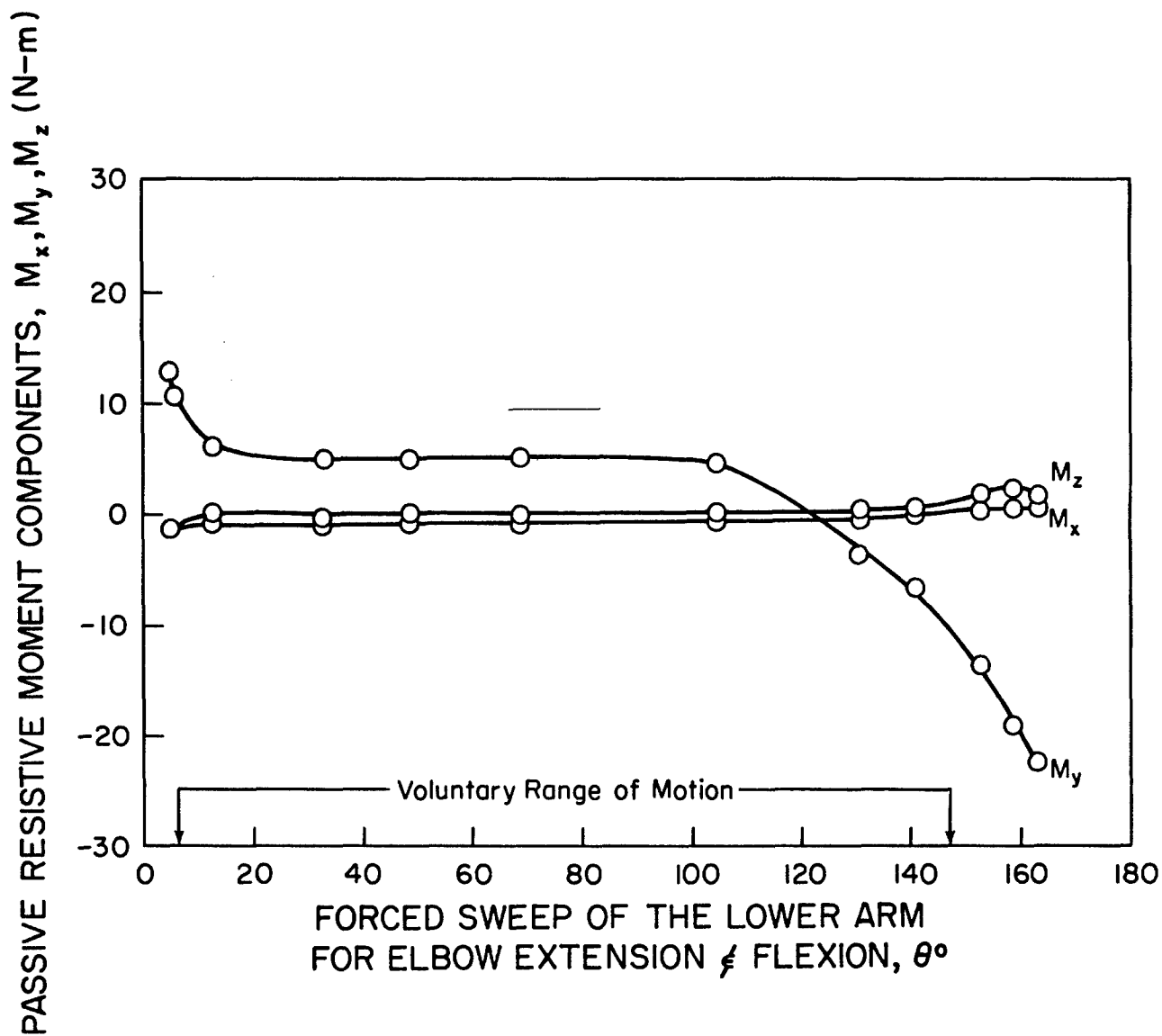
Fig. 49. Components of the passive resistive moment vector at the elbow joint of the first subject during forced sweep of the lower arm.
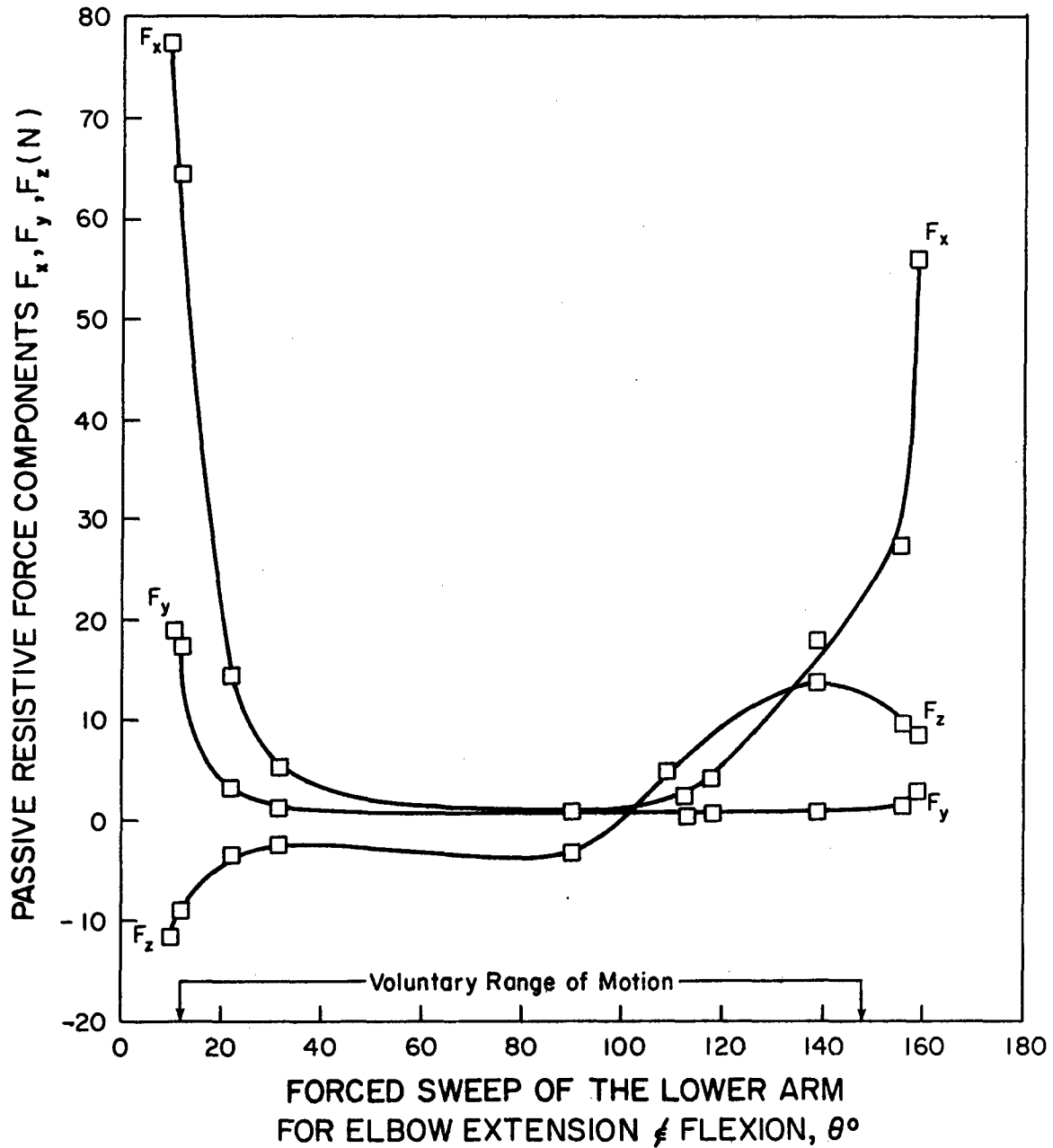
Fig. 50. Components of the passive resistive force vector at the elbow joint of the second subject during forced sweep of the lower arm.
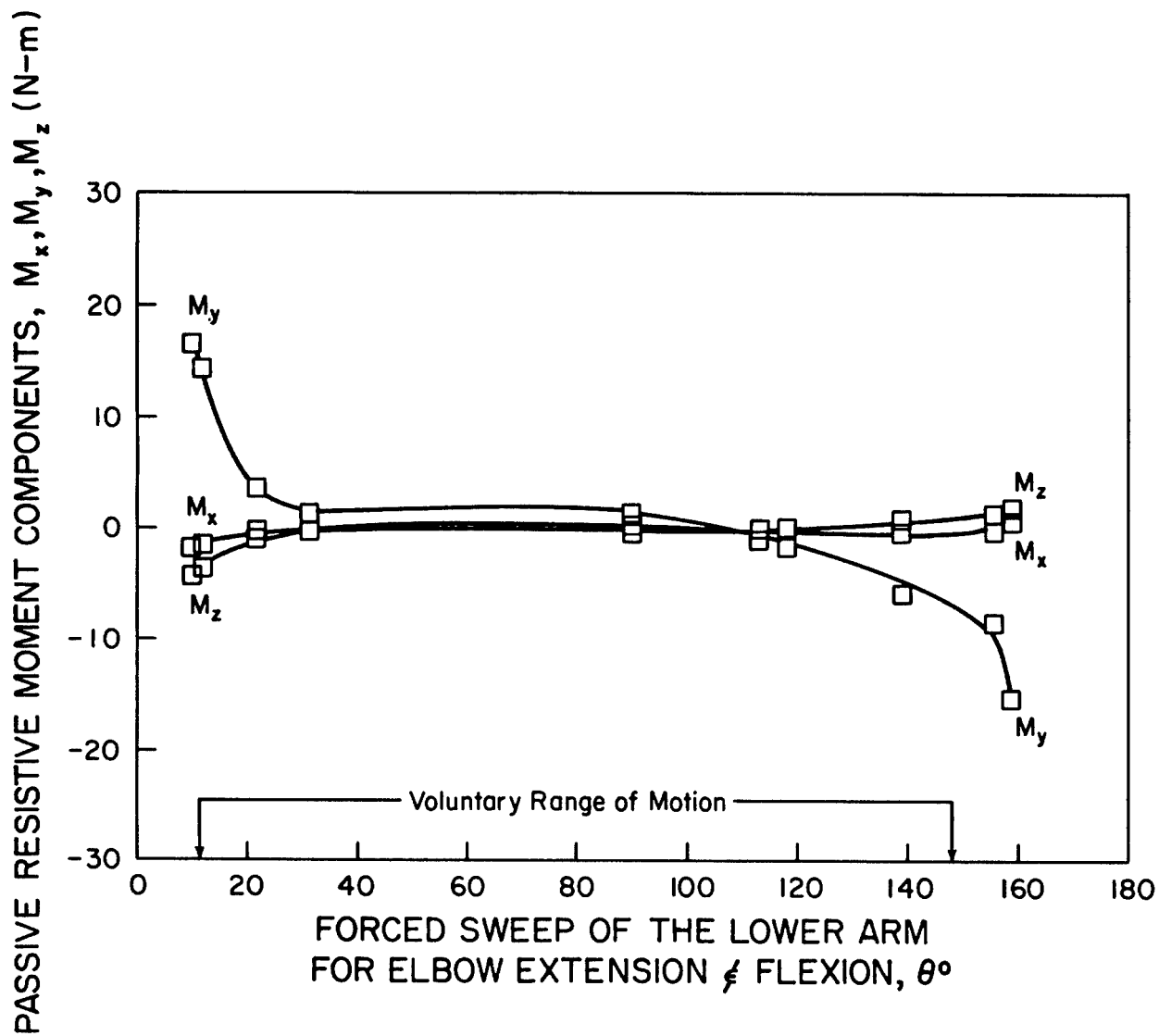
Fig. 51. Components of the passive resistive moment vector at the elbow joint of the second subject during forced sweep of the lower arm.

82
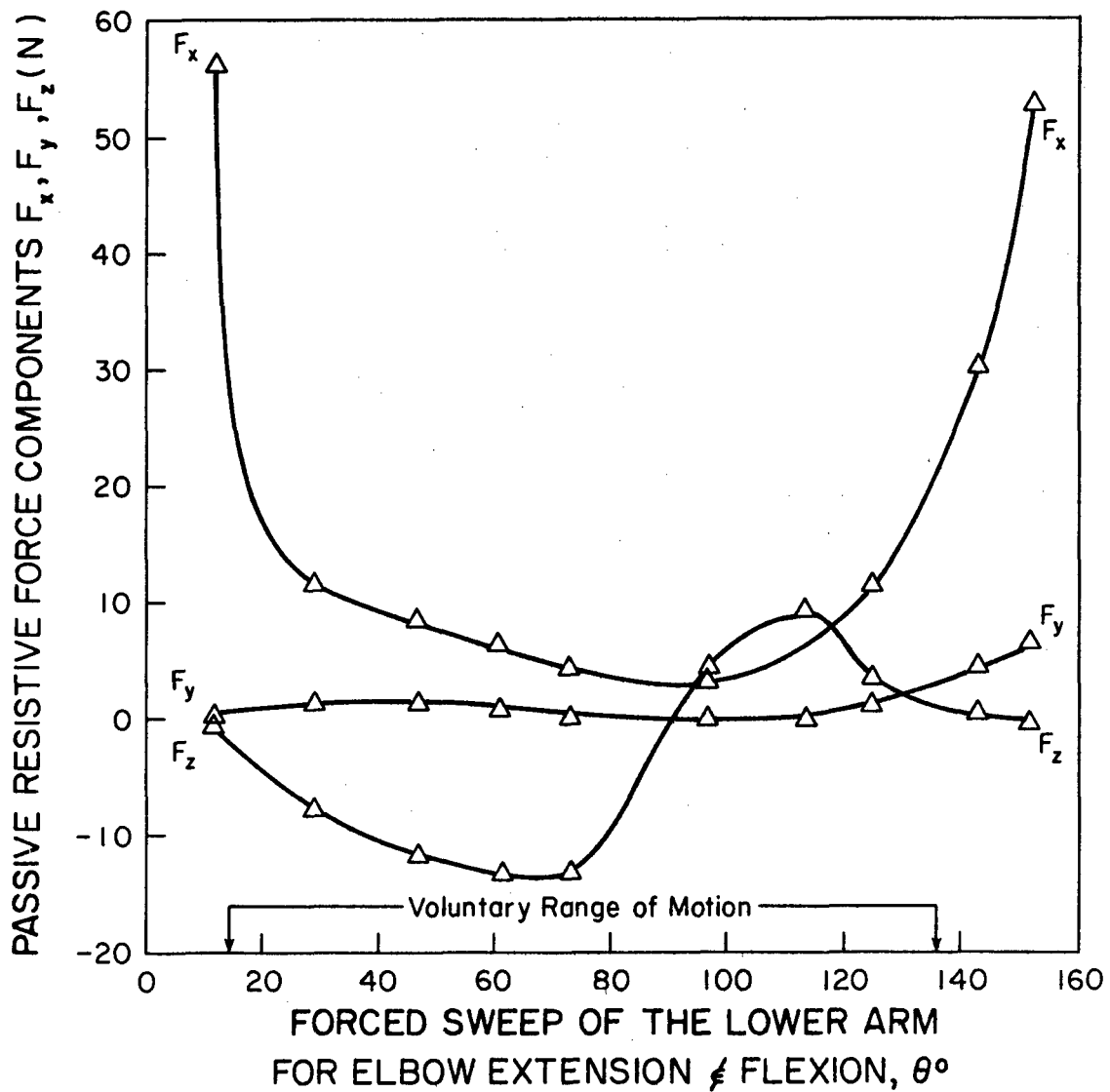
Fig. 52. Components of the passive resistive force vector
at the elbow joint of the third subject during forced
sweep of the lower arm.
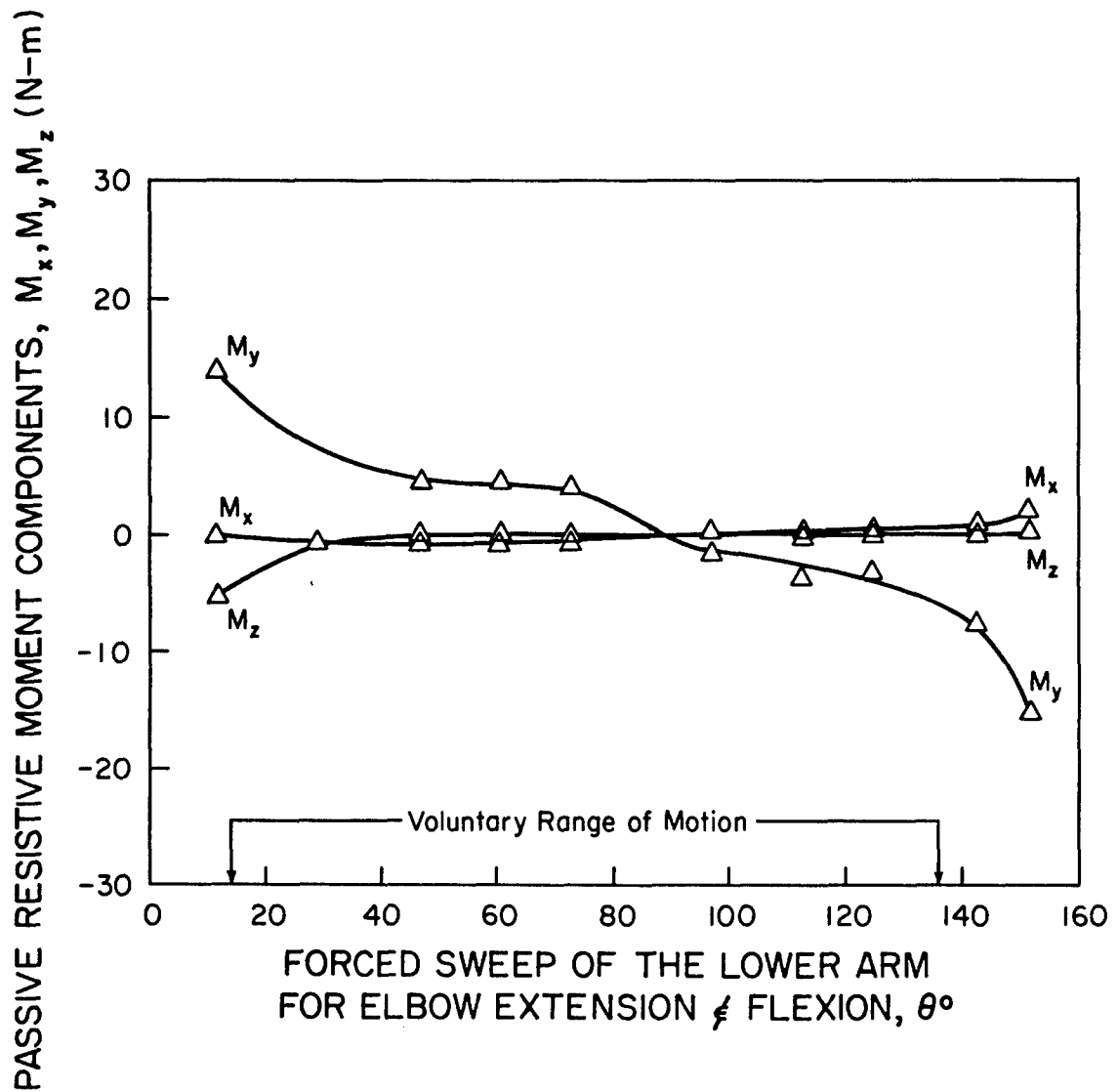
Fig. 53. Components of the passive resistive moment vector at the elbow joint of the third subject during forced sweep of the lower arm.
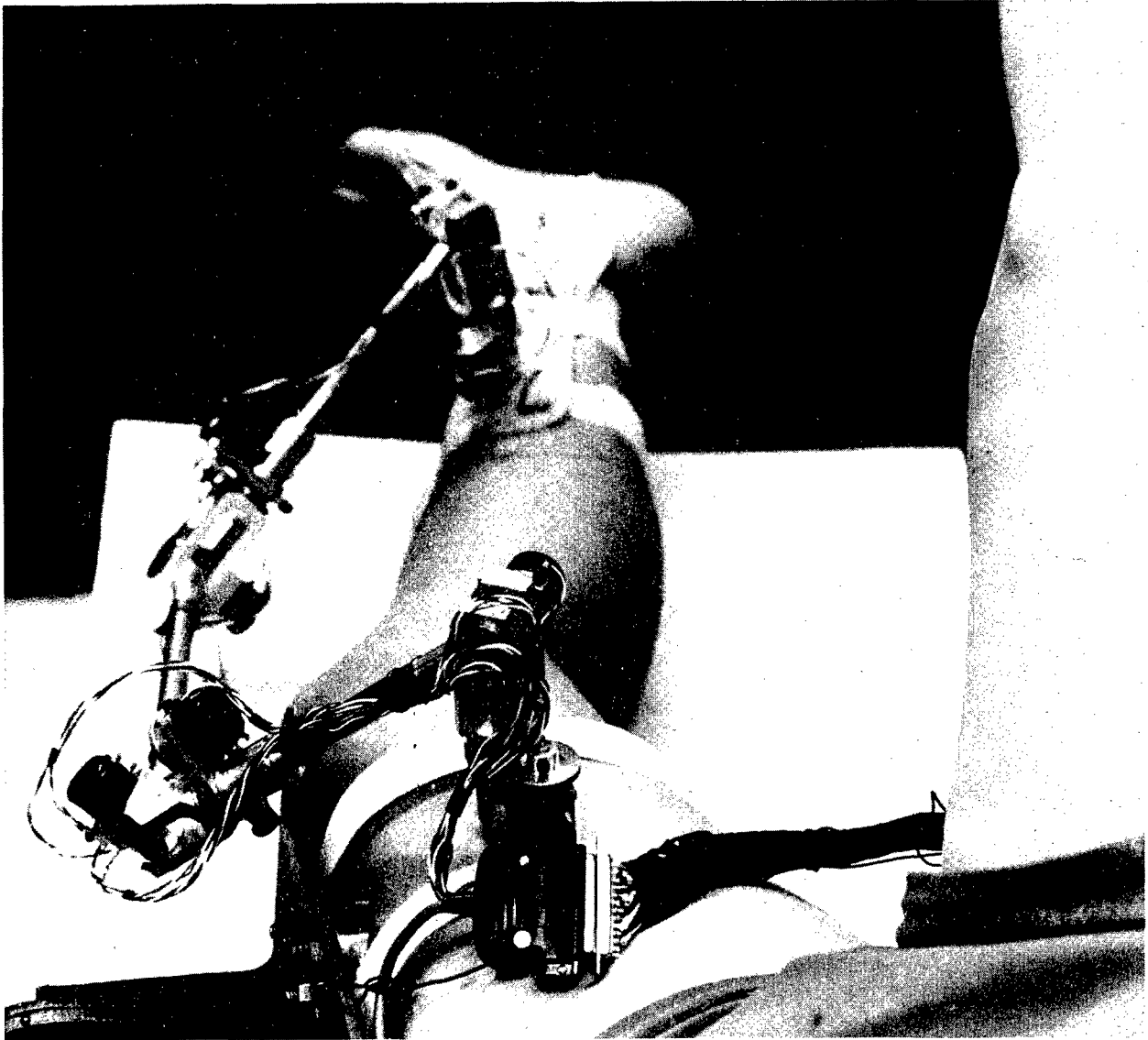
Fig. 54. Subject is prepared for the knee joint resistive force and moment data collection.
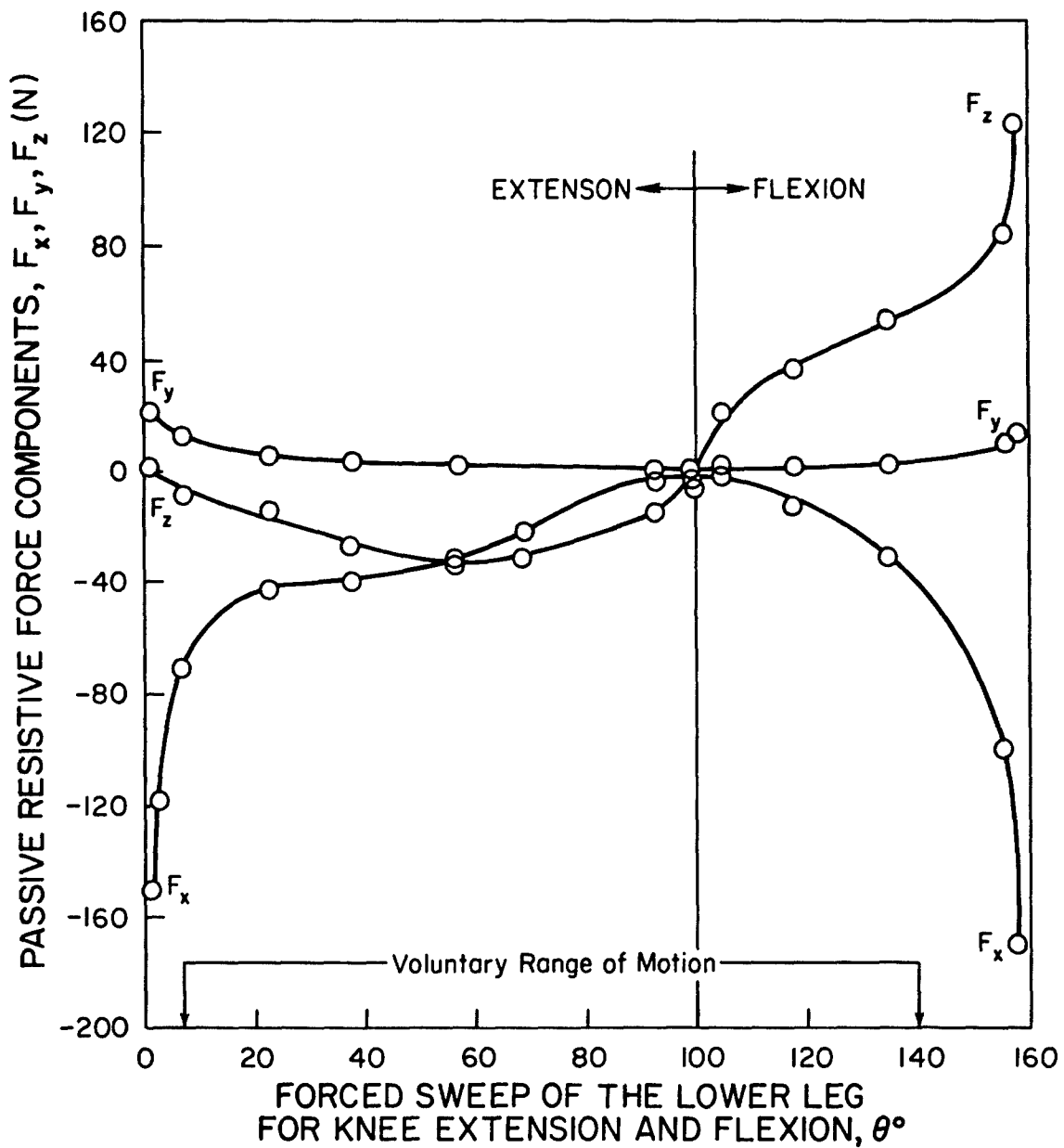
Fig. 55. Components of the passive resistive force vector at
the knee joint of the first subject during forced sweep of
the lower leg.
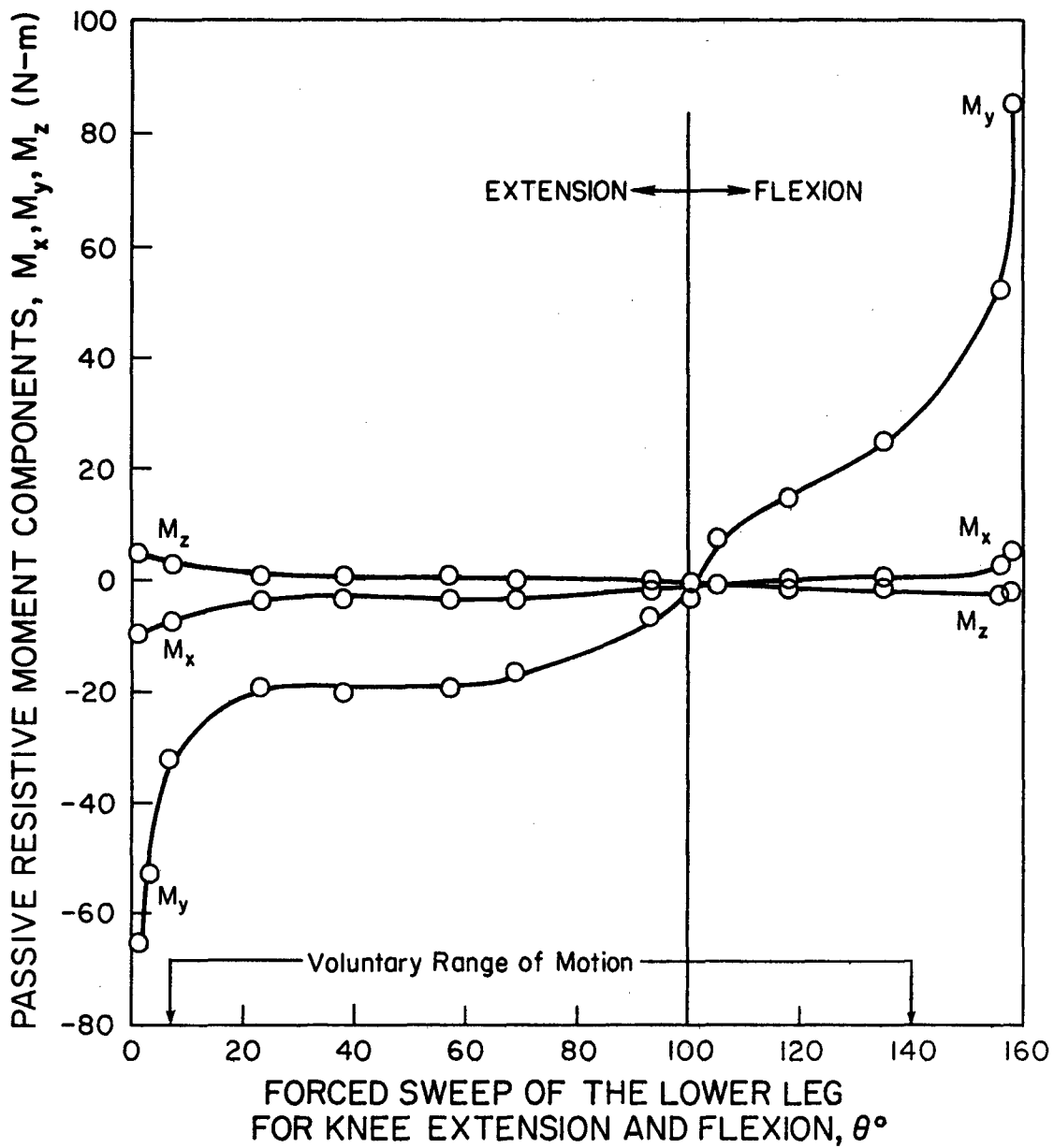
Fig. 56. Components of the passive resistive moment vector at the knee joint of the first subject during forced sweep of the lower leg.

87
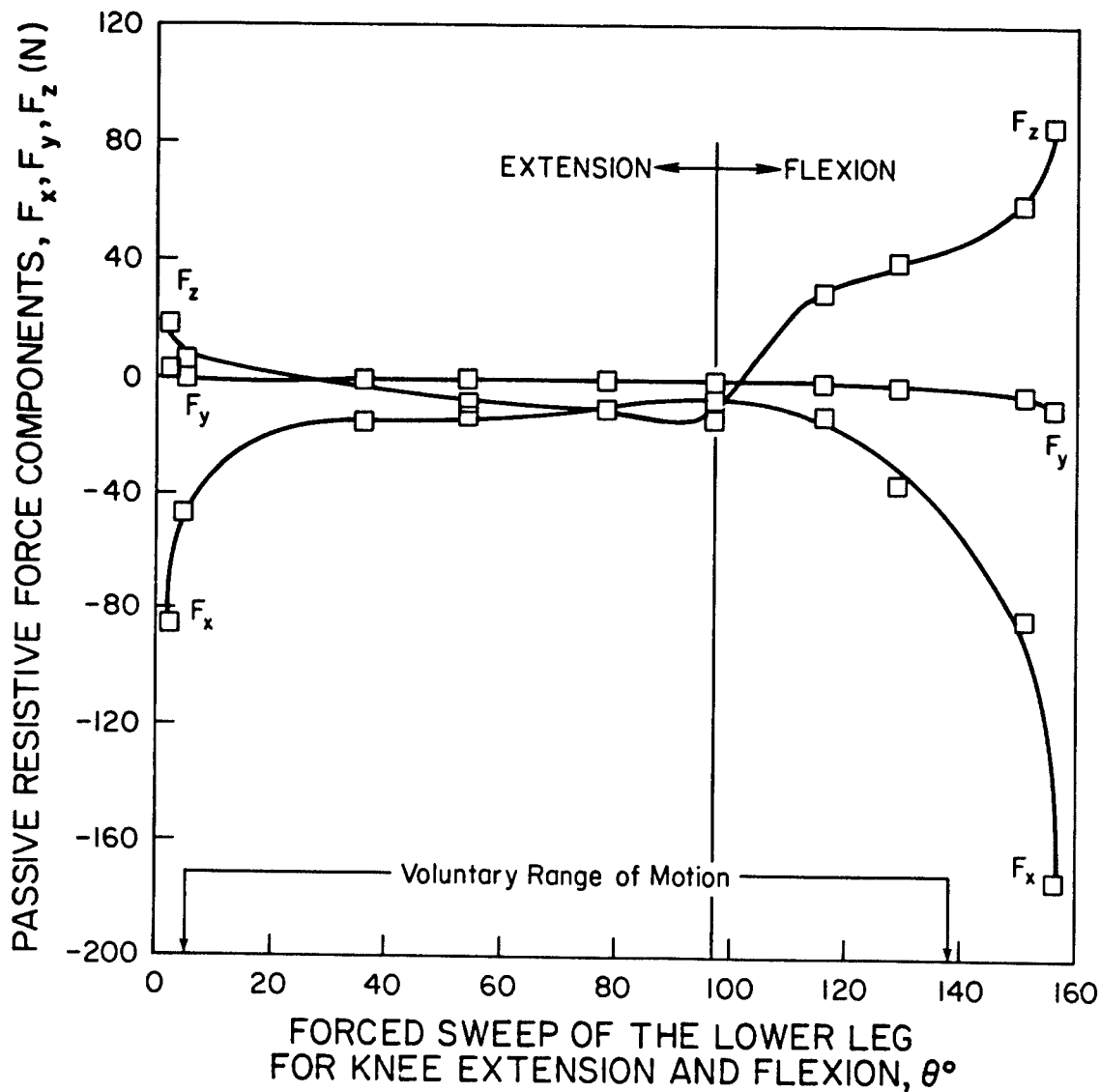
Fig. 57. Components of the passive resistive force vector at the knee joint of the second subject during forced sweep of the lower leg.

88
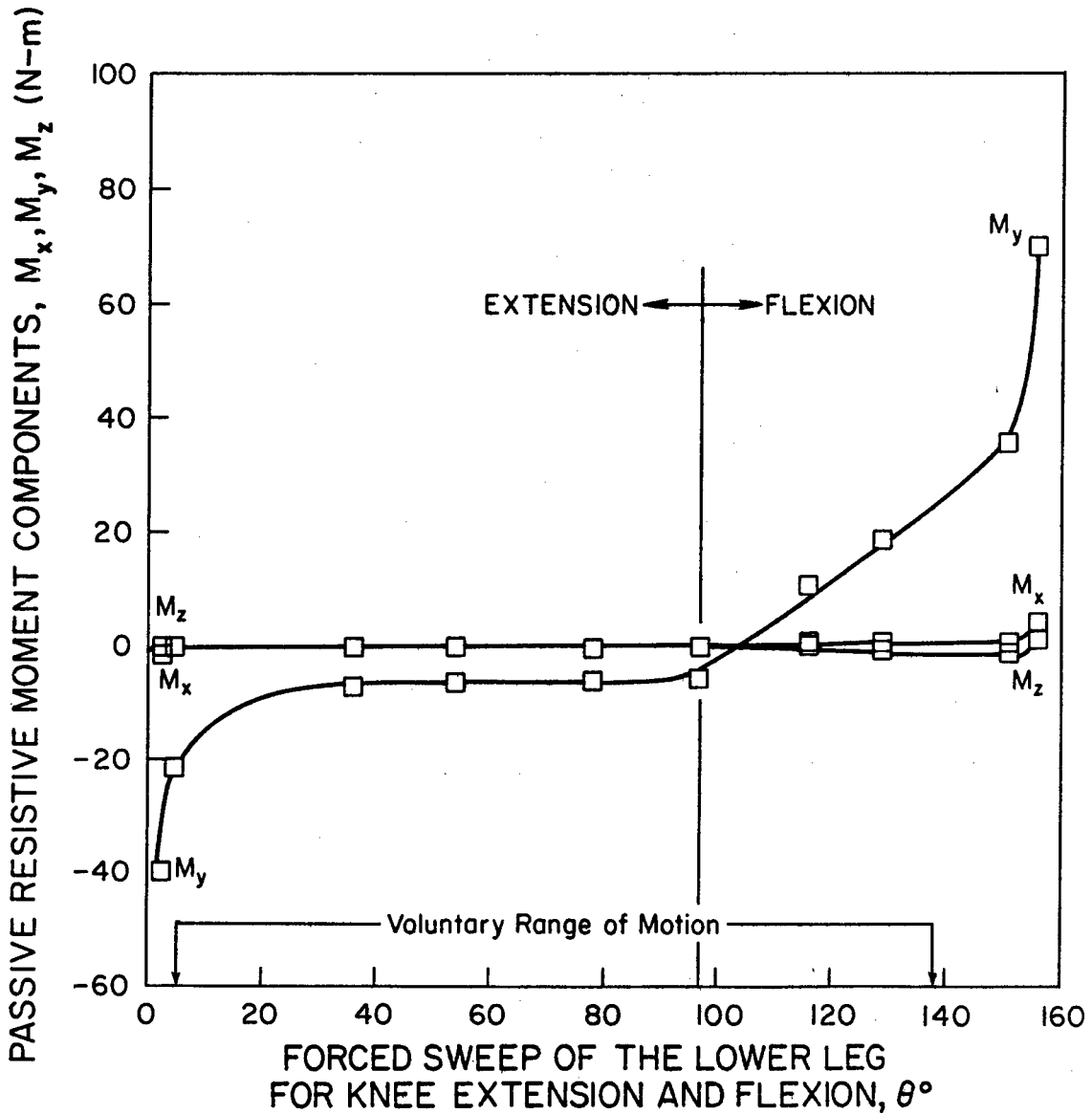
Fig. 58. Components of the passive resistive moment vector at the knee joint of the second subject during forced sweep of the lower leg.

89
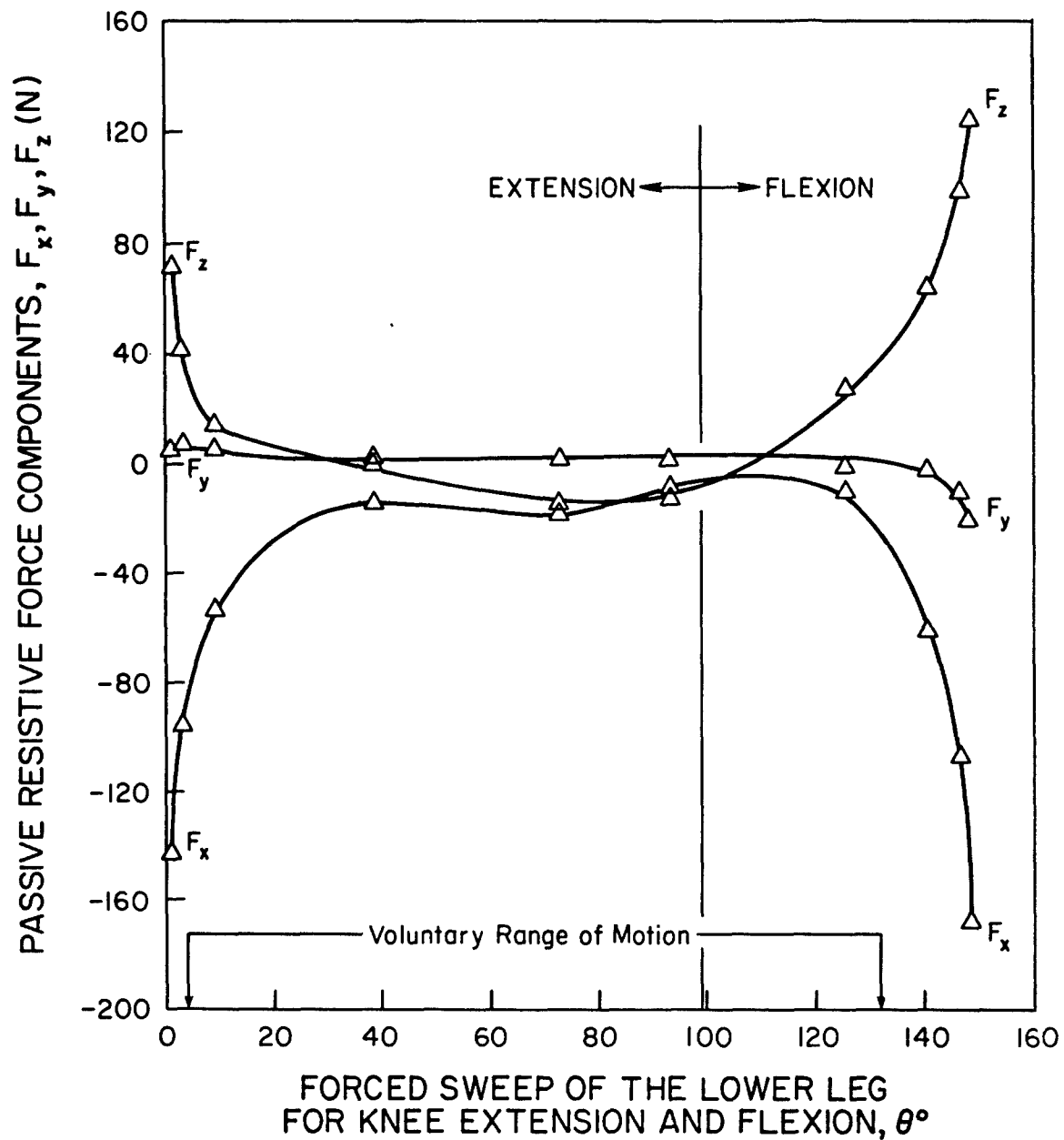
Fig. 59. Components of the passive resistive force vector at the knee joint of the third subject during forced sweep of the lower leg.

90
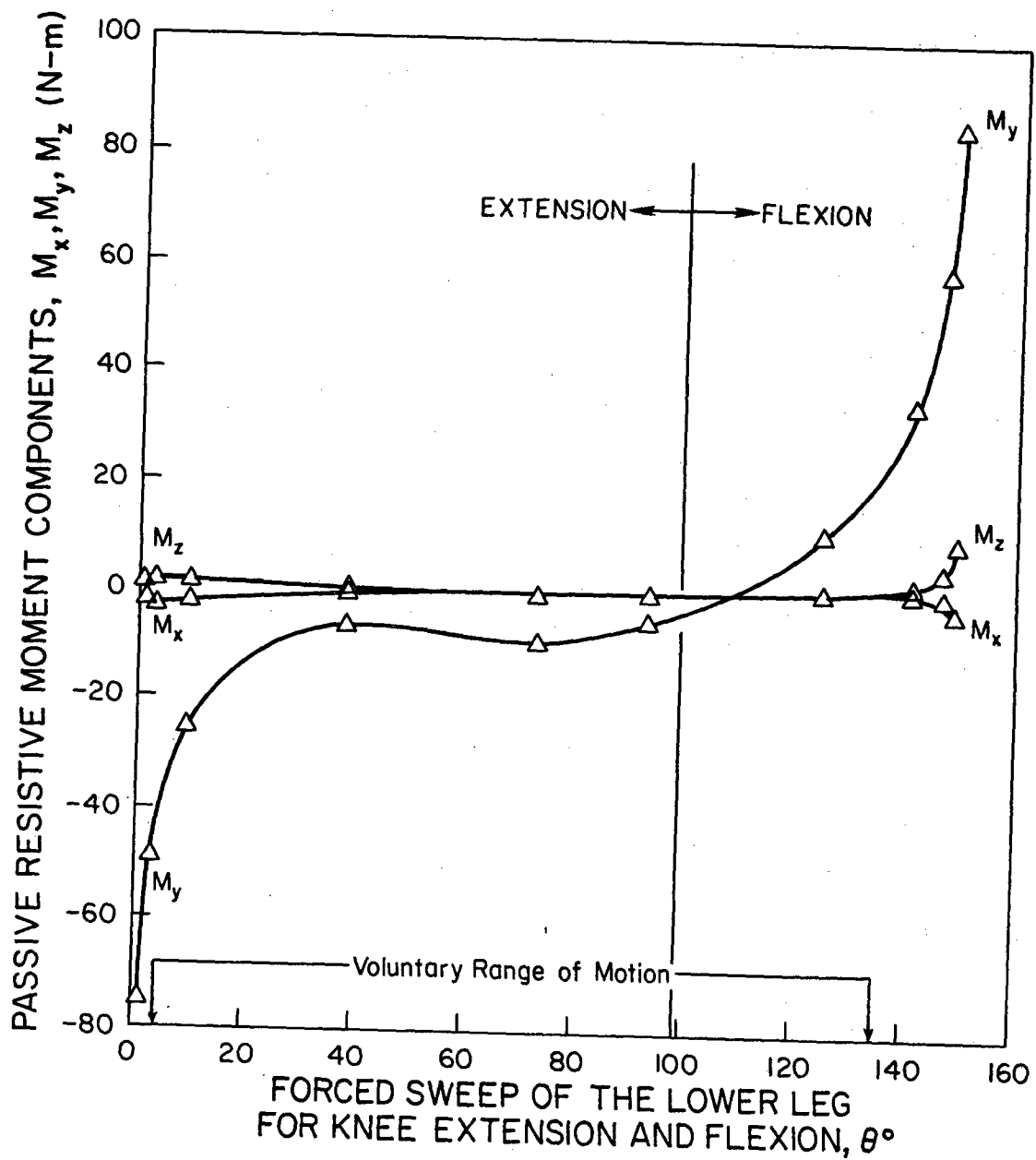
Fig. 60. Components of the passive resistive moment vector
at the knee joint of the third subject during forced
sweep of the lower leg.

91
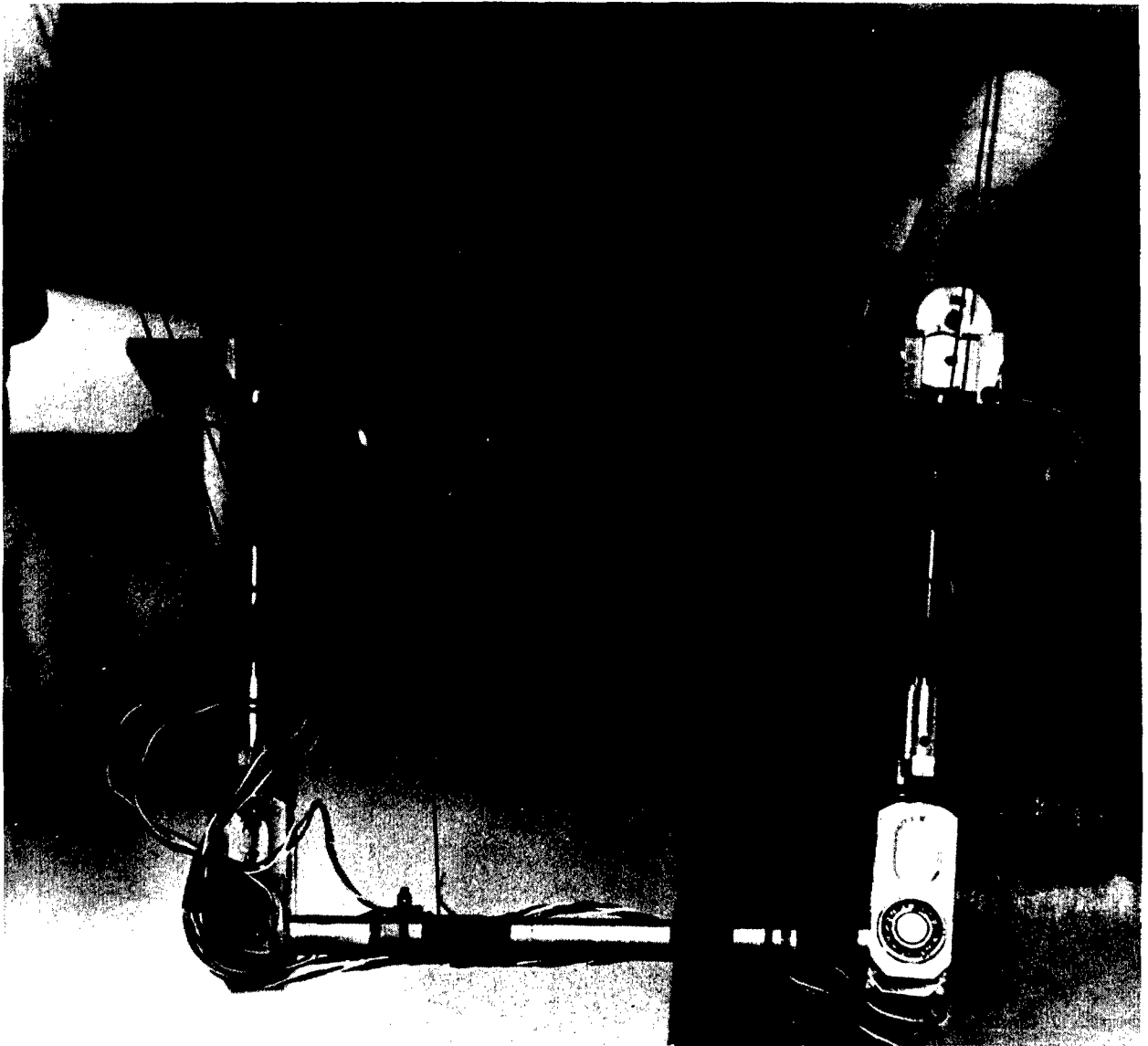
Fig. 61. Subject is prepared for the ankle joint resistive force
and moment data collection.
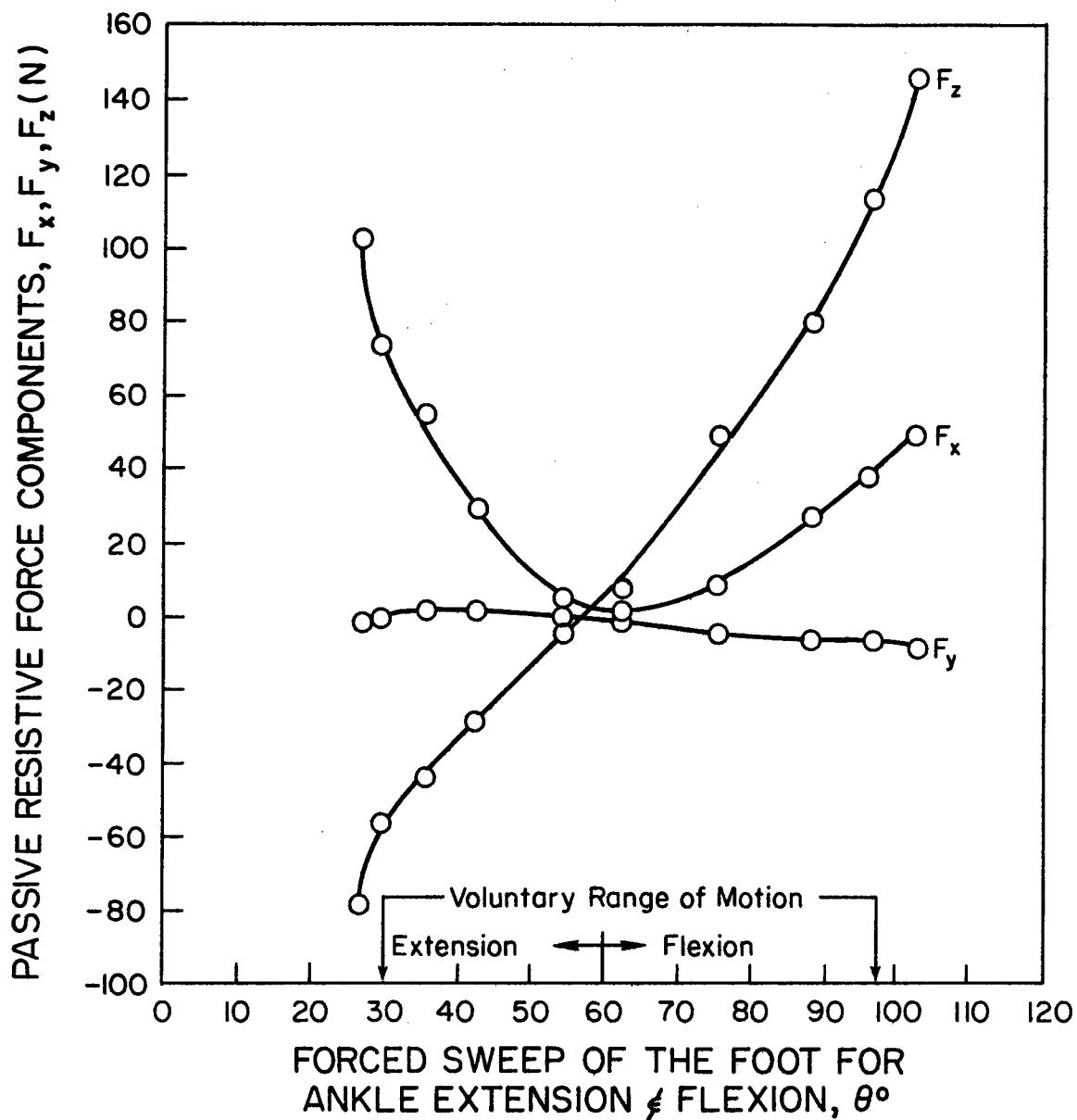
Fig. 62. Components of the passive force vector at the ankle joint of the first subject during forced sweep of the foot.
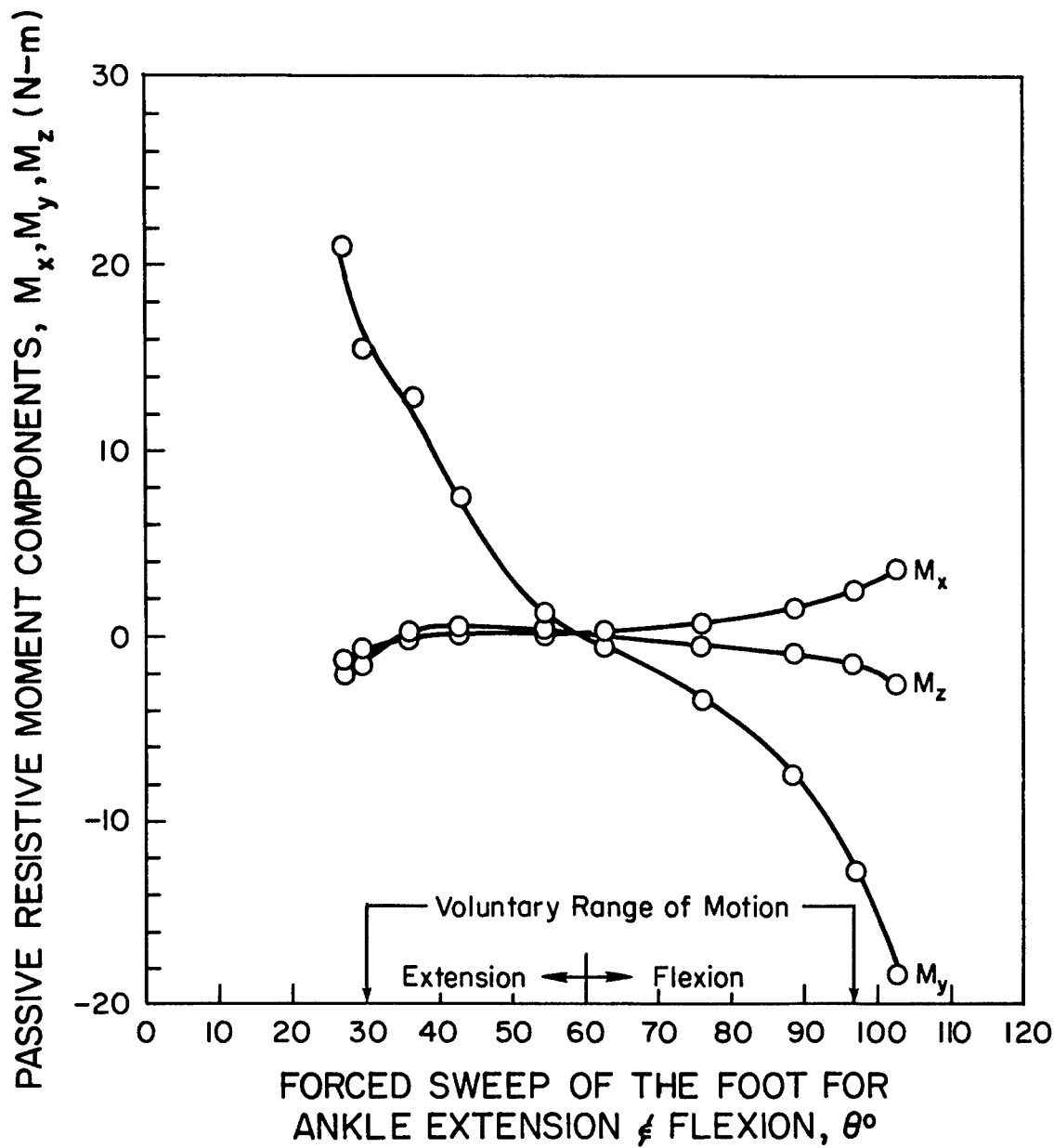
Fig. 63. Components of the passive moment vector at the ankle
joint of the first subject during forced sweep of the foot.

94
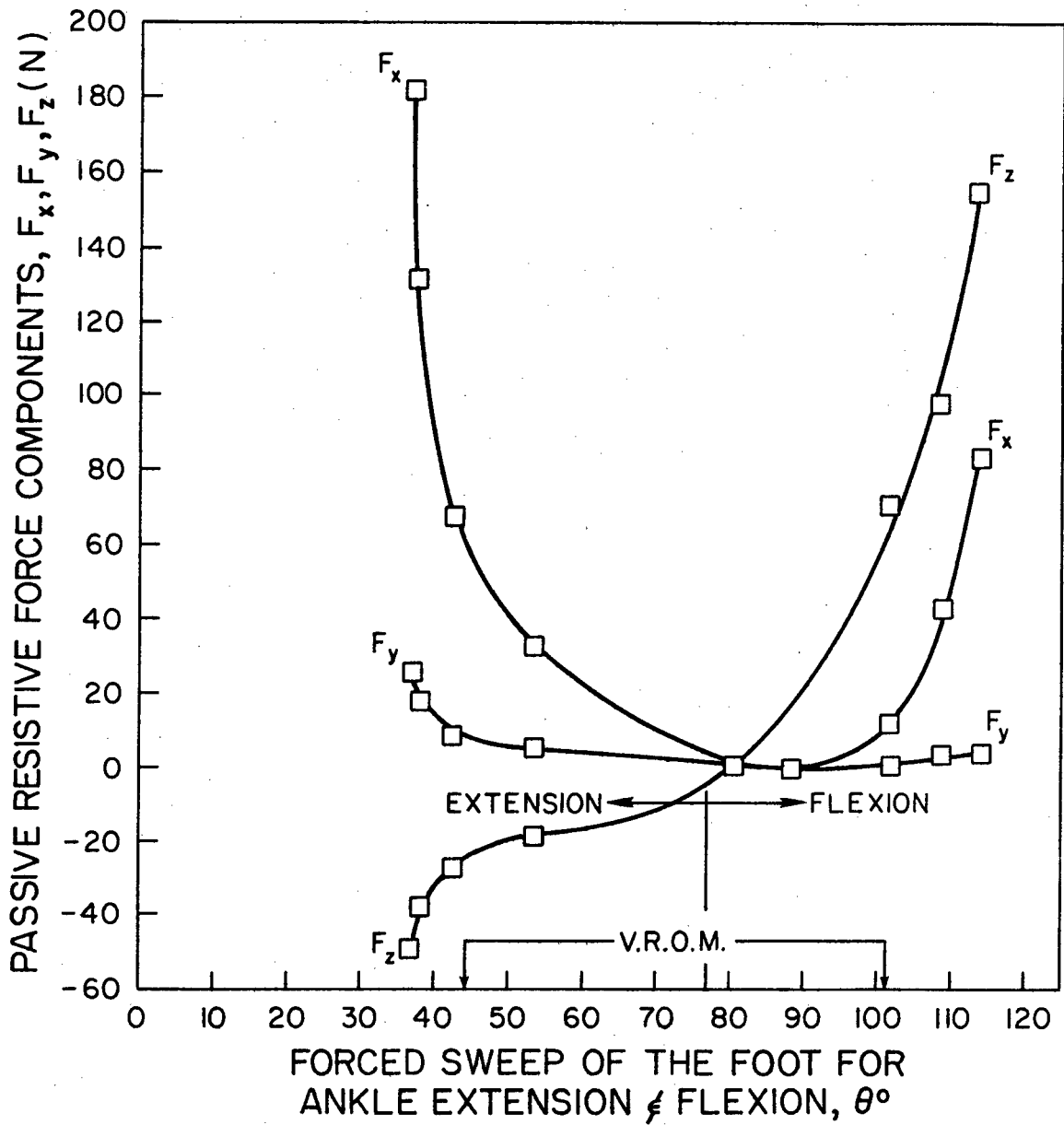
Fig. 64. Components of the passive force vector at the ankle joint of the second subject during forced sweep of the foot.

Fig. 65. Components of the passive moment vector at the ankle joint of the second subject during forced sweep of the foot.

PASSIVE RESISTIVE FORCE COMPONENTS, F_x, F_y, F_z (N)

140

120

100

80

60

40

20

0

-20

-40

-60

-80

-100

F_z

F_x

F_y

Voluntary Range of Motion

EXTENSION ← → FLEXION

0   10   20   30   40   50   60   70   80   90   100   110   120
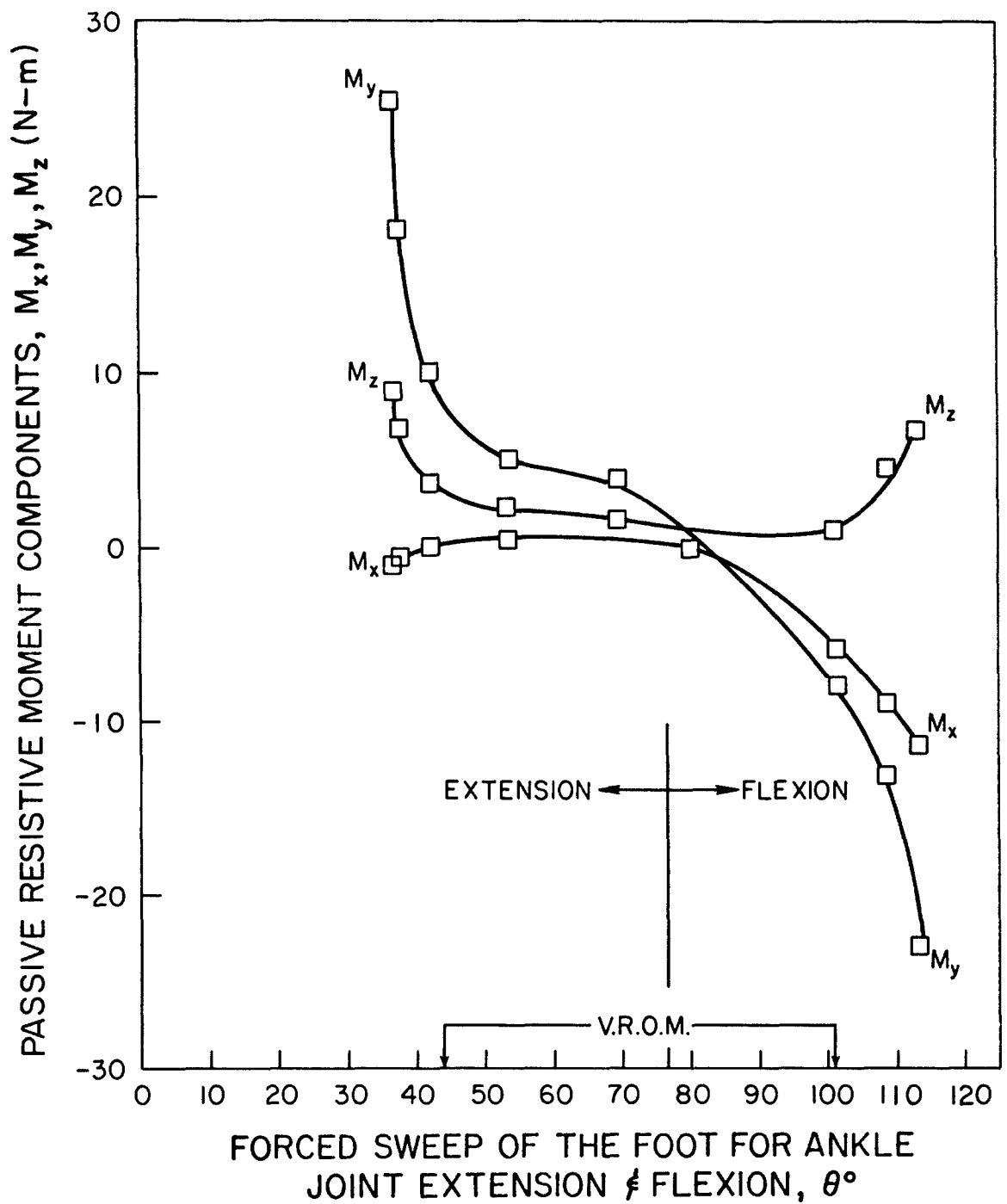
FORCED SWEEP OF THE FOOT FOR ANKLE
JOINT EXTENSION $\notin$ FLEXION, $\theta°$
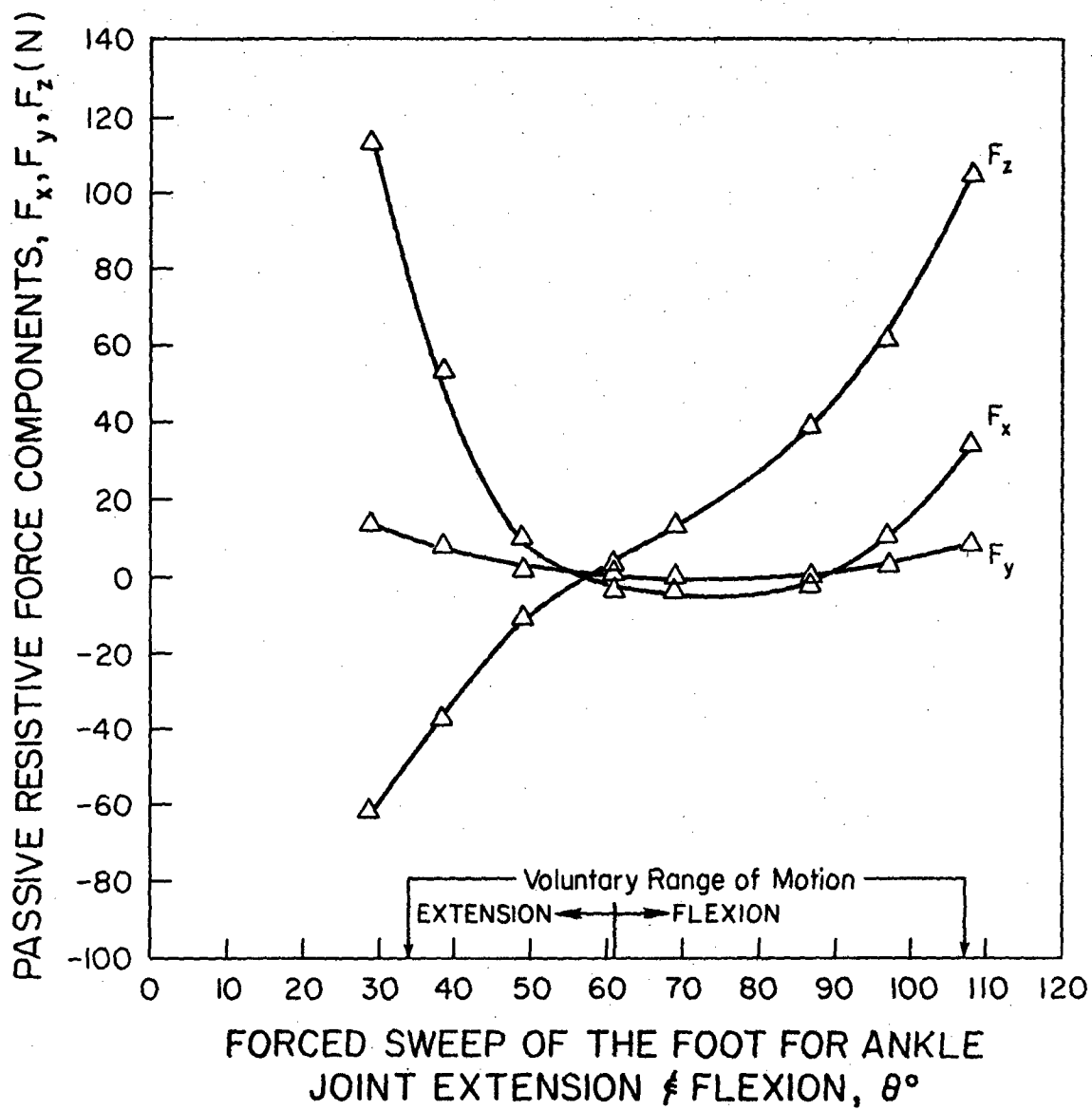
Fig. 66. Components of the passive force vector at the ankle
joint of the third subject during forced sweep of the foot.

97
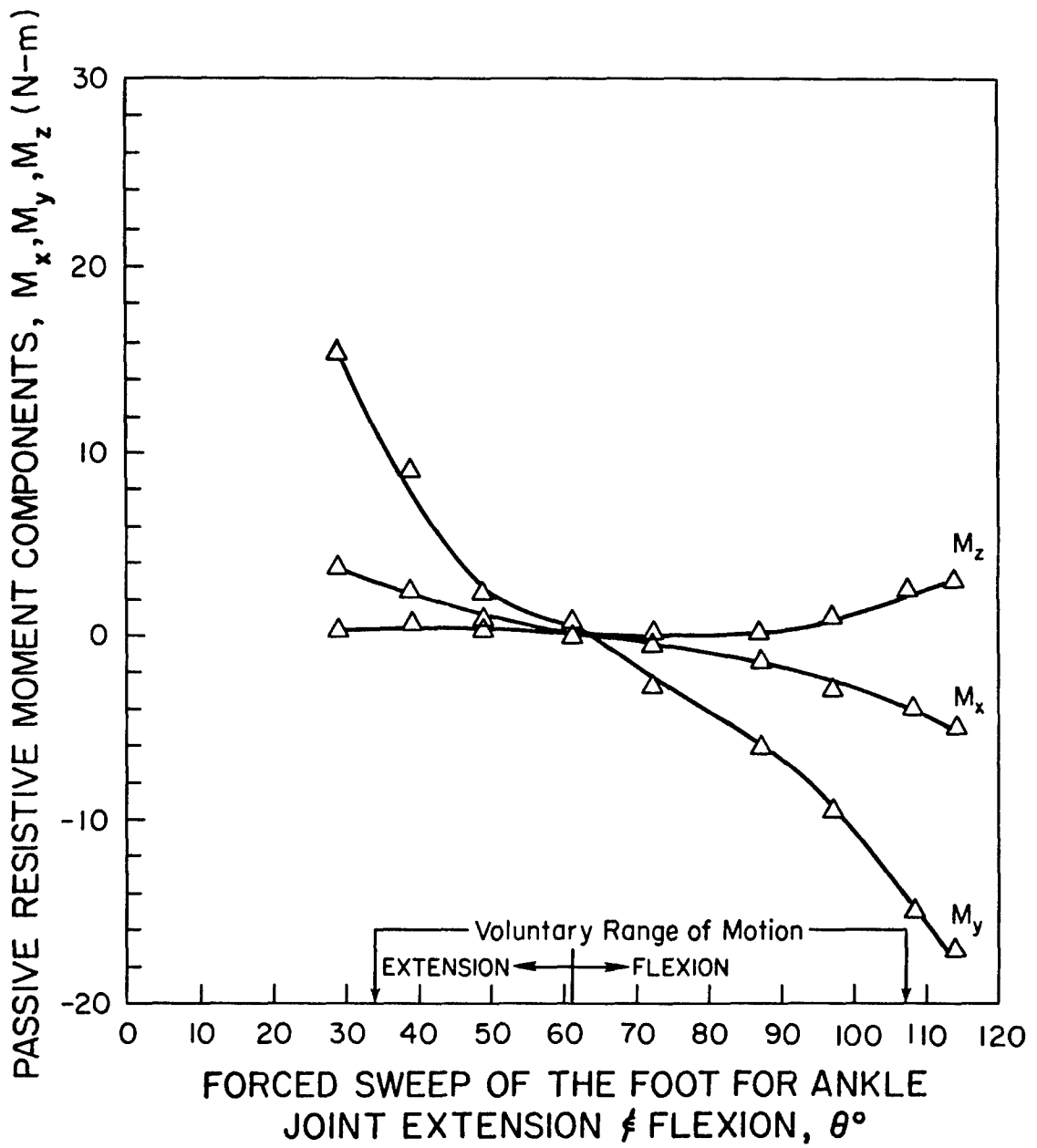
Fig. 67. Components of the passive moment vector at the ankle joint of the third subject during forced sweep of the foot.

Table 3

POLYNOMIAL EXPANSIONS FOR THE RESISTIVE FORCE & MOMENT COMPONENTS FOR THE SHOULDER JOINT

SHOULDER ABDUCTION and ADDUCTION	$F_x = 0.50 + 1.75\phi + 13.04\phi^2 - 20.27\phi^3 + 18.05\phi^4 - 9.4\phi^5 + 2.6\phi^6 - 0.29\phi^7$ $F_y = 5.48 - 24.23\phi + 0.64\phi^2 + 10.63\phi^3 + 12.94\phi^4 - 14.33\phi^5 + 3.32\phi^6$ $F_z = 0.15 + 0.16\phi + 4.81\phi^2 - 6.4\phi^3 + 4.84\phi^4 - 1.98\phi^5 + 0.31\phi^6$ $M_x = -0.45 + 2.69\phi - 1.39\phi^2 + 1.74\phi^3 - 2.32\phi^4 + 0.99\phi^5 - 0.12\phi^6$ $M_y = -0.07 - 0.04\phi + 1.1\phi^2 - 0.59\phi^3 + 0.087\phi^4 - 0.004\phi^5$ $M_z = 0.77 - 9.21\phi + 4.99\phi^2 + 5.46\phi^3 + 0.86\phi^4 - 10.12\phi^5 + 6.42\phi^6 - 1.18\phi^7$
SHOULDER ABDUCTION in the FRONTAL PLANE	$F_x = 16.45 - 43.24\theta + 40.53\theta^2 - 16.26\theta^3 + 2.39\theta^4$ $F_y = -317.20 + 554.37\theta - 315.47\theta^2 + 58.84\theta^3$ $F_z = -106.13 + 264.14\theta - 298.70\theta^2 + 179.89\theta^3 - 54.64\theta^4 + 6.62\theta^5$ $M_x = -592.67 + 1766.31\theta - 2070.46\theta^2 + 1190.19\theta^3 - 335.65\theta^4 + 37.28\theta^5$ $M_y = -2.39 + 2.40\theta - 0.65\theta^2 + 0.056\theta^3$ $M_z = -34.68 + 85.35\theta - 76.89\theta^2 + 30.16\theta^3 - 4.37\theta^4$
SHOULDER EXTENSION	$F_x = -41.49 + 262.72\theta - 459.86\theta^2 + 330.51\theta^3 - 80.66\theta^4$ $F_y = 24.80 - 180.76\theta + 480.73\theta^2 - 583.42\theta^3 + 331.70\theta^4 - 70.02\theta^5$ $F_z = 73.19 - 547.83\theta + 1570.58\theta^2 - 2032.69\theta^3 + 1219.34\theta^4 - 263.70\theta^5$ $M_x = 3.93 - 19.21\theta + 33.22\theta^2 - 25.64\theta^3 + 6.67\theta^4$ $M_y = 18.58 - 146.52\theta + 468.62\theta^2 - 650.84\theta^3 + 407.75\theta^4 - 90.82\theta^5$ $M_z = -14.8 + 95.51\theta - 234.60\theta^2 + 272.59\theta^3 - 150.35\theta^4 + 30.89\theta^5$

Table 4

POLYNOMIAL EXPANSIONS FOR THE RESISTIVE FORCE & MOMENT COMPONENTS FOR THE ELBOW & KNEE JOINTS

ELBOW

$$F_x = 129.87 - 839.23\theta + 2234.05\theta^2 - 2721.18\theta^3 + 1645.30\theta^4 - 482\theta^5 + 54.67\theta^6$$

$$F_y = 14.37 - 89.46\theta + 235.14\theta^2 - 284.96\theta^3 + 171.90\theta^4 - 50.30\theta^5 + 5.7\theta^6$$

$$F_z = 18.83 - 108.07\theta + 172.37\theta^2 - 147.34\theta^3 + 59.31\theta^4 - 8.49\theta^5$$

$$M_x = -1.96 + 4.64\theta - 3.98\theta^2 + 0.98\theta^3$$

$$M_y = 37.07 - 305.37\theta + 1069.54\theta^2 - 1804.17\theta^3 + 1615\theta^4 - 782.5\theta^5 + 193.3\theta^6 - 12070\theta^7$$

$$M_z = -3.25 + 21.7\theta - 44.76\theta^2 + 39.06\theta^3 - 15.06\theta^4 + 2.12\theta^5$$

KNEE

$$F_x = -181.84 + 1614.4\theta - 8319.6\theta^2 + 24642.8\theta^3 - 45719.4\theta^4 + 55080.8\theta^5 - 43496\theta^6 + 22265.2\theta^7 - 7096.2\theta^8 + 1276.6\theta^9 - 98.8\theta^{10}$$

$$F_y = 24.49 - 118.54\theta + 419.19\theta^2 - 946.62\theta^3 + 1277.62\theta^4 - 1013.08\theta^5 + 459.4\theta^6 - 109.77\theta^7 + 10.69\theta^8$$

$$F_z = 9 - 435.75\theta + 3967.8\theta^2 - 16698.8\theta^3 + 37075.5\theta^4 - 48362\theta^5 + 39032.6\theta^6 - 19744\theta^7 + 6100.97\theta^8 - 1054.03\theta^9 + 78.08\theta^{10}$$

$$M_x = 9.81 + 18.46\theta + 51.29\theta^2 - 277.2\theta^3 + 460.44\theta^4 - 383.64\theta^5 + 174.28\theta^6 - 41.2\theta^7 + 3.97\theta^8$$

$$M_y = -74.7 + 498.11\theta - 1319.27\theta^2 - 5.44\theta^3 + 6165.2\theta^4 - 13011.5\theta^5 + 13303.16\theta^6 - 7943.69\theta^7 + 2762.49\theta^8 - 524.17\theta^9 + 41.94\theta^{10}$$

$$M_z = 5.34 - 21.84\theta + 40.42\theta^2 - 33.04\theta^3 + 11.90\theta^4 - 1.57\theta^5$$

Table 5

POLYNOMIAL EXPANSIONS FOR THE RESISTIVE FORCE & MOMENT COMPONENTS FOR THE HIP & ANKLE JOINTS

HIP ABDUCTION	$F_x = -5.91 - 64.79\phi - 125.91\phi^2 - 87.23\phi^3$ $F_y = 4.32 - 95.24\phi - 275.55\phi^2 - 287.55\phi^3 - 92.25\phi^4$ $F_z = 0.93 - 12.40\phi - 22.36\phi^2 - 19.52\phi^3$ $M_x = 0.98 + 15.13\phi + 29.84\phi^2 + 20.21\phi^3$ $M_y = -0.12 + 0.36\phi - 1.76\phi^2$ $M_z = -1.43 - 77.48\phi - 179.4\phi^2 - 148.97\phi^3 - 29.81\phi^4$
HIP ABDUCTION in the FRONTAL PLANE	$F_x = -0.92 + 6.03\theta - 19.41\theta^2 + 24.76\theta^3 - 11.78\theta^4$ $F_y = 12.60 - 25.15\theta + 38.10\theta^2 - 9.91\theta^3$ $F_z = 13.48 - 108.34\theta + 306.62\theta^2 - 309.89\theta^3 + 120.4\theta^4$ $M_x = 10.36 - 200.1\theta + 769.16\theta^2 - 1396.18\theta^3 + 1131.05\theta^4 - 333.37\theta^5$ $M_y = 1.57 - 13.14\theta + 26.37\theta^2 - 14.58\theta^3$ $M_z = 0.68 - 4.35\theta + 6.89\theta^2 - 4.25\theta^3$
ANKLE	$F_x = 440.71 - 1202.82\theta + 1343.57\theta^2 - 842\theta^3 + 315.96\theta^4 - 52.16\theta^5$ $F_y = -35.1 + 132.42\theta - 168.38\theta^2 + 86.7\theta^3 - 16.48\theta^4$ $F_z = -769.41 + 3575.15\theta - 6713\theta^2 + 6236\theta^3 - 2789.6\theta^4 + 485.4\theta^5$ $M_x = -8.86 + 26.16\theta - 25.05\theta^2 + 8.05\theta^3$ $M_y = 73.59 - 165.94\theta + 130.22\theta^2 - 36.9\theta^3$ $M_z = -10.56 + 27.39\theta - 21.29\theta^2 + 4.8\theta^3$

RESULTS ON PASSIVE RESISTIVE TORQUES

The second phase of our experimental program was to collect resistive torque data at the joints for the rotational motion of the body segments about their long bone axes. To achieve this task we designed and built different kinds of body segment shells as shown in Figs. 68, 70, 72, 74 and 76. For the shoulder, the hip and the knee joints the design of the shells is similar, i.e., they involve an "L" shape construction. For the shoulder joint the L is fitted to the upper arm and the lower arm by making the elbow joint at a 90° flexion. The same is done for the hip joint shell where the L is fitted to the upper and the lower leg. In the case of the knee joint the foot is fitted with an L shaped half boot covering the sides of the ankle and terminating above the malleoli. For the elbow and ankle torque measurements design of the shells was quite different from the ones mentioned above. The shell designed for the elbow torque measurements was fist fitted which covered most of the fist and had a sufficient opening to put the hand in it. The shell for the ankle was almost like a shoe with an opening at the toes region and some opening on the top. All the shells were made of heat formable plastic material and their strength was reinforced by fiberglass compound. To each shell a steel inverted T shape rail was also attached rigidly such that the top part of the T was buried by fiberglass to the shell, leaving only the lower part exposed. This exposed part was parallel to the lower arm in the shoulder shell, thus, perpendicular to the upper arm. When the force transducer is attached and aligned properly its axis coincides closely with the humeral axis as shown in Fig. 68. Similar statements apply to the other shells.

The plots of the passive resistive torques about the long bone axes for all three subjects are given in Figs. 69, 71, 73, 75 and 77. In all these torque versus angle of rotation plots, the value of ψ was obtained by adding incremental screw axis rotations, α, given in Eq. 3.17. In particular, Fig. 69 shows the behavior of the passive resistive torques about the upper arm (humeral) axis during the medial and lateral torque application on the upper arm. For this test the upper arm was oriented along the positive x direction and the zero value of the angle ψ

Fig. 68. Torque application on the upper arm along the ψ direction.
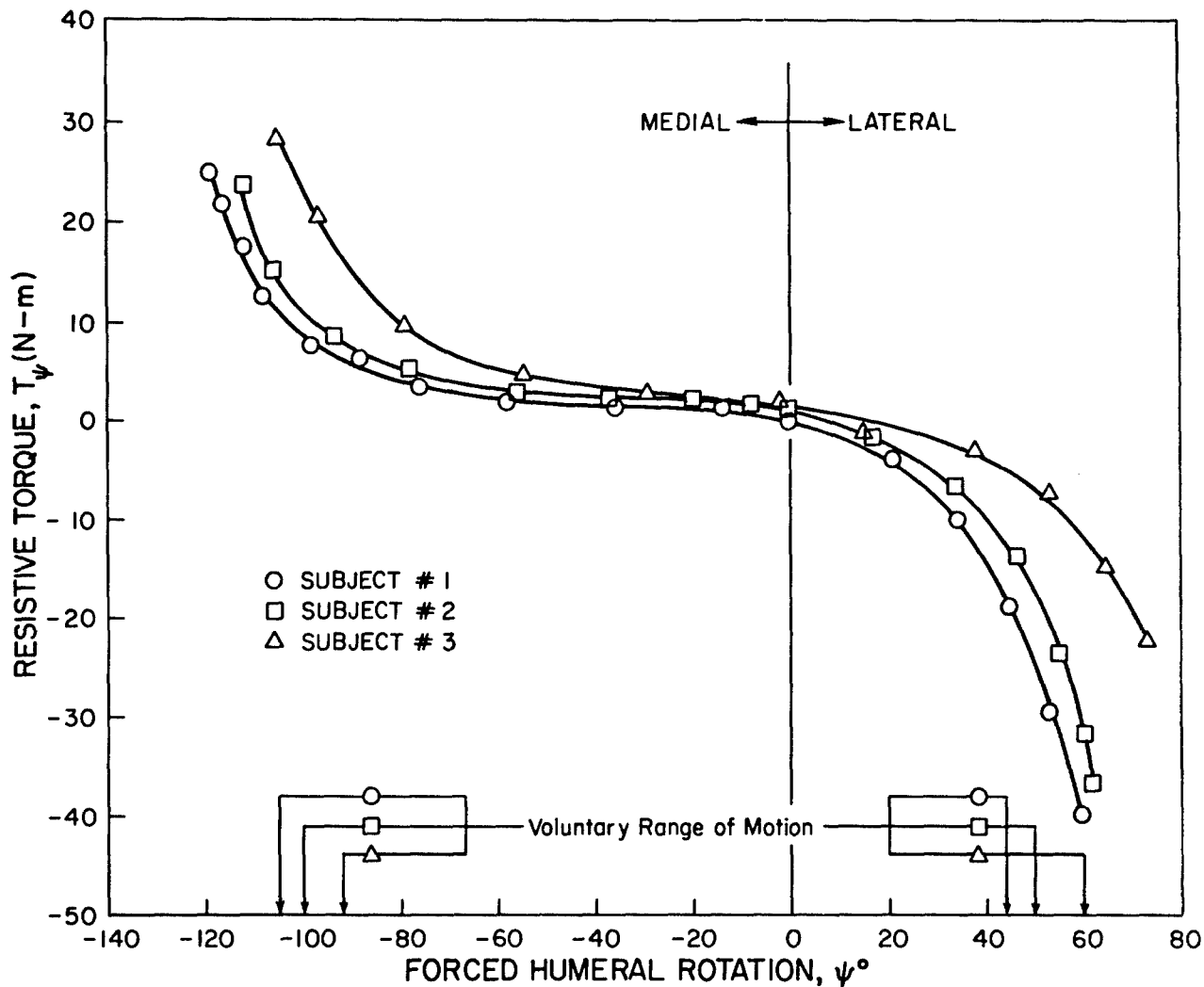
Fig. 69. Passive resistive torques about the humeral axis of the shoulder joint of the three subjects during the medial & lateral torque application on the upper arm.

Fig. 70. Torque application on the upper leg along the ψ direction.
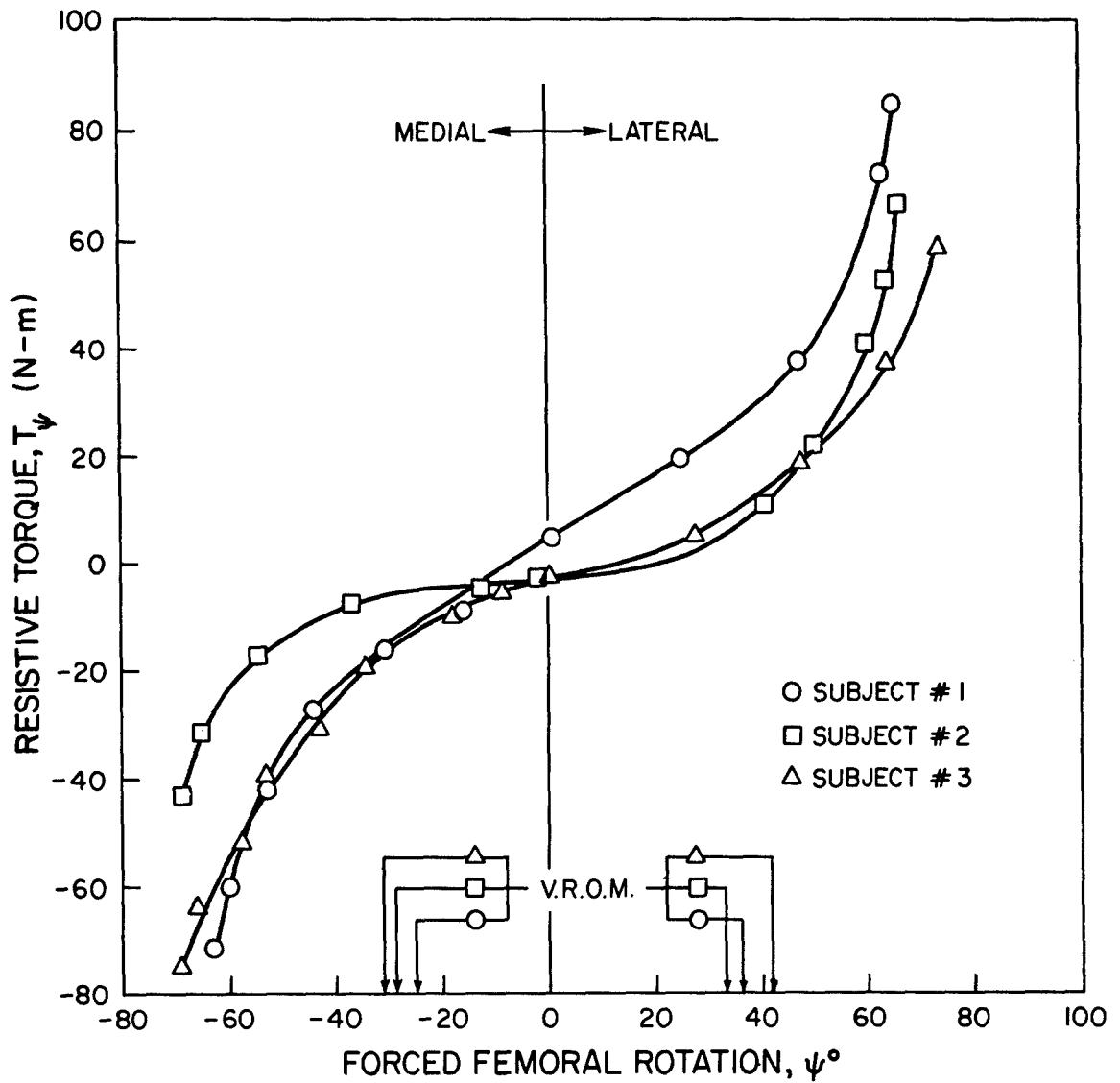
Fig. 71. Passive resistive torques about the femoral axis of the
hip joint of the three subjects during the medial & lateral
torque application on the upper leg.
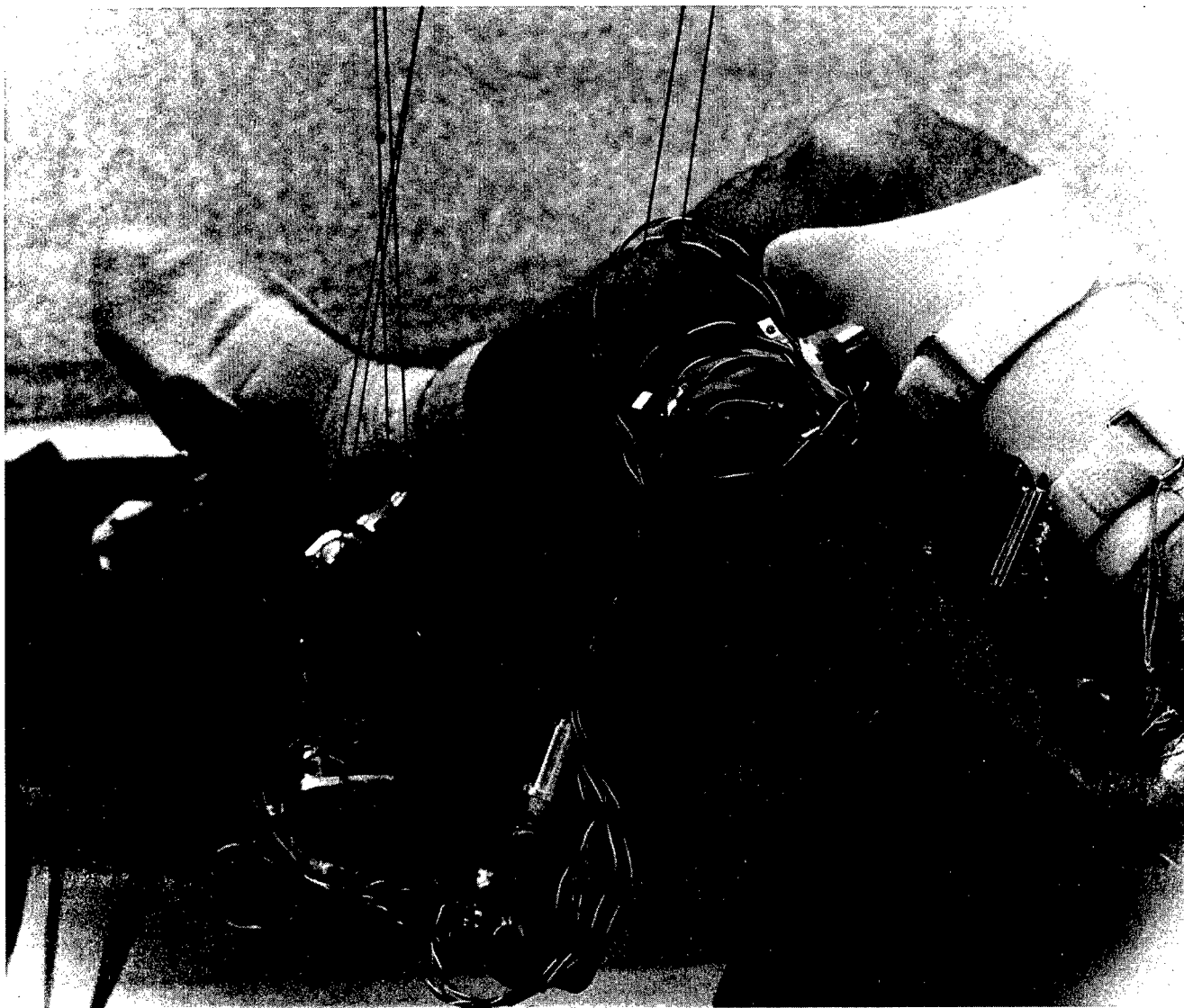
Fig. 72. Torque application on the lower leg along the ψ direction.
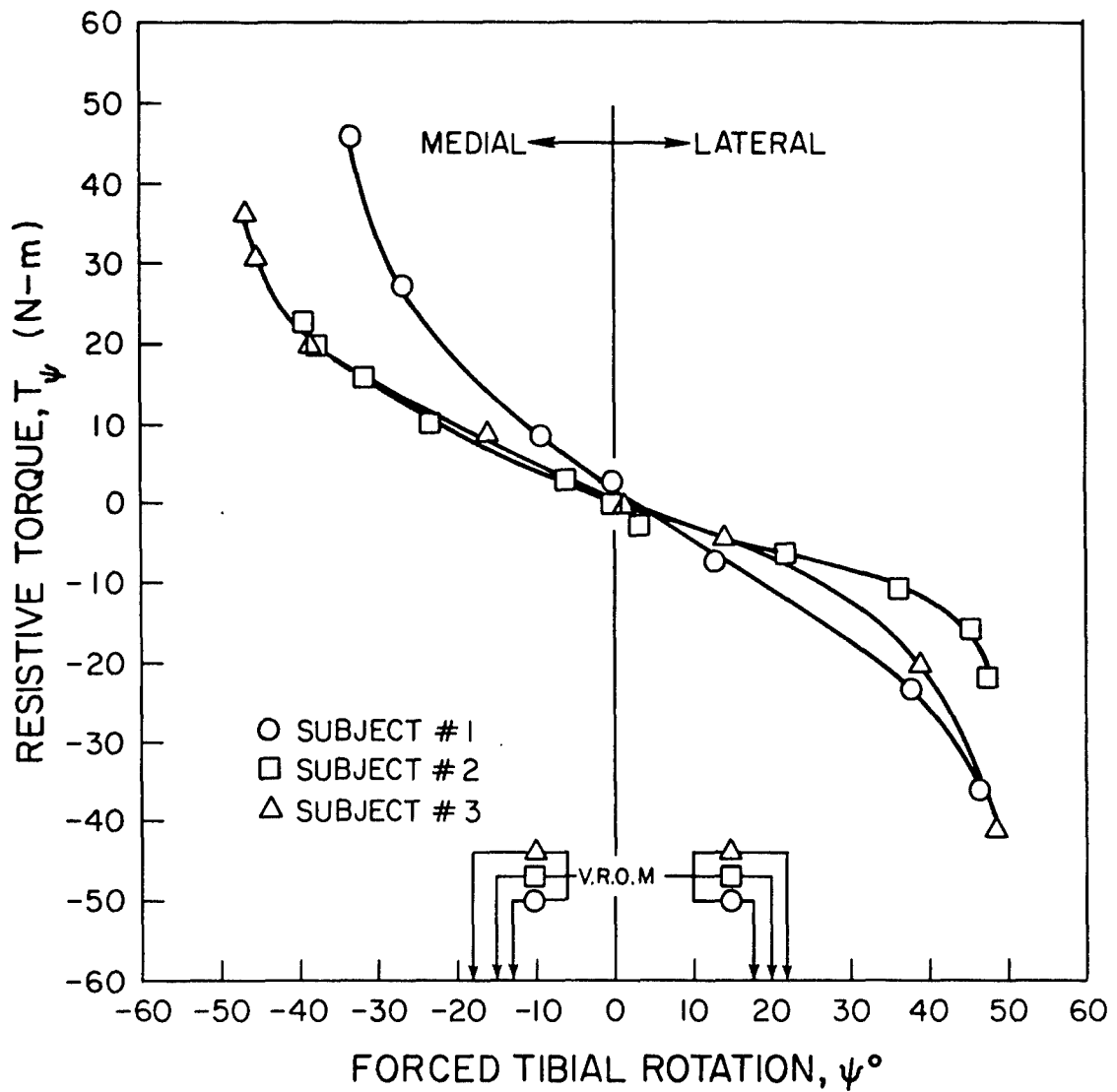
Fig. 73. Passive resistive torques about the tibial axis of the
knee joint of the three subjects during the medial & lateral
torque application on the lower leg.
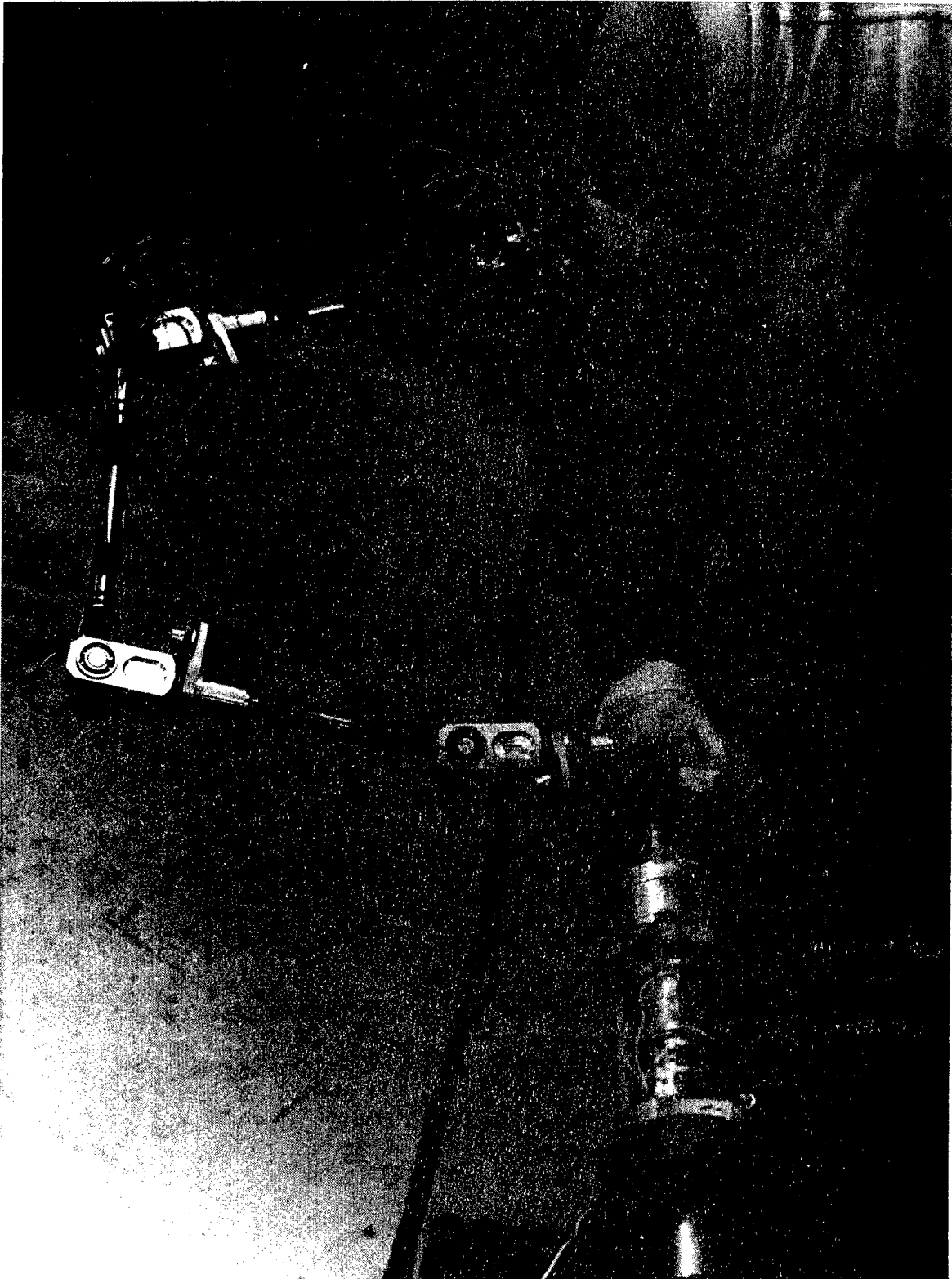
Fig. 74. Torque application on the fist along the ψ direction.
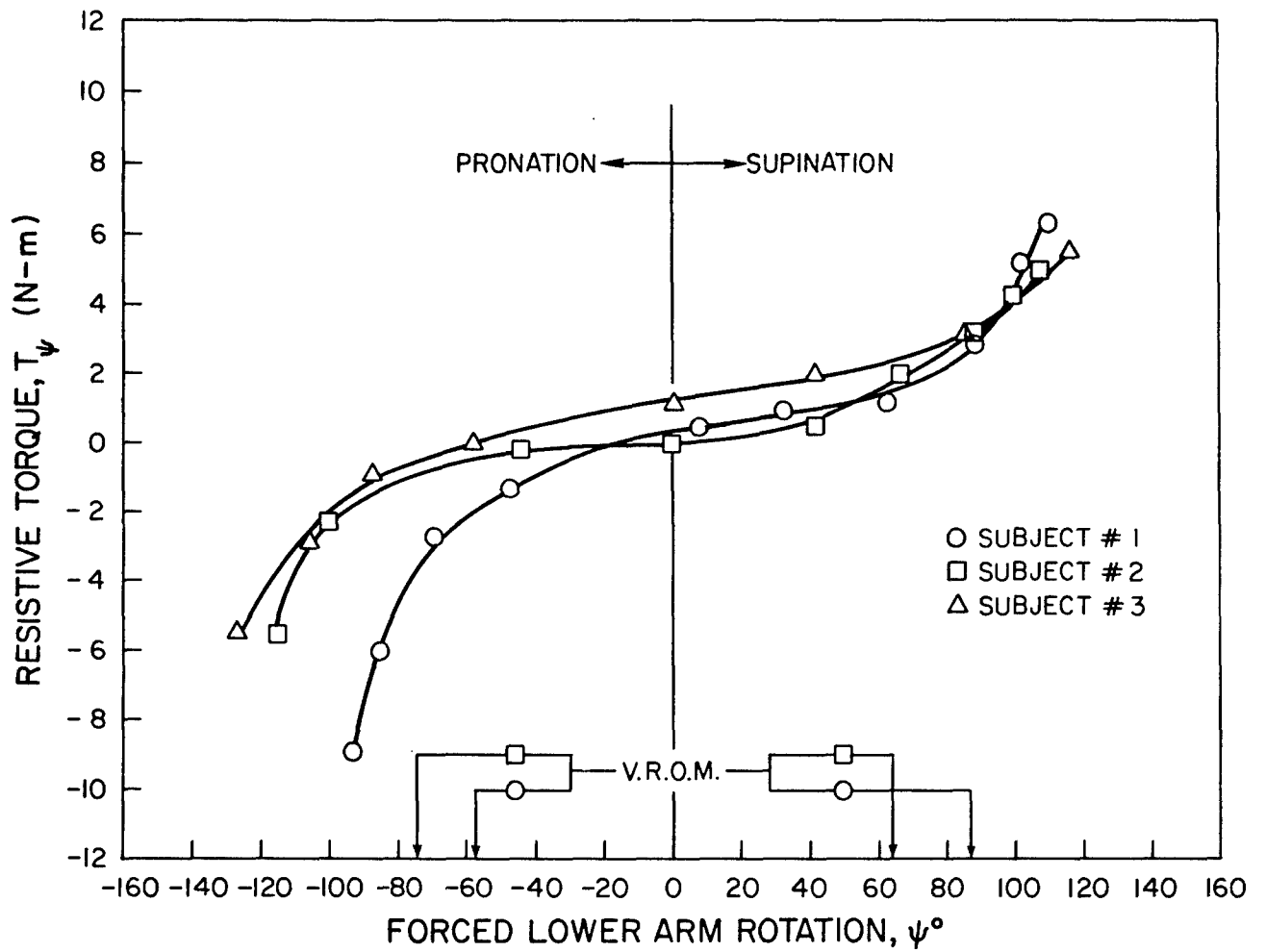
Fig. 75. Passive resistive torques about the radius-ulna axis of the elbow joint of the three subjects during the pronation & supination torque application.
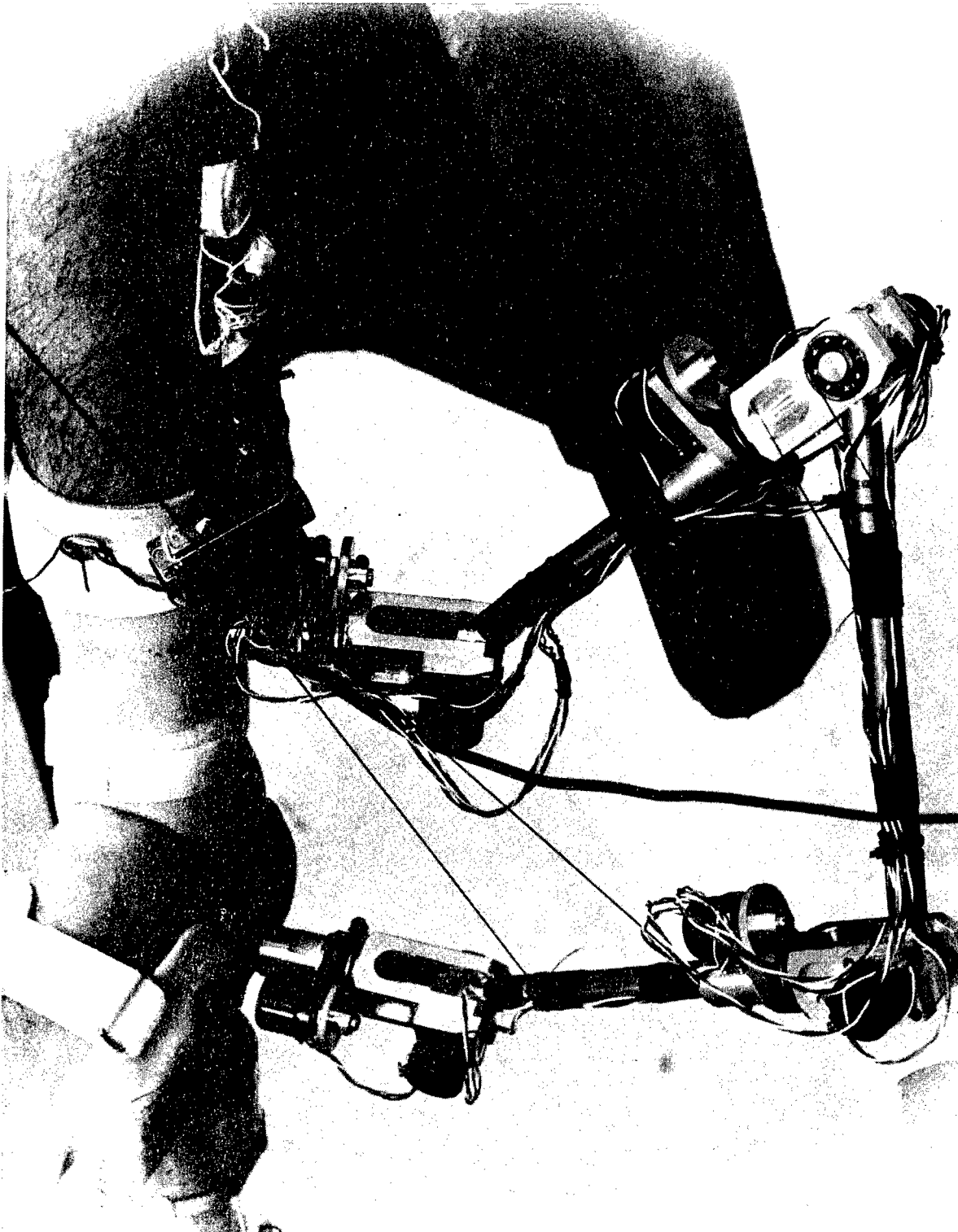
Fig. 76. Torque application on the foot along the ψ direction.
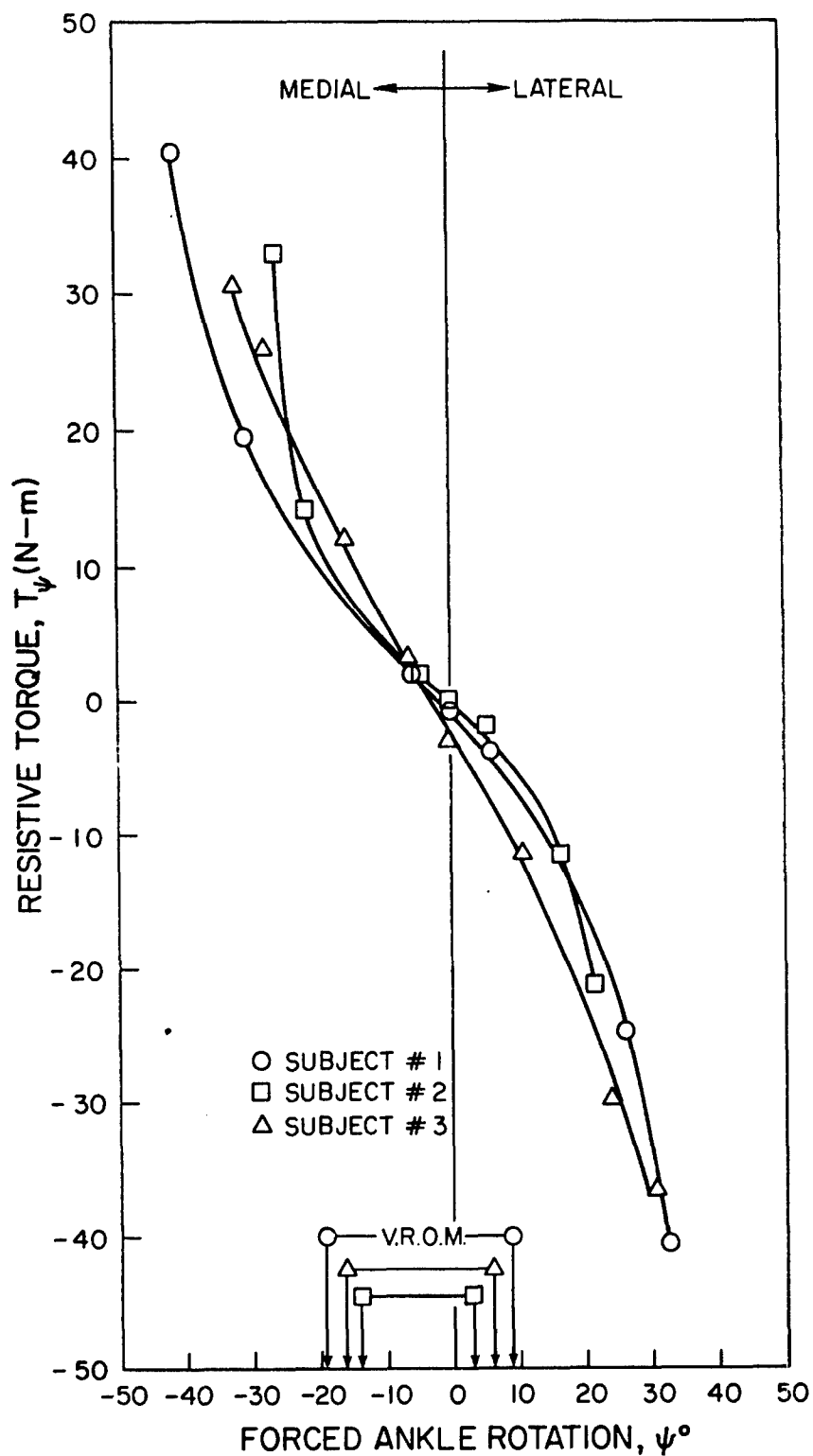
Fig. 77. Passive resistive torques for the ankle rotation of the three subjects during the medial & lateral torque application.

112

Table 6

POLYNOMIAL EXPANSIONS FOR THE RESISTIVE TORQUES ABOUT THE LONG BONE AXES

SHOULDER	#1	$T_\psi = 0.485 - 5.140\psi - 11.778\psi^2 - 12.894\psi^3 - 4.722\psi^4 - 0.652\psi^5 - 0.731\psi^6 - 0.422\psi^7$
SHOULDER	#2	$T_\psi = 1.456 - 5.627\psi - 11.104\psi^2 - 5.259\psi^3 + 3.766\psi^4 - 2.119\psi^5 - 5.834\psi^6 - 2.055\psi^7$
SHOULDER	#3	$T_\psi = 1.626 - 4.433\psi - 0.397\psi^2 + 0.752\psi^3 - 4.767\psi^4 - 4.506\psi^5 + 1.106\psi^6 + 0.825\psi^7$
HIP	#1	$T_\psi = 4.438 + 26.018\psi + 3.838\psi^2 + 63.355\psi^3 - 12.096\psi^4 - 100.87\psi^5 + 5.341\psi^6 + 62.637\psi^7$
HIP	#2	$T_\psi = -1.693 + 9.685\psi + 6.398\psi^2 + 11.649\psi^3 - 5.031\psi^4 - 10.44\psi^5 + 7.956\psi^6 + 15.65\psi^7$
HIP	#3	$T_\psi = -2.391 + 11.017\psi - 11.711\psi^2 + 51.398\psi^3 + 6.995\psi^4 - 40.70\psi^5 - 2.442\psi^6 + 16.47\psi^7$
KNEE	#1	$T_\psi = 2.289 - 42.265\psi - 8.814\psi^2 + 15.245\psi^3 + 120.561\psi^4 - 167.807\psi^5$
KNEE	#2	$T_\psi = -0.347 - 26.777\psi + 14.940\psi^2 + 39.227\psi^3 - 5.615\psi^4 - 71.967\psi^5$
KNEE	#3	$T_\psi = 1.303 - 25.870\psi - 1.783\psi^2 + 22.756\psi^3 + 0.381\psi^4 - 72.433\psi^5$
ELBOW	#1	$T_\psi = 0.198 + 1.283\psi + 0.036\psi^2 - 0.189\psi^3 - 0.429\psi^4 + 0.423\psi^5$
ELBOW	#2	$T_\psi = -0.116 + 0.548\psi + 1.079\psi^2 + 0.024\psi^3 - 0.248\psi^4 + 0.136\psi^5$
ELBOW	#3	$T_\psi = 1.233 + 0.925\psi - 0.035\psi^2 + 0.086\psi^3 - 0.021\psi^4 + 0.065\psi^5$
ANKLE	#1	$T_\psi = -0.776 - 28.679\psi - 14.189\psi^2 - 50.974\psi^3 - 32.918\psi^4 - 99.039\psi^5$
ANKLE	#2	$T_\psi = 0.653 - 22.523\psi - 62.427\psi^2 + 14.139\psi^3 + 244.363\psi^4 - 1329.89\psi^5$
ANKLE	#3	$T_\psi = -2.222 - 45.452\psi - 13.315\psi^2 - 143.47\psi^3 + 28.554\psi^4 + 305.67\psi^5$

113

corresponds to 45° medially rotated (θ = 135°) lower arm position. The
passive resistive torques about the femoral axis are shown in Fig. 71.
The orientation of the upper leg was along the positive x direction and
the zero value of ψ corresponds to the lower leg orientation along the
positive z axis (θ = 0°). During most of these torque tests, and
especially for the hip torques for which the values are relatively high,
one or two degrees (not more than two percent of the total range of the
forced motion) of shell rotation with respect to the body segments were
observed at the torqued limits of the motion. Of course, this was a
direct consequence of applying the torque on the shell.

In Fig. 73 passive resistive torques about the tibial axis for 90°
of knee flexion are plotted. The same is done for 90° of elbow flexion
for the torques about the lower arm in Fig. 75. Fig. 77 shows the
torques for the ankle rotation. In regards to the knee and the elbow
torques the following statement applies. The boundaries of the forced
motion for both plots may contain some ankle motion in the case of the
knee torques and some wrist motion in the case of the elbow torques.
This extraneous motion was carefully monitored and we tried to minimize
it if it were observed. Of course, working with live subjects one can not
fix pins through the bones; even with this obvious and some other
restrictions we feel in vivo test results are more realistic than the
in vitro ones. Finally, polynomial expansions for the resistive torques
about the long bone axes for all the three subjects are presented in
Table 6. T_ψ functions in this table approximate in the least square
sense the data and the curves shown in the figures; the units are N-m for
the T_ψ and radians for ψ.

RESULTS ON ACTIVE RESISTIVE FORCE, MOMENT AND TORQUES

Thus far, we presented results on the passive resistive force,
moment and torques. In this last section we will present some results in
tabular form for the magnitudes of the active resistive muscle force,
moment and torque vectors. In Table 7 the results of three test runs for
each subject are tabulated for four positions of the arm. For position
#1 the subject in seated position kept his arm in such a way that his
hand was close to his crotch and he applied muscle force about 5 seconds

Table 7

MAGNITUDES OF THE ACTIVE RESISTIVE MUSCLE FORCE & MOMENT
VECTORS AT THE SHOULDER JOINTS OF THREE SUBJECTS

ARM POSITION	MAGNITUDE	SUBJECT #1	SUBJECT #2	SUBJECT #3
POSITION #1	FORCE (N)	113.40 118.30 120.40	112.00 127.41 136.51	104.30 147.02 155.42
	MOMENT (N-m)	47.15 49.00 49.18	38.73 46.13 52.32	37.41 57.59 57.70
POSITION #2	FORCE (N)	102.90 113.40 131.61	160.32 179.93 202.34	121.10 122.50 179.23
	MOMENT (N-m)	39.41 43.41 50.80	45.35 50.72 59.75	38.03 39.06 58.03
POSITION #3	FORCE (N)	140.01 163.82 198.14	144.91 147.02 160.32	138.61 151.92 177.83
	MOMENT (N-m)	49.38 57.76 68.93	55.15 56.84 62.29	56.29 62.28 69.48
POSITION #4	FORCE (N)	153.32 163.82 169.42	122.50 154.02 163.82	128.81 137.91 160.32
	MOMENT (N-m)	43.02 43.49 45.03	21.23 26.47 31.74	23.66 25.21 27.87

115

approximately along the negative y direction, i.e. medially, on the force cuff of the GFA which was placed in the y direction on the lower arm about 10 cm away from the wrist. For position #2 everything was the same as in position #1 except the elbow flexion was changed to 90° and the upper arm took the natural along the torso position. For position #3 the subject extended his arm laterally along the y direction and exerted force along the x direction on the force cuff of the GFA which was again placed about the same location on the lower arm in the negative x direction. This position simulates the wind blast condition on the arm. For position #4 the subject flexed his elbow and brought his hand toward the lateral side of his face as if he were holding the face curtain of his helmet. At this position he applied a force in the negative y direction on the force cuff of the GFA which was placed on the lower arm very close to the elbow joint.

Magnitudes of the muscle torques about the axes of the long bones which are connected to the joints are tabulated in Tables 8-10. In these tables the maximum torque magnitudes of three test runs for each subject are tabulated according to their values. The duration of the torque application by the subject in the directions indicated at the tables was about 5 seconds. In table 8 magnitudes of the active muscle torques about the humeral axis for various positions of the upper arm are tabulated. The positions indicated in the first column of this table describe the angular ψ orientation of the upper arm whose axis remains fixed parallel to the x direction for all positions. The initial condition of the upper arm was defined such that the lower arm was parallel to the z axis. The other positions refer to this initial condition. With the exception of the limits of the motion for each position of the upper arm, subjects applied torques along the long bone axes both in the medial and lateral directions.

In table 9, magnitudes of the active muscle torques about the femoral axis for the hip and the tibial axis for the ankle joints are shown. For the hip torques the orientation of the upper leg was along the x direction and the initial condition for the value of ψ corresponds to the lower leg orientation along the z axis. Finally, magnitudes of

Table 8

MAGNITUDES OF THE ACTIVE MUSCLE TORQUES ABOUT THE HUMERAL
AXIS FOR VARIOUS POSITIONS OF THE UPPER ARM (N-m)

BODY SEGMENT POSITION	TORQUE APPLICATION DIRECTION BY SUBJECT	SUBJECT #1	SUBJECT #2	SUBJECT #3
UPPER ARM AT THE INITIAL CONDITION	MEDIAL	54.19 58.90 79.45	71.65 72.63 87.16	37.90 50.83 50.93
UPPER ARM AT THE INITIAL CONDITION	LATERAL	20.96 21.88 27.92	6.36 11.66 21.87	37.52 37.68 42.30
UPPER ARM 30° MEDIALLY ROTATED	MEDIAL	55.00 62.83 65.48	59.77 60.75 72.53	31.29 33.05 54.89
UPPER ARM 30° MEDIALLY ROTATED	LATERAL	33.07 33.35 34.36	28.26 29.86 31.23	51.66 52.61 56.41
UPPER ARM 90° MEDIALLY ROTATED	MEDIAL	41.89 44.01 44.11	56.00 58.59 59.96	38.06 39.41 42.19
UPPER ARM 90° MEDIALLY ROTATED	LATERAL	45.50 46.61 51.12	29.04 31.82 33.72	28.03 30.68 37.29
UPPER ARM ROTATED TO THE MEDIAL LIMIT	LATERAL	38.44 40.46 40.85	19.52 25.24 26.88	28.12 32.25 33.07

117

Table 9

MAGNITUDES OF THE ACTIVE MUSCLE TORQUES ABOUT THE FEMORAL AXIS
FOR THE HIP AND ABOUT THE TIBIAL AXIS FOR THE ANKLE (N-m)

BODY SEGMENT POSITION	TORQUE APPLICATION DIRECTION BY SUBJECT	SUBJECT #1	SUBJECT #2	SUBJECT #3
UPPER LEG AT THE INITIAL CONDITION	MEDIAL	66.13 66.23 70.83	43.44 48.49 61.78	44.23 62.56 65.44
UPPER LEG AT THE INITIAL CONDITION	LATERAL	86.49 113.38 116.74	68.70 71.45 74.33	84.91 112.50 136.07
UPPER LEG 30° MEDIALLY ROTATED	MEDIAL	47.50 47.97 59.60	43.64 48.75 51.04	34.93 35.52 59.48
UPPER LEG 30° MEDIALLY ROTATED	LATERAL	92.45 124.71 131.14	62.22 64.58 68.38	80.16 136.01 154.53
UPPER LEG ROTATED TO THE MEDIAL LIMIT	LATERAL	121.64 124.91 139.21	55.67 72.24 75.77	120.88 112.50 126.91
UPPER LEG ROTATED TO THE LATERAL LIMIT	MEDIAL	76.32 77.36 80.72	36.37 44.30 48.94	123.97 135.49 143.28
FOOT AT THE INITIAL CONDITION	MEDIAL	41.92 47.11 50.38	17.83 23.40 25.36	58.16 65.04 74.14
FOOT AT THE INITIAL CONDITION	LATERAL	30.11 30.68 32.04	20.99 22.49 24.52	52.61 58.63 61.78

Table 10

MAGNITUDES OF THE ACTIVE MUSCLE TORQUES ABOUT THE TIBIAL AXIS
FOR THE KNEE AND ABOUT THE LOWER ARM AXIS FOR THE ELBOW (N-m)

BODY SEGMENT POSITION	TORQUE APPLICATION DIRECTION BY SUBJECT	SUBJECT #1	SUBJECT #2	SUBJECT #3
LOWER LEG AT THE INITIAL CONDITION	MEDIAL	42.88 45.58 48.35	16.20 16.20 19.14	50.50 61.11 64.19
LOWER LEG AT THE INITIAL CONDITION	LATERAL	47.68 49.80 50.87	24.85 31.86 35.00	43.25 54.05 55.69
LOWER LEG ROTATED TO THE LATERAL LIMIT	MEDIAL	36.92 - -	23.07 25.17 32.24	43.63 46.71 49.59
LOWER LEG ROTATED TO THE MEDIAL LIMIT	LATERAL	55.47 - -	31.07 35.65 41.81	63.94 93.14 101.78
LOWER ARM AT THE INITIAL CONDITION	PRONATION	12.15 13.30 13.79	11.56 11.95 13.13	12.41 15.82 16.41
LOWER ARM AT THE INITIAL CONDITION	SUPINATION	18.20 18.96 19.46	7.69 7.82 8.28	16.20 20.71 20.78
LOWER ARM AT 90° SUPINATION	PRONATION	18.78 22.05 22.91	14.25 14.97 16.93	13.53 14.77 15.03
LOWER ARM AT 90° PRONATION	SUPINATION	21.95 26.16 29.35	14.17 17.18 20.78	18.23 22.81 25.10

the active muscle torques about the tibial axis for the 90° of knee flexion and about the lower arm axis for 90° of elbow flexion are tabulated in Table 10. For the elbow joint torques the initial condition of the lower arm was defined in such a way that the unit normal vector to the palm of the subject was along the y direction. The rest of the table is self-explanatory.

CONCLUDING REMARKS

The research work discussed and presented in this report was performed on live subjects with some obvious limitations. The immediate application of these results is the development of more realistic joint models for the articulated total body models of the human body. Although the resistive force and moment values which are displayed by the figures of the previous section are relatively low, they provide sufficient data for extrapolation beyond the test regions. Near the boundaries of the test regions the critical item of interest is the rate of change of the slopes of curves. For example, if we represent the predominant moment component, M_y, of the knee joint by a tenth degree least squares polynomial as shown in Table 4, the value of M_y, for an additional two degrees of knee flexion beyond the forced range, increases more than three times the maximum test value. Of course, extrapolated values corresponding to a very small change in extension angles for the locked joint conditions that occur at some joints, should easily reach to values which are an order of magnitude higher than those obtained from experiments, provided suitable expansion functions are introduced. One of the primary tasks of the joint modeling is the distribution of the passive resistive force and moments as forces on the bony structure and various ligaments of the joint. One can expect that the total number of unknowns, i.e., contact and ligaments forces, will exceed the number of equations that can be written for each joint; thus, the problem becomes indeterminate. The solution of this indeterminate problem requires more research on the subject matter.

Although one can base the development of the joint models on data which are collected on human subjects by means of quasi-static testing of the joints, these joint models must somehow reflect dynamic and

viscoelastic effects since their final application is on the articulated total body model of the human body. It is a well established fact that biological materials display strain rate sensitivity of varying magnitudes. Thus, the force response of a ligament at a given strain level will be different at different rates of loading; in general, the higher the rate of loading, the higher the magnitude of force. There are only a very few studies reported in the literature which deal with strain rate effects on ligaments. One must investigate their applicability on the modeling task or at least get some indications about the type of modifications one can make on the quasi-static data so that they can be more suitably applied for dynamic situations.

Finally, substantially more experimental data and modeling efforts are needed on the long bone fractures and joint dislocations. Research must be conducted on cadavers as well as on primates. The strength and fracture data obtained from primates should be appropriately scaled to humans so that models which have the capability of predicting fractures and dislocations in long bones and major articulating joints can be developed.

APPENDIX A

SUBJECT RESTRAINT SYSTEM

RESTRAINT SYSTEM DESIGN CRITERION

The restraint system consists of, in the global sense, a chair to
provide subject support and, in the local sense, segmental support forms
along with a space framework to aid the support of the body segments
associated with the joint under consideration. The design of the subject
support and segmental support forms is governed first by safety. The
subject must be firmly supported in such a way that the security of the
restraint system allows total relaxation and the external force appli-
cation is performed on a particular body segment by the method prescribed
in the main part of this report. The head, torso and legs should be
firmly supported by the segmental support forms for the subject will be
in various abnormal seating positions for extended periods of time. To
fit the broad subject population, an adaptable seat form must be
constructed. It must reasonably fit the full range of population
differences in a similar manner without crowding or stretching either end
of the anthropometric range. The angular velocity and accelerations of
the chair motion should be low enough so as not to shock the subject
during positioning.

To provide easy experimental procedure for the experimenters, it is
wise to reduce the physical effort required to position the subject at
the various positions which are required to examine the entire joint
range of motion in a horizontal or gravity negating mode. During force
application on a particular body segment, constant elevation support
assures a relaxed floating type of motion of the body segment in addition
to elimination of the gravitational moment component at the joint under
consideration.

DESIGN ITERATION

Several methods were examined starting with the simplest concept of a balanced polar mount (similar to a telescope mount). The obvious variation of subject weights in the population would necessitate a variable balance weight and the large size of the device required to support such a mass would be very cumbersome. With the goal of fitting through a conventional door without disassembly, a search for various mechanical positioning devices was commenced.

Hydraulic actuators for units such as dentist or barber chairs do not provide the type of motion we require, and therefore were eliminated. Commercially available industrial hydraulic actuators were examined and found to be of limited length or strength or of excessive price. The cost of a hydraulic power supply (i.e. integral, pump, motor, reservoir, accumulator) was prohibitive. In addition, no automatic positioning would have been possible without the use of servo control which would have added more to the basic cost. The final drawback was the difficulty of efficiently converting linear hydraulic powered motion from a cylinder into rotation about an axis. Slider-crank mechanisms have non-linear torque output over their possible range of motion. Attempts to power the necessarily large cylinders with a hydraulic hand pump would require excessive pumping to get a very small chair motion and was therefore eliminated.

FINAL DESIGN

The final design choice for the drive mechanism of the chair was made to be an electro-mechanical device with a double worm gear train. The gear train provides 800 to 1 reduction; thus, a 1725 rpm motor speed is reduced to little over 2 rpm. This speed is low enough to be comfortable for the subject but would allow the full traverse of the range desired in eight seconds. This means that incremental positionings will take approximately 12°/sec. Furthermore, this design lended itself to low voltage hand held controls which actuate power and reversing relays. Positional control is also facilitated by the easy introduction of limit switches and positional stops at incremental pitch and yaw angles. This also allowed consistent positioning of the chair to

eliminate positioning variation both intra and inter subject wise.
Figure 78 shows a schematic overall view of the subject restraint system.

To firmly and comfortably secure the subject, a segmental fiberglass
seatform which can be adjusted to fit various size subjects was designed
and fabricated. The segmental forms support the head, ribcage below the
scalpula, hips, and legs as units. The design of the chair allows body
width, seated height, torso diameter, leg length and torso support to be
adjusted. The hip and leg supports have right and left sections so that
the hip joint can be tested by removing one of the sections. In addition
to these segmental forms both torso and hip belts are provided, not shown
in Fig. 78 but can be seen in Fig. 79 which shows an overall view of the
subject restraint system with a subject.

To provide support for the moving body segment associated with the
joint under test, an expanded metal grid was suspended from the ceiling
of the biomechanics laboratory. A support cable containing a force
transducer was attached to the grid at a suitable point determined
according to the location of the joint.
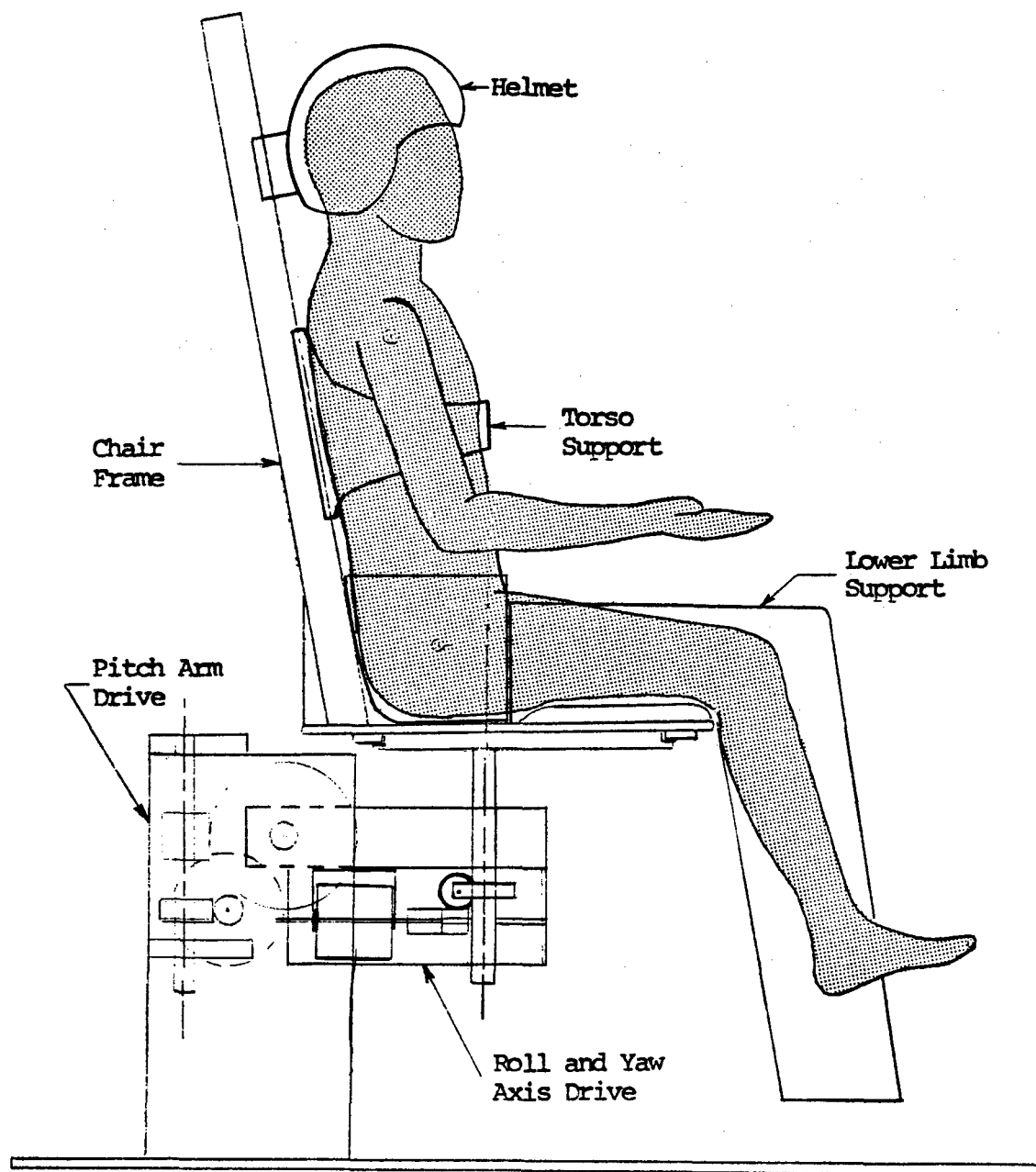
Fig. 78. Schematic view of the subject restraint system.
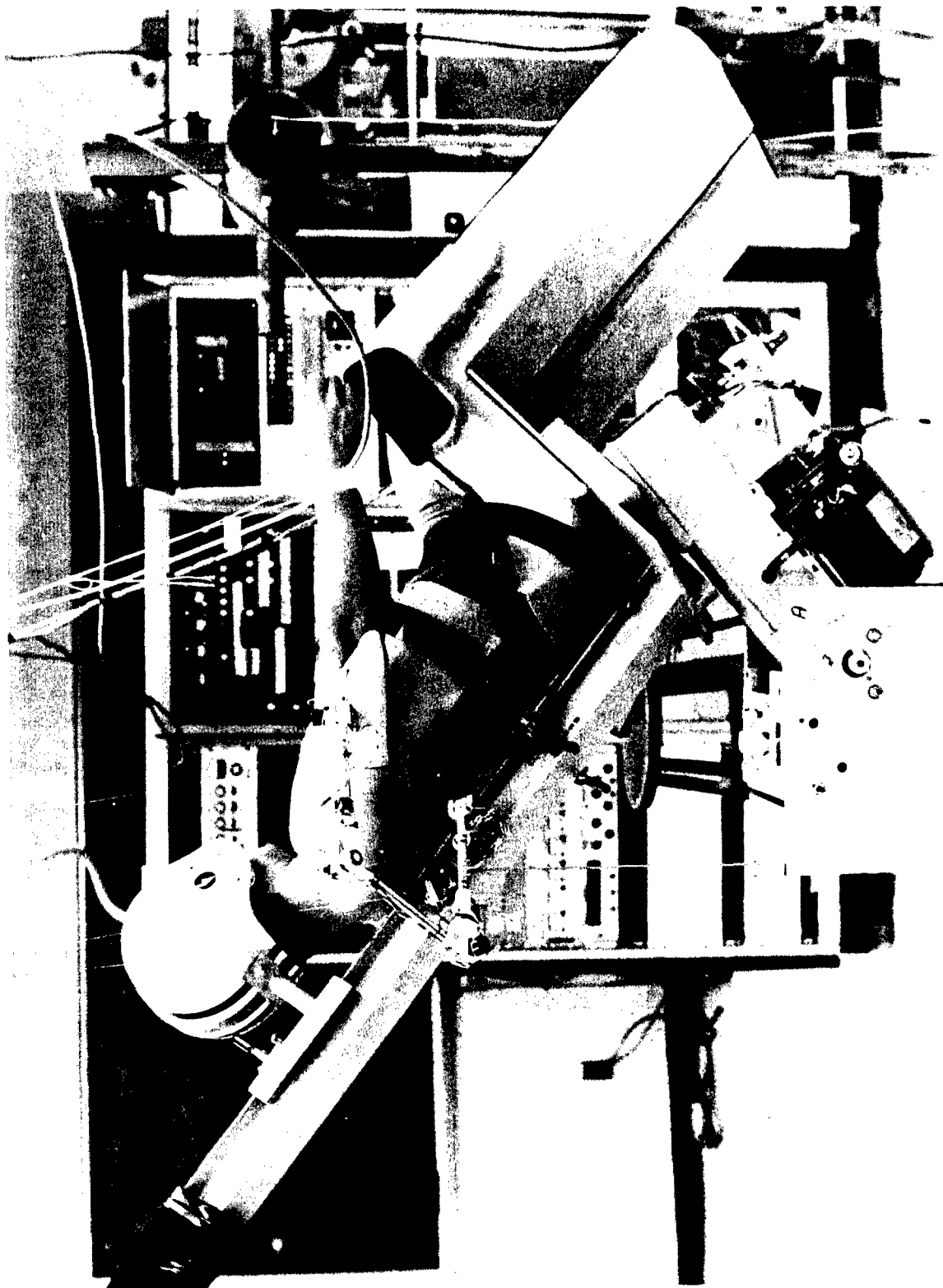
Fig. 79. Overall view of the subject restraint system with a subject.

GLOBAL FORCE APPLICATOR (GFA) & FORCE TRANSDUCER

The global force applicator (GFA) consists of a series of four moving links attached together with four polar joints. The first mobile link is attached to a fixed link secured to the floor of the laboratory and the last mobile link is terminated with a force transducer and a force cuff as shown in Fig. 80. Each polar joint is made of two precision potentiometers whose outputs along with those of the other joints as well as the length dimensions of the links are utilized to perform two functions; (1) to determine the direction of the force application, and (2) to determine the location of the force application on the body segment with respect to the inertial coordinate system.

DETERMINATION OF THE DIRECTION OF THE FORCE APPLICATION

Referring to Fig. 80, we establish that rotations about the x_i ($i = 1,2,3,4$) axes are given as θ_i, and rotations about the z_i axes are given as ϕ_i. We can consider that the initial configuration of the GFA has all of the axis systems, formed by the four polar-hinge joints, parallel to each other and to the inertial coordinate system X,Y,Z. A rotation about the z axis can be written as,

$$\begin{bmatrix} x_1' \\ y_1' \\ z_1' \end{bmatrix} = [D_1] \begin{bmatrix} x_1 \\ y_1 \\ z_1 \end{bmatrix} \tag{B1a}$$

where the transformation matrix $[D_1]$ is found to be

$$[D_1] = \begin{bmatrix} \cos\phi_1 & \sin\phi_1 & 0 \\ -\sin\phi_1 & \cos\phi_1 & 0 \\ 0 & 0 & 1 \end{bmatrix} \tag{B1b}$$
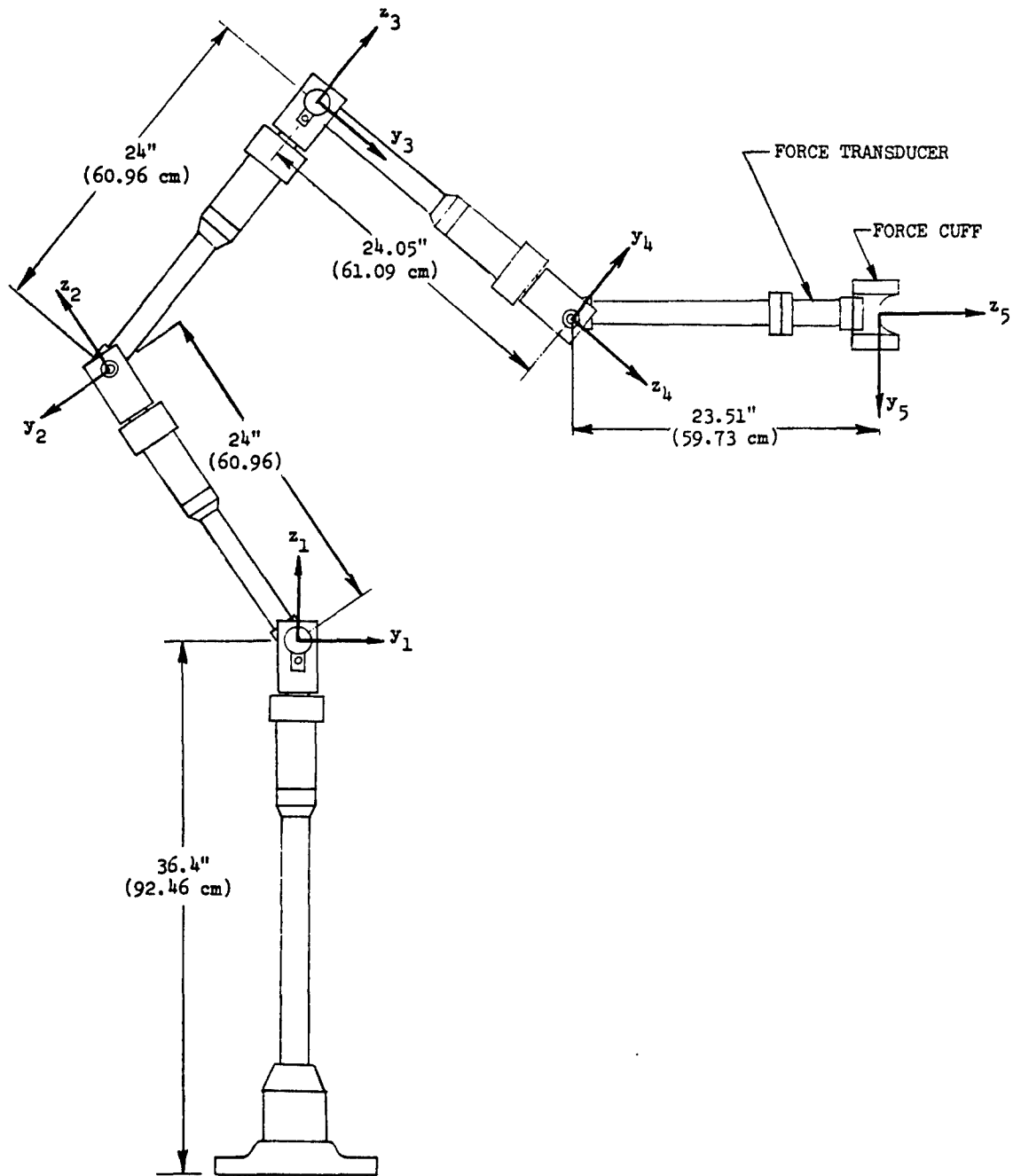
Fig. 80. Schematic drawing of the global force applicator

Likewise, a rotation about the x_1' axis is written as:

$$\begin{bmatrix} x_2 \\ y_2 \\ z_2 \end{bmatrix} = [D_2] \begin{bmatrix} x_1' \\ y_1' \\ z_1' \end{bmatrix} \tag{B2a}$$

where $[D_2]$ is

$$[D_2] = \begin{bmatrix} 1 & 0 & 0 \\ 0 & -\cos\theta_1 & \sin\theta_1 \\ 0 & -\sin\theta_1 & \cos\theta_1 \end{bmatrix} \tag{B2b}$$

Therefore, the new axis system $x_2 y_2 z_2$ can be related to the $x_1 y_1 z_1$ axis system by the transformation matrix formed by $[D_1]$ and $[D_2]$ as shown below:

$$\begin{bmatrix} x_2 \\ y_2 \\ z_2 \end{bmatrix} = [D_2][D_1] \begin{bmatrix} x_1 \\ y_1 \\ z_1 \end{bmatrix} \tag{B3}$$

We can use the same method to show that for the other joints, the relative orientation of consecutive axis systems is always given as:

$$\begin{bmatrix} x_{i+1} \\ y_{i+1} \\ z_{i+1} \end{bmatrix} = \begin{bmatrix} \cos\phi_i & \sin\phi_i & 0 \\ -\sin\phi_i\cos\theta_i & \cos\phi_i\cos\theta_i & \sin\theta_i \\ \sin\phi_i\sin\theta_i & -\cos\phi_i\sin\theta_i & \cos\theta_i \end{bmatrix} \begin{bmatrix} x_i \\ y_i \\ z_i \end{bmatrix} \tag{B4}$$

Let us call the above transformation matrix the $[K_i]$ matrix. Hence, the final orientation of the force applicator with respect to the inertial reference system XYZ can be given as

$$\begin{bmatrix} x_5 \\ y_5 \\ z_5 \end{bmatrix} = [K_5][K_4][K_3][K_2][K_1] \begin{bmatrix} x_1 \\ y_1 \\ z_1 \end{bmatrix}$$

We will define the overall transformation matrix formed by the product of the $[K_i]$ matrices as the $[L]$ matrix, and then Eq. (B5) becomes

$$\begin{bmatrix} x_5 \\ y_5 \\ z_5 \end{bmatrix} = [L] \begin{bmatrix} x_1 \\ y_1 \\ z_1 \end{bmatrix} \tag{B6}$$

The matrix $[L]$ is a 3 x 3 matrix, and since we are only concerned about the direction along the axis of the force application, we need to consider only the third row of the matrix $[L]$. This gives us

$$z_5 = (L_{31} \; L_{32} \; L_{33}) \begin{bmatrix} x_1 \\ y_1 \\ z_1 \end{bmatrix} \tag{B7}$$

where L_{ij} denotes the elements of the matrix $[L]$. The direction of force application has now been determined with respect to the inertial reference system. Note that in general the force vector may have transverse components along the x_5 and y_5 directions, hence, z_5 and the direction of the force vector will not coincide. However, the design of the force transducer is such that these transverse force components are also known; thus, the precise orientation of the force vector can be determined with respect to the z_5 direction.

DETERMINATION OF THE LOCATION OF THE FORCE APPLICATION

If we consider the links of the GFA as vectors in space, we can then determine the position of the force cuff in the inertial reference system. Referring to Fig. 81, we find the position of the force application ($\vec{r}_5$), with respect to a given point 0, by adding the vectors $\vec{r}_1$, $\vec{A}$, $\vec{B}$, $\vec{C}$ and $\vec{D}$. Let $\vec{r}_1$ be the position vector which locates the first joint (point P) in the inertial reference system XYZ. Then we have

$$\vec{r}_1 = x_p \hat{i} + y_p \hat{j} + z_p \hat{k} \tag{B8}$$

130
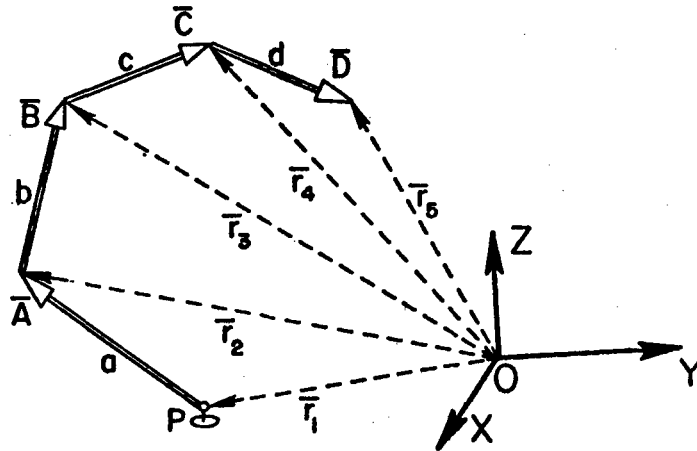
Fig. 81. Vector representation of the links of the global force applicator.
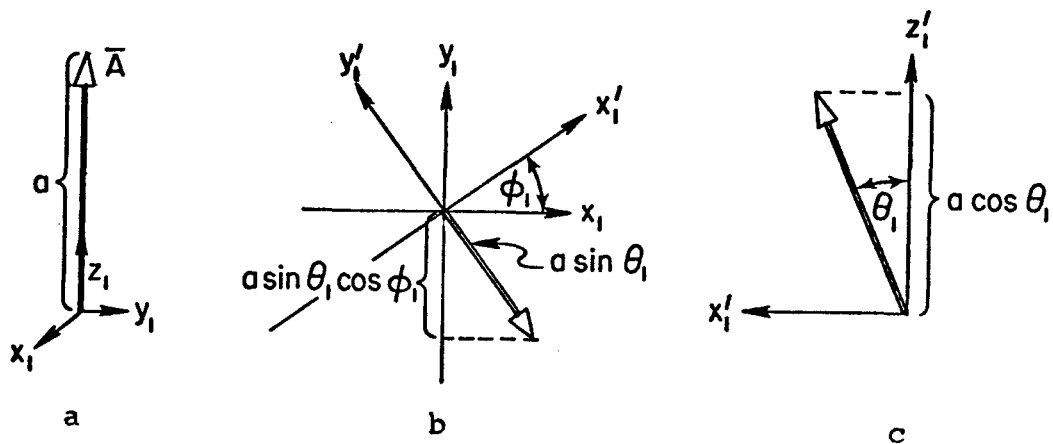
Fig. 82. Various positions of vector A associated with the first link of
the global force applicator: (a) initial configuration, (b) view on the
x-y plane, (c) view on the x_1'-z_1' plane.

131

In the actual usage of the GFA, x_p, y_p, and z_p were established as constant parameters.

Let us consider the first link individually in its starting position. Referring to Fig. 82, if we rotate about the z_1-axis by an angle ϕ, we do not change the orientation of A, but we have shifted the x_1 and y_1 axes to new positions x_1' and y_1'. A subsequent rotation about the x_1' axis gives us the following result

$$\bar{A}_{new} = (a\sin\theta_1\sin\phi_1)\hat{i}_1 - (a\sin\theta_1\cos\phi_1)\hat{j}_1 + (a\cos\theta_1)\hat{k}_1 \qquad (B9)$$

where $\hat{i}_1$, $\hat{j}_1$ and $\hat{k}_1$ are unit vectors along the corresponding x_1, y_1 and z_1 directions. This is more clearly illustrated in Figs. 82b and 82c. Therefore, once again referring to Fig. 81, the position of the second joint with respect to the origin of the inertial coordinate system is given by

$$\bar{r}_2 = (x_p + a\sin\theta_1\sin\phi_1)\hat{i}_1 + (y_p - a\sin\theta_1\cos\phi_1)\hat{j}_1 + (z_p + a\cos\theta_1)\hat{k}_1 \qquad (B10)$$

Using the same method as is illustrated in Fig. 81 we obtain for the second link

$$\bar{B}_{new} = (b\sin\theta_2\sin\phi_2)\hat{i}_2 - (b\sin\theta_2\cos\phi_2)\hat{j}_2 + (b\cos\theta_2)\hat{k}_2 \qquad (B11)$$

However, in order to add this vector to $\bar{r}_2$, we must transform its components into components along the x_1, y_1, and z_1 directions. From our previous discussion, we have established the fact that

$$\begin{bmatrix} x_2 \\ y_2 \\ z_2 \end{bmatrix} = [K_1] \begin{bmatrix} x_1 \\ y_1 \\ z_1 \end{bmatrix} \qquad (B12)$$

Utilizing Eq. B12 in Eq. B11 gives us the following

$$\bar{B}_{new} = b[(\sin\theta_2\sin\phi_2\cos\phi_1 + \sin\theta_2\cos\phi_2\sin\phi_1\cos\theta_1 + \cos\theta_2\sin\phi_1\sin\theta_1)\hat{i}_1$$

$$+ (\sin\theta_2\sin\phi_2\sin\phi_1 - \sin\theta_2\cos\phi_2\cos\phi_1\cos\theta_1 - \cos\theta_2\sin\theta_1\cos\phi_1)\hat{j}_1 \quad \text{(B13)}$$

$$+ (\cos\theta_2\cos\theta_1 - \sin\theta_2\cos\phi_2\sin\theta_1)\hat{k}_1]$$

Finding the suitable components for the $\bar{C}$ and $\bar{D}$ vectors is done by the same method with the aid of the two equations below.

$$\begin{bmatrix} x_3 \\ y_3 \\ z_3 \end{bmatrix} = [K_2][K_1]\begin{bmatrix} x_1 \\ y_1 \\ z_1 \end{bmatrix}$$

and

(B14)

$$\begin{bmatrix} x_4 \\ y_4 \\ z_4 \end{bmatrix} = [K_3][K_2][K_1]\begin{bmatrix} x_1 \\ y_1 \\ z_1 \end{bmatrix}$$

After tabulating the components of all the vectors, the final answer for $\bar{r}_5$ is given in terms of $\hat{i}_1$, $\hat{j}_1$, and $\hat{k}_1$ which are also the unit vectors corresponding to the XYZ inertial reference axes. The point location of the force application is now determined.

CALIBRATION OF THE GFA

To calibrate each of the eight high precision potentiometers of the GFA we collected sufficient voltage versus angle data points and applied a linear regression fit. Although the correlation coefficients, r^2, were all 0.9999--changing only at the 5th and 6th digits, thus, indicating high quality fit, the linear calibration curves did not provide satisfactory performance test results for the GFA. Note that both the GFA and the ESD must perform in such a way that at all times the same three dimensional coordinates with sufficient accuracy must be obtained no matter what their linkage configurations are. We detected up to 1% nonlinearity introduced by the data collection system, which was estimated to cause approximately 10% errors in the GFA performance. This non-linearity was attributed to

the input impedance level of the data collection system not being high enough for the potentiometers of the GFA and the ESD. First, we tried two different types of operational amplifiers at the inputs of the data collection system to see whether we could reduce substantially the 1% nonlinearity of the data collection system by increasing the existing 10kΩ input impedance of the system to 400 kΩ. Unfortunately, this increase in the input impedance did not improve the nonlinearity and the results were still unsatisfactory.

In view of this we decided to solve this problem by means of software techniques. We increased the calibration data points approximately _four_ times and used a curve fitting computer program to fit the data for each potentiometer into (up to) the tenth degree polynomial curve. The first term i.e. the constant term of the polynomial, was calculated for each potentiometer by using the voltage value read from the tape output at a known pre-set position of the GFA for a particular potentiometer. The accurate calculation of these constant values were very critical since a small variation in the calibration voltages recorded would significantly change the location of the end point of the last link of the GFA.

Since these voltage values were read after positioning the GFA in a particular configuration by the help of eye sight, it was believed that errors might have been introduced. To eliminate or minimize these errors, the constant terms of the polynomials were calculated in the range of ± 10 m volts of the read values, i.e., three readings per potentiometer. Then, two 3 x 4 matrices were constructed; one for the four elbow potentiometers and one for the four in-line potentiometers.

A computer program was developed to permute 12 voltage values (81 combinations, four potentiometers taken at a time). With every permutation the position vector for a known point was determined for two different linkage configurations of the GFA. The same procedure was repeated for the second set of values and the optimum values for the constants were determined. For the three different test positions and for the two arbitrary configurations of the GFA we obtained results within 2% range

of the actual values for the magnitudes of the vectors. In the light of this result we considered the performance of the GFA quite satisfactory.

The above mentioned calibration-curve fitting method resulted in the following relations for each potentiometer of the GFA:

$$\phi_1 = -3.204539 + (6.252397\times10^{-1})v - (1.403477\times10^{-3})v^2 + (3.203624\times10^{-3})v^3$$
$$- (4.964594\times10^{-4})v^4 - (3.997871\times10^{-5})v^5 + (1.199071\times10^{-5})v^6$$
$$- (6.151504\times10^{-7})v^7$$

$$\theta_1 = -3.101679 + (6.230784\times10^{-1})v - (1.331289\times10^{-2})v^2 + (6.059082\times10^{-3})v^3$$
$$- (8.354521\times10^{-4})v^4 + (3.583653\times10^{-5})v^5$$

$$\phi_2 = -1.764398 + (6.157800\times10^{-1})v + (9.225758\times10^{-3})v^2 - (9.352272\times10^{-4})v^3$$
$$- (1.705075\times10^{-5})v^4 + (2.448528\times10^{-6})v^5$$

$$\theta_2 = 3.074066 - (6.345027\times10^{-1})v - (7.855841\times10^{-3})v^2 + (1.663551\times10^{-3})v^3$$
$$- (7.101155\times10^{-5})v^4 \hspace{4cm} \text{(B15)}$$

$$\phi_3 = -3.223025 + (6.279128\times10^{-1})v + (1.294406\times10^{-3})v^2 + (6.281585\times10^{-4})v^3$$
$$- (1.535056\times10^{-4})v^4 + (7.134855\times10^{-6})v^5$$

$$\theta_3 = -3.133787 + (6.258071\times10^{-1})v + (5.446690\times10^{-3})v^2 - (6.839129\times10^{-4})v^3$$
$$+ (1.096645\times10^{-6})v^4$$

$$\phi_4 = (2.112579\times10^{-2}) + (6.261723\times10^{-1})v + (1.159564\times10^{-4})v^2$$
$$+ (1.673239\times10^{-3})v^3 - (3.296351\times10^{-4})v^4 + (1.576043\times10^{-5})v^5$$

$$\theta_4 = -3.222161 + (6.386217\times10^{-1})v - (1.435807\times10^{-2})v^2 + (5.453679\times10^{-3})v^3$$
$$- (7.443236\times10^{-4})v^4 + (3.222329\times10^{-5})v^5$$

where ϕ_i and θ_i are the rotations in radians of the in-line and elbow potentiometers, respectively; and v represents the corresponding voltage values.

THE FORCE AND MOMENT TRANSDUCER

The force and moment transducer which is referred as the force transducer in the main section of this report was designed to be a force and moment measuring device. It is essentially a cylindrical shell containing on the surface of the shell 8 single strain gages and 4 T-Rossettes which are strategically located to sense all three components of the force and moment vectors as shown in Fig. 83. The modular construction of this transducer enabled us to take it from the last link of the GFA and place it at the torque application apparatus.

After the installation of the strain gages and wiring tasks completed the transducer was calibrated for the axial, pure torsion, and bending moments about two perpendicular directions. The linear calibration curves and associated linear regression equations were obtained. These linear calibration equations are given below with their correlation coefficients:

$$\text{Axial:} \quad y_a = 157.441x_a + 0.304 \qquad (r^2 = .99975)$$

$$\text{Torsion:} \quad y_t = 53.390x_t - 0.428 \qquad (r^2 = .99987)$$

$$\text{Bending about } y: \begin{cases} y_{b11} = 64.316x_{11} + 0.385 & (r^2 = .99997) \\ y_{b22} = 63.386x_{22} - 0.264 & (r^2 = .99997) \end{cases}$$

$$\text{Bending about } x: \begin{cases} y_{b33} = 64.630x_{33} + 0.493 & (r^2 = .99997) \\ y_{b44} = 64.162x_{44} + 0.565 & (r^2 = .9997) \end{cases}$$

$$(B16)$$

where the x values represent the amplified voltages obtained from the strain gages at the indicated locations in Fig. 83 and y values represent either force in lbs. or torques in in-lbs. Using these calibration equations and some dimensions of the transducer in a straightforward analysis we obtained the following equations for the components of the force and moment vectors.

8 SINGLE STRAIN
GAGES AT 90°
SEPARATION & LOCATED
AT TWO ROWS

4 T-ROSSETTES
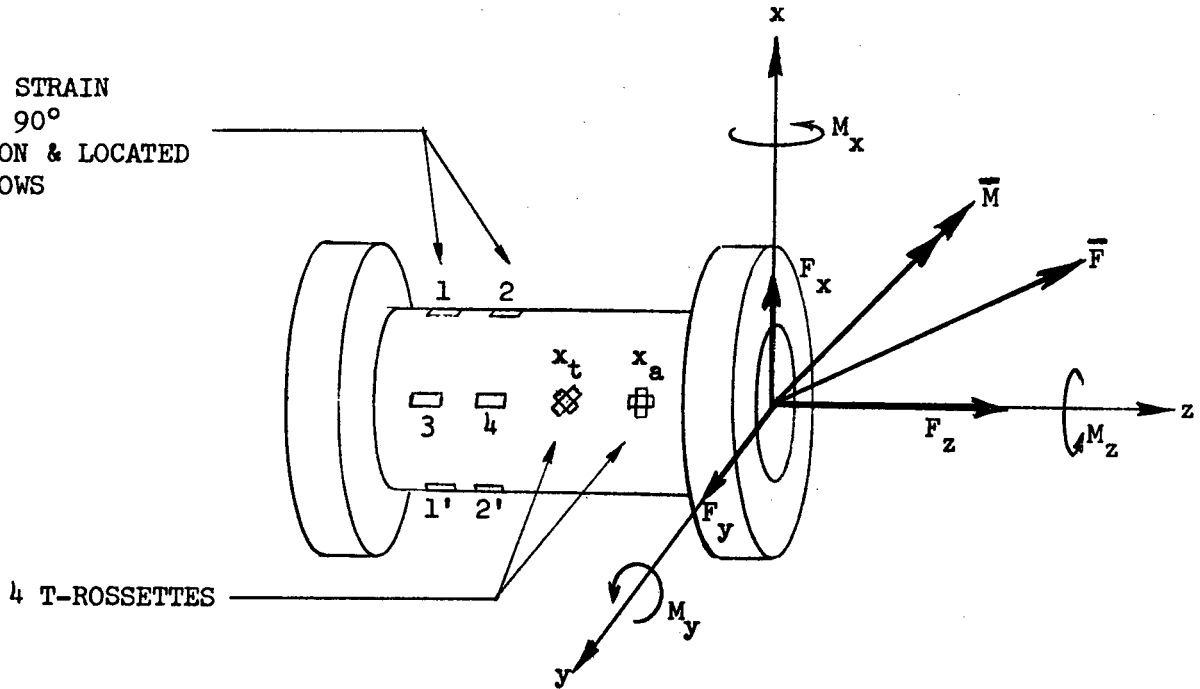
Fig. 83. Schematic drawing of the force transducer

$$F_x = 178.656x_{11} - 176.072x_{22} + 1.803$$

$$F_y = 179.528x_{33} - 178.229x_{44} - 0.072$$

$$F_z = 157.441x_a + 0.304$$

$$M_x = 374.284x_{44} - 312.382x_{33} + 0.913$$

$$M_y = 369.752x_{22} - 310.862x_{11} - 1.224$$

$$M_z = 53.390x_t - 0.428.$$

(B17)

Note that during force application on the moving body segment the predominant force component is obviously F_z which is along the direction of the last link of the GFA if one maintains approximately perpendicular force application on the moving body segment.

137

APPENDIX C

EXOSKELETAL DEVICE (ESD)

The exoskeletal device (ESD) consists of five links which are connected by four joints as shown in Figures 84 and 85. Each joint allows flexion (or elbow-like rotation) and axial rotation (or in-line rotation). The ESD uses the same principle as the GFA to determine the relative orientations and positions between two body segments although this was done by augmented matrix transformations. In Figures 84 and 85 principal features of the ESD and reference axes which are attached to each link at the joint center are shown.

The in-line rotation of the links about the z-axes are measured by ϕ angles (PH) and elbow-type rotations are measured by θ angles (TH). Since the joints of the ESD are inverted after the midpoint (see Figure 85) and in order that the same matrix transformation matrix can be used throughout the analysis, two constant angles ϕ_3 and θ_5 are introduced and set equal to zero. A link of length equal zero, CL5, is introduced for the same reason. Hence, the last matrix transformation is used only to obtain the orientation of the final axis system $x_5 y_5 z_5$.

The transformation matrix for coordinates and orientation of the axes $x_2 y_2 z_2$ with respect to the base reference axes $x_1 y_1 z_1$ has the form:

$$[AK1] = \begin{bmatrix} 1 & 0 & 0 & 0 \\ 0 & \cos\phi_1 & \sin\phi_1 & 0 \\ 0 & -\sin\phi_1\cos\theta_1 & \cos\phi_1\cos\theta_1 & \sin\theta_1 \\ CL_1 & \sin\phi_1\sin\theta_1 & -\cos\phi_1\sin\theta_1 & \cos\theta_1 \end{bmatrix} \quad (C1)$$

and will be called [AK1]. The transformation matrix of the axis system $x_3 y_3 z_3$ into the axis system $x_2 y_2 z_2$ will have the same form but with angle θ_2 and ϕ_2 instead of θ_1 and ϕ_1, and length CL_2 instead of CL_1. This transformation is called [AK2] and further transformations proceed in like manner. There are 5 transformation matrices required to transform the coordinates and orientation of the final axis system $x_5 y_5 z_5$ into

138
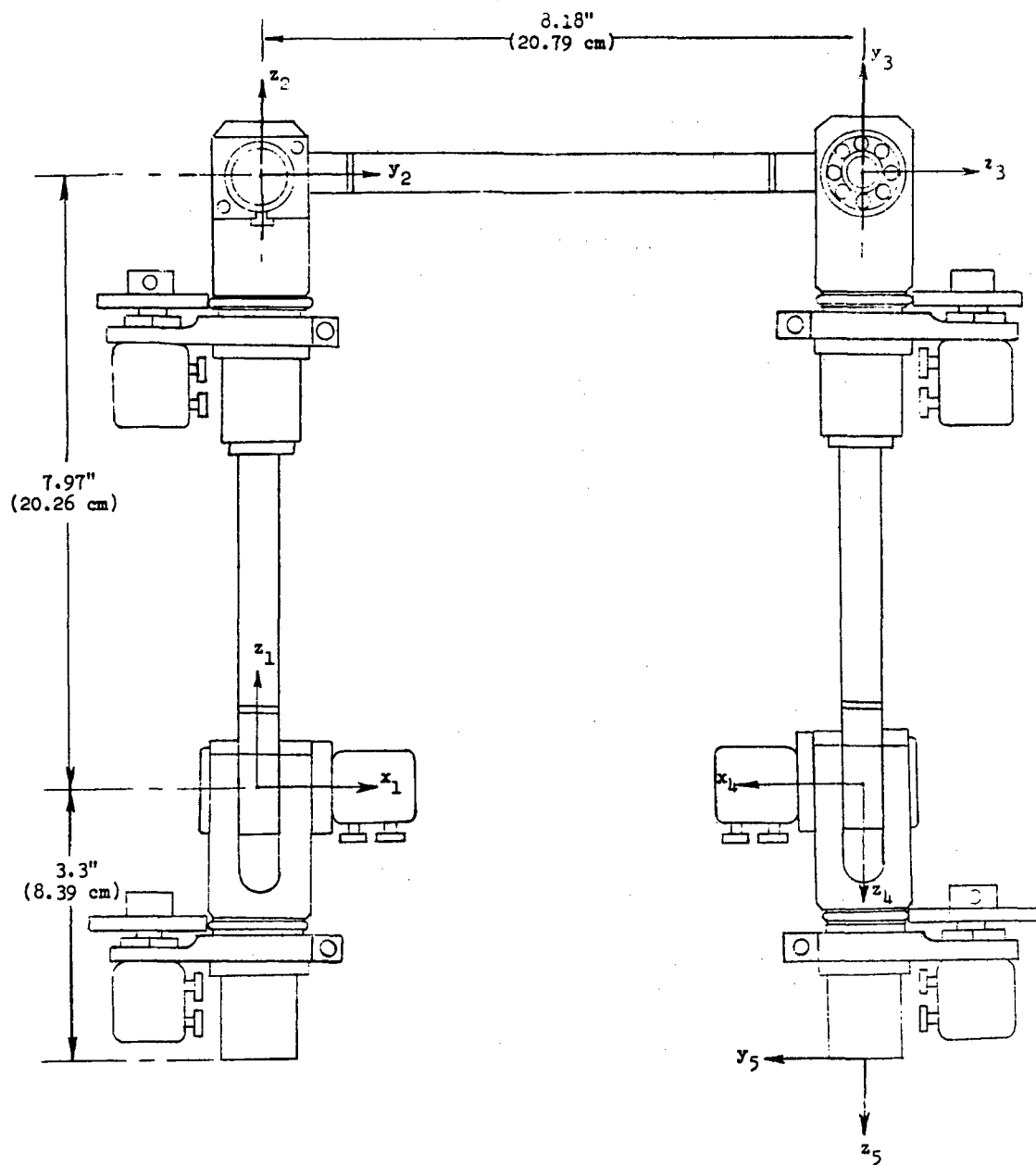
Figure 84 Schematic drawing of the exoskeletal device.
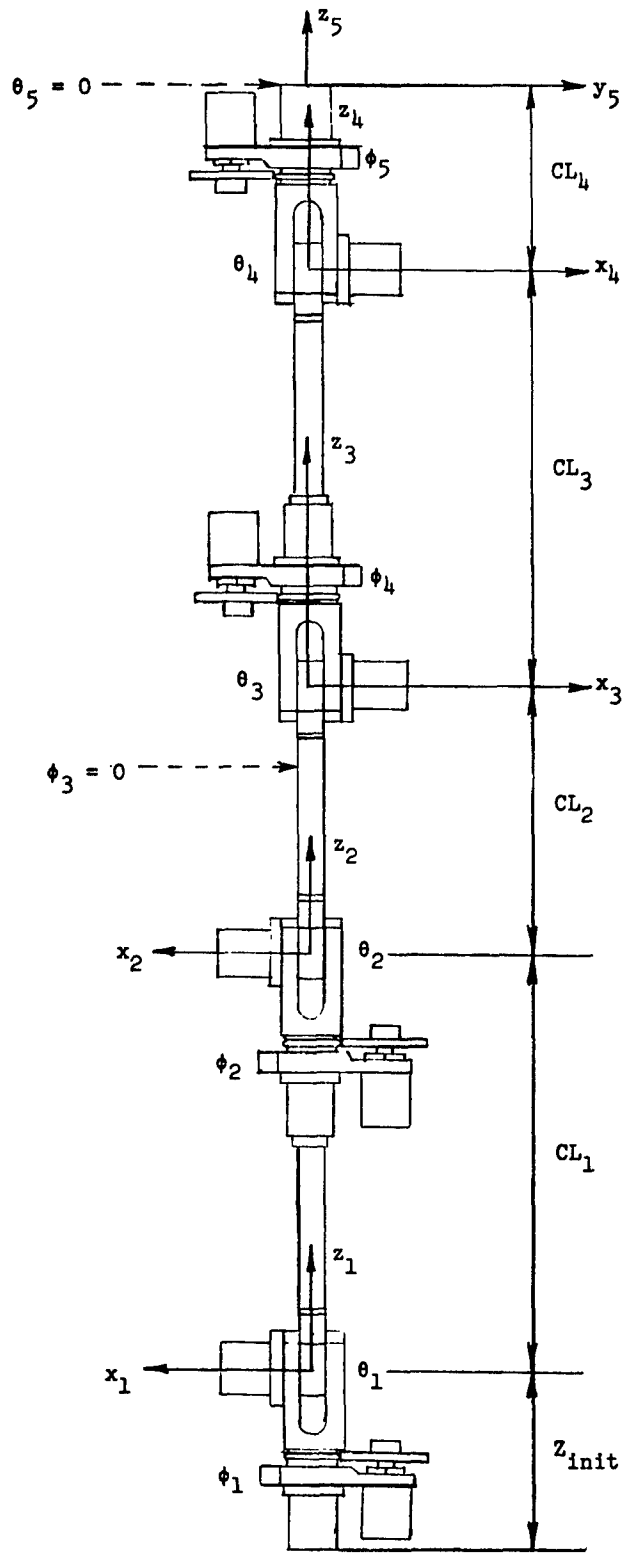
Figure 85 Initial reference configuration of the ESD.

the base reference axis system $x_1 y_1 z_1$.

The final matrix transformation has the form:

$$[A51] = [AK5] [AK4] [AK3] [SID] [AK2] [AK1] \qquad \text{(C2)}$$

where,

$$[SID] = \begin{bmatrix} 1 & 0 & 0 & 0 \\ 0 & -1 & 0 & 0 \\ 0 & 0 & -1 & 0 \\ 0 & 0 & 0 & 1 \end{bmatrix}$$

is the semi-identity matrix used to change signs of the angles measured by the potentiometers of joints 3 and 4 since these joints are oriented in the opposite direction of the joint of the base axis system $x_1 y_1 z_1$. Also, since the orientation of the axis system at the base of the ESD is usually different from that of the fixed body $x_b y_b z_b$, a matrix called [AK6] is used to transform the coordinates and directions of the ESD end axis system $x_5 y_5 z_5$ into the fixed body axis system. The final transformation matrix obtained in this manner is called [WRTB], (with respect to body) which has the form:

$$\begin{bmatrix} 1 & 0 & 0 & 0 \\ a_{21} & a_{22} & a_{23} & a_{24} \\ a_{31} & a_{32} & a_{33} & a_{34} \\ a_{41} & a_{42} & a_{43} & a_{44} \end{bmatrix} \qquad \text{(C3)}$$

WRTB is thus an augmented transformation matrix. The elements of the submatrix shown above (a_{ij} where i = 2, 3, 4 and j = 2, 3, 4) consist of the direction cosines of the $x_5 y_5 z_5$ axes with respect to the fixed body axis system $x_b y_b z_b$. The elements a_{21}, a_{31}, and a_{41} are multiplicative factors used to calculate the position of a given point (the end point of the ESD) on the moving body segment.

The calibration procedure for the ESD was very similar to that of the GFA. For the ESD the configuration shown in Figure 85, i.e. the

141

straight line configuration for which the axes of rotation of the elbow potentiometers are parallel, was called the reference configuration. The voltages read from the potentiometers at this reference configuration were used to calculate reference points on the calibration (angle v.s. voltage) curves. For example, if v_0 is the voltage read at the reference configuration for a particular potentiometer the reference angle for this potentiometer is $\theta(v_0)$ radians. If the voltage read at some arbitrary position is v, then the corresponding angle is $\theta(v)$ radians, and this angle is $\theta(v) - \theta(v_0)$ radians away from the reference configuration, i.e., the reference angle subtracted from the calibration function.

The same permutation procedure explained for the GFA calibration was also applied for the ESD with ± 5 m volts. The calibration functions for each potentiometer of the ESD are as follows:

$$\phi_1 = -4.639687 + 3.210859 \, v$$

$$\theta_1 = 11.104414 + 0.090359 \, v - 0.805363 \, v^2 + 0.062857 \, v^3$$

$$\phi_2 = -4.737862 + 3.061055 \, v + 0.052142 \, v^2$$

$$\theta_2 = 29.113821 - 11.199511 \, v + 1.583857 \, v^2 - 0.103915 \, v^3$$

$$\theta_3 = 1.690876 + 5.870352 \, v - 2.104249 \, v^2 + 0.159421 \, v^3$$

$$\phi_4 = -4.646166 + 3.246798 \, v$$

$$\theta_4 = 7.590080 + 1.892096 \, v - 1.126615 \, v^2 + 0.081798 \, v^3$$

$$\phi_5 = -5.006343 + 2.746649 \, v + 0.334164 \, v^2 - 0.060329 \, v^3$$

$$(C4)$$

where ϕ_i and θ_i are the rotations in radians of the in-line and elbow potentiometers, especially; v represents the corresponding voltage values. Note that for the ESD similar accuracy to that of the GFA was achieved with calibration functions of lower degrees.

APPENDIX D

DATA COLLECTION SYSTEM

Fig. 86 shows a chart of the major operations and functions of the NWL (Naval Weapons Laboratory) 610 data collection system which was installed in our laboratory. We extended the data collection capability of this system from 16 channels to 24 channels by building an additional electronics board into the multiplexer. In our application, we sampled 24 channels of analog data and one zero reference channel. The first 16 channels of data coming from the ESD and the GFA and ranging between 0.1 volts to 10 volts were sent directly to the multiplexer while eight of the last nine coming from the force transducers were preamplified to a three-volt range and sent to the multiplexer. The last, i.e. the twenty-fifth channel, was the zero volts reference channel which was not accessed outside of the multiplexer. In the next few paragraphs technical information on the general operation of the data collection system is presented.

The multiplexer, driven by a controllable digital clock, selects each channel of data in sequence and applies it to the analog to digital (A/D) converter. A signal from the A/D initiates a write cycle into the memory to store the 14-bit digital value of the signal at the moment of sampling. In addition, a parity bit is created and stored as the 15th bit. This bit produces an odd bit sum for each data word, which is confirmed when it is read from memory, in order to detect memory errors.

Data is continuously read into memory, channel by channel, up to a possible 4096 data points. At some pre-programmed point, the contents are unloaded onto magnetic tape on the IBM 729 tape drive under the control of additional bits previously stored in memory locations by the user. When bit 19 is sensed (during the above loading process) it signals the tape drive that "unloading minus 5 milliseconds" has occurred. The short delay allows the tape drive to reach full speed and to insure an adequate gap between each record (group of data) on the tape. While the memory is unloading, it continues to collect data without interruption. Bit 20

143
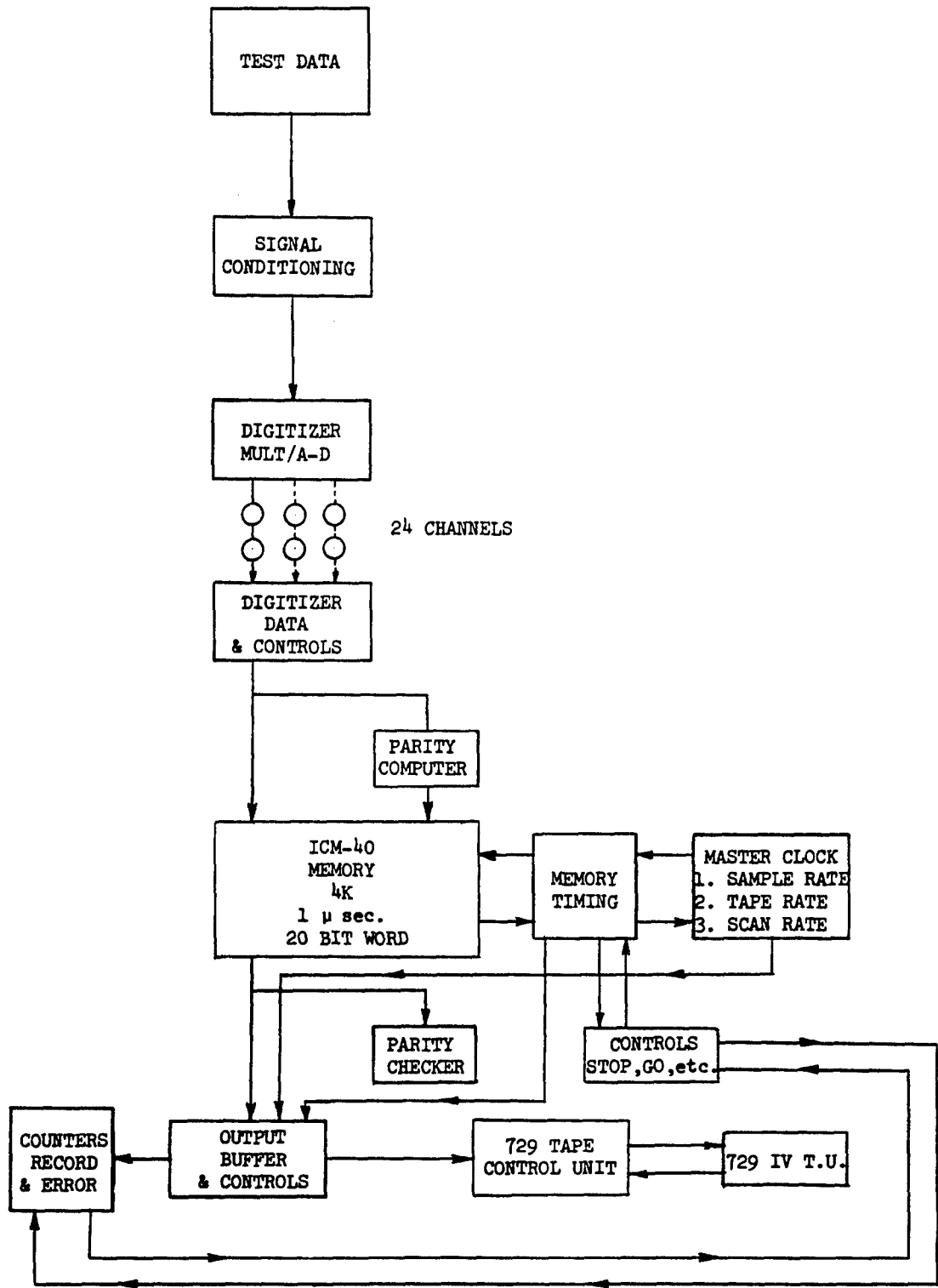
Fig. 86. Block diagram for the data conversion system

marks the upper end of the data record stored in memory, and starts the unloading of memory onto the magnetic tape of the IBM 729-VI.

Data is stored in binary form on the tape as a series of two vertical tape characters of seven bits each. The uppermost bit of each character is a parity bit for the entire column. The next lowest bit of the first tape character is the sign bit -1 for positive values, 0 for negative values. The remainder are the most significant bits of the data word originally stored in memory. The second tape character likewise has a parity bit and six data bits, representing the six least most significant data bits. Therefore, 12 bits of data (sign plus 11 bits) are stored as two tape characters.

At the end of each record a longitudinal parity character is recorded which provides a check of bit parity over each row of data bits in the record, for additional error detection. The tape drive has "read" as well as "write" electronics. Each tape character is read after it is written and checked for parity errors, and the entire record is checked and compared with the longitudinal parity character for further error detection. The NWL 610 can be programmed to stop on the detection of these errors.

The cycle of scanning channels, loading memory, and unloading onto tape can be done once (to write a single record) or as many times as desired, all under user control. Likewise, the sampling rate, number of channels scanned, and length of record are also predetermined by the user, within the constraints of the data conversion system.

To make the data collection system operational a number of problems had to be first diagnosed and later resolved. These problems included frequent memory errors, both longitudinal and vertical tape parity errors, irregular scanning of the input channels by the multiplexer, deviations from the linear input/output format for the A/D convertor, and inability to attain READY status and load tape properly on the IBM 729-VI. We resolved each of these problems and others. After calibration and numerous checks we started our testing program. Data were gathered at a sampling rate of 1500 samples/sec. or 62.5 samples/sec/channel. After collecting data over three months we discovered that A/D converter at times deviated

from the normal operation by either .32 volt jumps between 0 to 5 volt
range and thereafter by series of repetitions of magnitudes from 20
milivolts to 150 milivolts staggered by 80 milivolts jumps in the 5 to 10
volt operating range. This behavior was discovered when the data were
run to get some numerical results. The problem was pin pointed to the
A/D converter and it was verified by inputting voltage increments of
10 milivolts from 0 to 10 volts and recording results on the IBM 729 tape.
Tape dump was further studied by plotting 1000 points on a large graph
paper as system voltage output versus system voltage input.

We next wrote a computer program to investigate the influence of the
irregular behavior of the A/D convertor on our data. This program
scanned the data tapes with very strict code conditions, i.e., reporting
if the data points fell into within 10 milivolt boundaries of the jumps
or repetition regions of the A/D converter. For each code condition the
number of channels whose data fell into the questionable regions was
also determined. Good data were defined as the data that passed all code
conditions for all the channels. Unfortunately, among over a million
data points not even a percent satisfied this requirement. Thus, after
repairing and recalibrating the A/D converter we embarked upon retesting
program.

REFERENCES

1. McHenry, R.R., "Analysis of the Dynamics of Automobile Passenger-Restraint System," <u>Proceedings of the 7th Stapp Car Crash Conference</u>, 207, (1963), Charles C. Thomas, Springfield, Ill., 1965.

2. Segal, D.J., "Revised Computer Simulation of the Automobile Crash Victim," Cornell Aeronautical Lab. Report No. VJ-2759-V-a, 1971.

3. Danforth, J.P. and Randall, C.D., "Modified ROS Occupant Dynamics Simulation User Manual," GM Research Labs., Publication No. GMR-1254 1972.

4. Glancy, J.J. and Larsen, S.E., "User Guide for Program SIMULA," Dynamic Science, Report TDR No. 72-23, 1972.

5. Robbins, D.H., Bowman, B.M. and Bennett, R.O., "The MVMA Two-Dimensional Crash Victim Simulations," <u>Proceedings of the 18th Stapp Car Crash Conference</u>, 657, 1974.

6. Karnes, R.N., Tocher, J.L. and Twigg, D.W., "Prometheus--A Crash Victim Simulator," <u>Symposium on Aircraft Crashworthiness</u>, 1975.

7. Robbins, D.H., Bennett, R.O. and Bowman, B.M., "User Oriented Mathematical Crash Victim Simulator," <u>Proceedings of the 16th Stapp Car Crash Conference</u>, 128, 1972.

8. Young, R.D., "A Three-Dimensional Mathematical Model of an Automobile Passenger," Texas Transportation Institute Research Report 140-2, 1970.

9. Huston, R.L., Hessel, R.E. and Passerello, C.E., "A Three-Dimensional Vehicle-Man Model for Collision and High Acceleration Studies," SAE Paper No. 740275, 1974.

10. Bartz, J.A. and Butler, F.E., "A Three-Dimensional Computer Simulation of a Motor Vehicle Crash Victim, Phase 2 Validation of the Model," Calspan Technical Report No. VJ-2978-V-2, 1972.

11. Fleck, J.T., Butler, F.E. and Vogel, S.L., "An Improved Three-Dimensional Computer Simulation of Motor Vehicle Crash Victims," Calspan Final Technical Report No. AQ-5180-L-1, 1974.

12. Fleck, J.T., "Calspan Three-Dimensional Crash Victim Simulation Program," <u>Aircraft Crashworthiness</u>, edited by K. Saczalski, G.T. Singley, W.D. Pilkey, and R.L. Huston, University Press of Virginia, Charlottesville, 299, 1975.

13. Engin, A.E., "Mechanics of the Knee Joint: Guidelines for Osteotomy in Osteoarthritis," _Orthopaedic Mechanics_, edited by D.N. Ghista and R. Roaf, Academic Press, London, England, 60, 1978.

14. Barnett, C.H., Davies, D.V. and Mac Conaill, M.A., _Joints, Their Structure and Mechanics_, Charles C. Thomas Publishers, Springfield, Ill. 1949.

15. Steindler, A., _Kinesiology of the Human Body_, Thomas, Springfield, 62, 1964.

16. Mac Conaill, M.A., "Joint Movement," _Physiotherapy_ (50), 359, 1964.

17. Murphy, W.W., Garcia, D.H. and Bird, R.G., "Measurement of Body Motion," ASME Paper No. 66-WA/BHF-2, 1966.

18. Adrian, M.J., "An Introduction to Electrogoniometry," _Kinesiology Review_, 12, 1968.

19. Ringer, L.B. and Adrian, M.J., "An Electrogoniometric Study of the Wrist and Elbow in the Crawl Arm Stroke," _The Research Quarterly_ (40), 353, 1969.

20. Murray, M.P., Sepic, S.B. and Barnard, E.J., "Patterns of Sagittal Rotation of the Upper Limbs in Walking," _Physical Therapy_ (47), 272, 1967.

21. Clayson, S.J., et al., "Goniometer Adaptation for Measuring Hip Extension," _Archives of Physical Medicine_ (47), 255, 1966.

22. Shoup, T.E., "Applying Burmester's Theory to the Mechanization of Human Motion," _Proceedings of the Third Canadian Congress of Applied Mechanics_, Calgary, Alberta, 1971.

23. Saunders, J.B., Inman, V.T. and Eberhart, H.D., "The Major Determinants in Normal and Pathological Gait," _The Journal of Bone and Joint Surgery_ (35-A), 543, 1953.

24. Leighton, J.R., "An Instrument and Technique for the Measurement of Range of Joint Motion," _Archives of Physical Medicine and Rehabilitation_ (36:5), 571, 1955.

25. Young, H., "Use of a Hinged Vitallium Prosthesis for Arthroplasty of the Knee," _The Journal of Bone and Joint Surgery_ (45-A), 1627, 1963.

26. Finley, F.R. and Karpovich, P.V., "Electrogoniometric Analysis of Normal and Pathological Gaits," _The Research Quarterly_ (35), 379, 1964.

27. Contini, R., Gage, H. and Drillis, R., "Human Gait Characteristics," Biomechanics and Related Bioengineering Topics, R.M. Kenedi, ed. Pergamon Press, New York, 413, 1965.

28. Liberson, W.T., "Biomechanics of Gait: A Method of Study," Archives of Physical Medicine and Rehabilitation (46), 37, 1965.

29. Klissouras, V. and Karpovich, P.V., "Electrogoniometric Study of Jumping Events," The Research Quarterly (38), 41, 1967.

30. Beckett, R. and Chang, K., "An Evaluation of the Kinematics of Gait by Energy," Journal of Biomechanics (1), 147, 1968.

31. Gollnick, P.D. and Karpovich, P.V., "Electrogoniometric Study of Locomotion and Some Athletic Movements," The Research Quarterly (35), 357, 1964.

32. Freedman, L. and Munro, R.H., "Abduction of the Arm in the Scapular Plane: Scapula and Glenohumeral Movements," The Journal of Bone and Joint Surgery (48-A), 1503, 1966.

33. Taylor, C.L. and Blaschke, A.C., "A Method for Kinematic Analysis of Motions in the Shoulder, Arm and Hand Complex," Annals New York Academy of Sciences (51), 1251, 1951.

34. Engen, T.J. and Spencer, W.A., "Method of Kinematic Study of Normal Upper Extremity Movements," Archives of Physical Medicine and Rehabilitation (49), 9, 1968.

35. Roebuck, J.A., Jr., "Kinesiology in Engineering," Kinesiology Review, 5, 1968.

36. Paul, J.P., "Forces Transmitted by Joints in the Human Body," Proceedings of the Institution of Mechanical Engineers (181), 8, 1967.

37. Eberhart, H. and Inman, V., "An Evaluation of Experimental Procedures Used in a Fundamental Study of Human Locomotion," Annals New York Academy of Sciences (51), 1213, 1951.

38. Hallen, L.G. and Lindahl, O., "The Lateral Stability of the Knee Joint," Acta Orthopaedica Scandinavica (36), 400, 1965.

39. Morrison, J.B., "Function of the Knee Joint in Various Activities," Biomedical Engineering (4), 573, 1969.

40. Dempster, S.T., "The Anthropometry of Body Motion," Annals New York Academy of Sciences (63), 559, 1955.

41. Lamoreux, L.W., "Kinematic Measurements of Walking," ASME Paper No. 72-MECH-80, 1972.

42. McKee, G.K., "Developments in Total Hip Joint Replacement," Proceedings of the Institution of Mechanical Engineers (181), 85, 1967.

43. Johnston, R.C. and Smidt, G.L., "Measurement of Hip Joint Motion during Walking," The Journal of Bone and Joint Surgery (51-A), 1083, 1969.

44. Chao, E.Y.S., et al., "The Application of 4x4 Matrix Methods to the Correction of the Measurements of Hip Joint Rotations," Journal of Biomechanics (3), 459, 1970.

45. Smidt, G.L., "Hip Motion and Related Factors in Walking," Physical Therapy (51), 9, 1971.

46. Smidt, G.L., "Biomechanical Analysis of Knee Flexion in Walking," Journal of Biomechanics (6), 79, 1973.

47. Bahniuk, E. and Wijnschenk, M.J., "Design Parameters for an Orthotic Arm Aid," ASME Paper No. 63-WA-282, 1963.

48. Bousso, D., "A Six Degree of Freedom Experimental Limb for Thalidomide Children," Bio-medical Engineering (4), 313, 1969.

49. Risteen, F.C. and Torfason, L.E., "Hydraulically Actuated Quadraplegic Arm Appliance with Six Degrees of Freedom," ASME Paper No. 70-MECH-55, 1970.

50. Barnett, C.H., "Locking at the Knee Joint," Journal of Anatomy (87), 91, 1953.

51. Radcliffe, C.W., "Prosthetic Mechanisms for Leg Amputees," Transactions of the Sixth Conference on Mechanisms, Purdue University, 143, 1960.

52. Burstein, A. and Frankel, V.H., "The Design of Orthopaedic Implants and Prostheses," ASME Paper No. 67-DE-38, 1967.

53. Shute, C.C.D., "Complex Movements at the Knee Joint," Proceedings of the Institution of Mechanical Engineers (181), 9, 1967.

54. Freudenstein, F. and Woo, L.S., "Kinematics of the Human Knee Joint," Bulletin of Mathematical Biophysics (31), 215, 1969.

55. Frankel, V.H., Burstein, A.H. and Brooks, D.B., "Biomechanics of Internal Derangement of the Knee," The Journal of Bone and Joint Surgery (53-A), 945, 1971.

56. Reilly, D.T. and Martin, M., "Experimental Analysis of Quadriceps Muscle Force and Patello-femoral Joint Reaction Force for Various Activities," Acta Orthopaedica Scandinavica (43), 126, 1972.

57. Evans, F.G., "Biomedical Implications of Anatomy," Proceedings of the C.P.C. Symposium on Biomechanics, J.M. Cooper, ed., Indiana University, 3, 1970.

58. Sammarco, G.J., Burstein, A.H. and Frankel, V.H., "Biomechanics of the Ankle: A Kinematic Study," Orthopedic Clinics of North America (4), 75, 1973.

59. Bick, H.O. and Morrison, W.E., "A Method for Reproduction of Movements of the Mandible," The Journal of Prosthetic Dentistry (12), 873, 1962.

60. Cannon, D.C., Instrumentation for the Investigation of Mandibular Movements, M.S. Thesis, Case Institute of Technology, 1965.

61. Messerman, T., "A Means for Studying Mandibular Movements," The Journal of Prosthetic Dentistry (17), 36, 1967.

62. Knap, F.J., Richardson, B.L. and Bogstad, J., "Study of Mandibular Motion in Six Degrees of Freedom," Journal of Dental Research (49), 289, 1970.

63. Thompson, C.T., A System for Determining the Spatial Motions of Arbitrary Mechanisms - Demonstrated on a Human Knee, Ph.D. Thesis, Stanford University, 1972.

64. Kinzel, G.L., Hillberry, B.M., Hall, A.S., Van Sickle, D.C. and Harvey, W.M., "Measurement of the Total Motion between Two Body Segments, Part II--Description of Application," Journal of Biomechanics (5), 283, 1972.

65. Chasles, M., Bull, Sci. Math. (14), 321, 1830.

66. Skreiner, M., "Study of the Geometry and the Kinematics of Instantaneous Spatial Motion," Journal of Mechanisms (1), 115, 1966.

67. Klein, F., Geometry translated by E.R. Hednick and C.A. Noble, No. S151, Dover Publications, Inc., New York, N.Y. 1939.

68. Bocher, M., Introduction to Higher Algebra No. S1238, Dover Publications, Inc., New York, N.Y., 1964.

69. Goldstein, H., Classical Mechanics, Addison-Wesley, Cambridge, Mass., 1959.

70. Marey, E.J., "De la locomotion terrestre chez les bipedes et les quadrupedes," J. de l'Anat. et de la Physiol. (9), 42, 1873.

71. Bresler, B. and Frankel, J.P., "The Forces and Moments in the Leg During Level Walking," Trans. Am. Soc. Mech. Engrs. (72), 27, 1950.

72. Hyzer, W.G., Engineering and Scientific High Speed Photography, New York: MacMillan, 1963.

73. Mascelli, J.V. and Miller, A., American Cinematographer Manual, Hollywood, Cal. Amer. Soc. of Cinematographers Holding Corp., 1966.